EXPERIMENTAL AND NUMERICAL SIMULATION OF HYDRAULIC FRACTURING

By

Mohammad Hoveidafar, B.S.

A Thesis Submitted in Partial Fulfillment of the Requirements

for the Degree of

Master of Science

in

Mining Engineering

University of Alaska Fairbanks

December 2017

APPROVED:

Gang Chen, Committee Chair

Paul Metz, Committee Member

Il Sang Ahn, Committee Member

Yin Zhang, Committee Member

Margaret M. Darrow, Chair

Department of Mining and Geological Engineering

Doug Goering, Dean

College of Engineering and Mines

Michael Castellini, *Dean of Graduate School*

Abstract

Hydraulic Fracturing (HF) has many applications in different fields such as stimulation of oil and gas reservoirs, in situ stress measurements, stress relief for tunneling projects as well as in underground mining applications such as block caving mining. In the HF process, high pressure fluid is injected into a well to generate fractures in tight rock formations. This technique is particularly suitable for developing hydrocarbon energy resources in tight rock formations such as shale with very low permeability.

An experimental setup was designed and developed to simulate the HF process in the laboratory. Cubic plaster specimens were molded and HF experiments were conducted with simulated plaster models. Five laboratory tests were performed on cubic specimens under different stress conditions. Because the uniaxial compressive strength of the plaster was about 1600 psi, in all experiments the applied vertical stress was 1000 psi to avoid breaking the specimens before injection of fluid. The differential horizontal stress varied from 100 to 500 psi. These stress levels are related to shallow formations in a real environment. It was observed that increasing the differential horizontal stress by 100 psi, the minimum pressure required to initiate HF decreases about 100 psi. These results were in agreement by 2D failure criterion of HF. All in all, the small scale HF experiments were conducted successfully in the rock mechanics lab. It was observed that vertical hydraulic fractures would propagate along maximum horizontal stress, which is in agreement with propagation of HF theory.

Three-dimensional (3D) numerical models were developed and computer simulations were conducted with ABAQUS, a commercially available finite element analysis (FEA) software. The numerical simulation results compared favorably with those from the laboratory experiments, and verification and analysis were carried out.

Since the results obtained from the numerical model were in agreement with the results of experiments and verified the correctness of the model, further investigation was carried out with developed computer models. Several scenarios with different vertical stresses and different levels of horizontal stress were simulated. A statistical software, R, was used to generate a 3D failure criterion for the HF in shallow formations. The statistical analysis indicated that the HF pressure required to initiate hydraulic fractures (P_{HF}) is a function of the vertical stress (σ_v), the maximum

horizontal stress (σ_H), the minimum horizontal stress (σ_h), and the tensile strength of the material (T) in the following relationship:

$$P_{HF} = 0.07(\sigma_v) + 3.01(\sigma_h) - (\sigma_H) + 0.79(T)$$

It can be stated that in shallow formations, vertical stress has the least effect among stress components on the minimum pressure required to initiate HF.

Dedication

I dedicate this work to my beloved family for their infinite love, support, and inspiration.

Table of Contents

List of Figures

Page

List of Tables

Page

Acknowledgements

Firstly, I would like to express my sincere gratitude to my advisor Prof. Gang Chen for the continuous support of my Master study and related research, for his support, guidance, and immense knowledge.

I also want to take this opportunity to thank my committee members Dr. Paul Metz, Dr. Yin Zhang, and Dr. Il Sang Ahn for their patience and motivation for completing this research.

The financial supports provided by the Department of Mining and Geological Engineering and the Institute of Northern Engineering are gratefully acknowledged.

Last but not least, I remain grateful to my family for their endless love, support, and encouragement that I relied on throughout my education at the University of Alaska Fairbanks. Finally, I would like to thank all of my friends and the faculties at the University of Alaska Fairbanks.

CHAPTER 1 INTRODUCTION

The hydraulic fracturing (HF) technique has been used in the petroleum industry since its introduction in 1948. In the HF process, by injecting high pressure fluid containing mostly water into a borehole, rock fractures are generated in unconventional reservoirs situated in low permeability formations. This technique is suitable for oil and gas extraction in formations such as shale with very low permeability (1).

In conventional reservoirs, when a well is drilled and reaches the formation containing hydrocarbons, the hydrocarbons migrate to the well from high pressure regions to low pressure regions. On the other hand, in some unconventional reservoirs due to low permeability of the formation, the hydrocarbons cannot migrate. So it is necessary to increase permeability to allow hydrocarbons to flow to the well and be extracted.

1.1 Brief History of HF

Modern HF can be traced back to 1857. Preston Barmore used gunpowder inside a gas well to create fractures and increase gas flow at Canadaway Creek, NY (2).

Col. Edward Roberts, a civil war veteran, started a new method called 'superincumbent fluid-tamping' in 1865. In this technique, water was used to avoid scattered pieces of rocks coming out of the well by dampening the explosion (2; 3).

In the 1940's, Floyd Farris stated that production from a well could be increased by using hydraulic pressure. In 1947, the first gas well was hydraulically fractured in Houghton Field, Kansas. At that time, the fracturing fluid contained naphthenic acid, palm oil, gasoline, and sand. Halliburton Company, by using crude oil as the hydraulic fluid, increased the oil production of 332 wells by 75% in 1949. Water was used as the hydraulic fluid for the first time in 1953 (2).

In the 1980s, Mitchell Company combined HF with horizontal drilling in the Barnett Shale near Fort Worth, Texas. The combination of HF with horizontal drilling was a great breakthrough in the oil and gas industry. Since then, this technique has been used in tight shale formations (unconventional reservoirs) in the U.S (3).

1.2 Applications of HF

HF has many applications in different engineering projects. In addition to unconventional oil and gas reservoirs, this technique has been used in different fields including (4):

- Water well production enhancement
- Block cave mining (hydraulic pre-conditioning)
- Rock stress determination for geotechnical design (tunnels, dams, foundations)
- Conventional oil and gas production
- Geothermal production (hot dry rock, or "enhanced' geothermal)
- Carbon sequestration (carbon capture and storage)
- Coalbed methane development
- Coal mine methane drainage
- Rock burst mitigation

1.3 The Importance of HF in the U.S.

Based on studies done by the U.S. Energy Information Administration in May 2016, half of the total crude oil production in the United States comes from hydraulically fractured wells. Although HF has been used since 1940s, it has been applied more frequently in tight formations containing hydrocarbons after the invention of horizontal drilling in recent years. For instance, in 2000 less than 2% of crude oil production by the U.S. came from hydraulically fractured wells (23,000 hydraulically fractured wells); but in 2015 the percentage of oil production using HF technique rose to 51% (300,000 hydraulically fractured wells). Figure 1-1 shows the percentage of oil production from hydraulically fractured wells and non-hydraulically fractured wells. Figure 1-2 shows the growing trend in application of HF from 2000 to 2015 (5).

The HF technique was used first in the Eagle Ford formation and Permian Basin of Texas, and the Bakken and Three Forks formation of Montana and North Dakota (5). Figure 1-3 shows the distribution of shale formations in lower 48 states (6).

Figure 1-4 shows the shale oil and gas production from prominent shale formations in billion cubic feet per day (7).

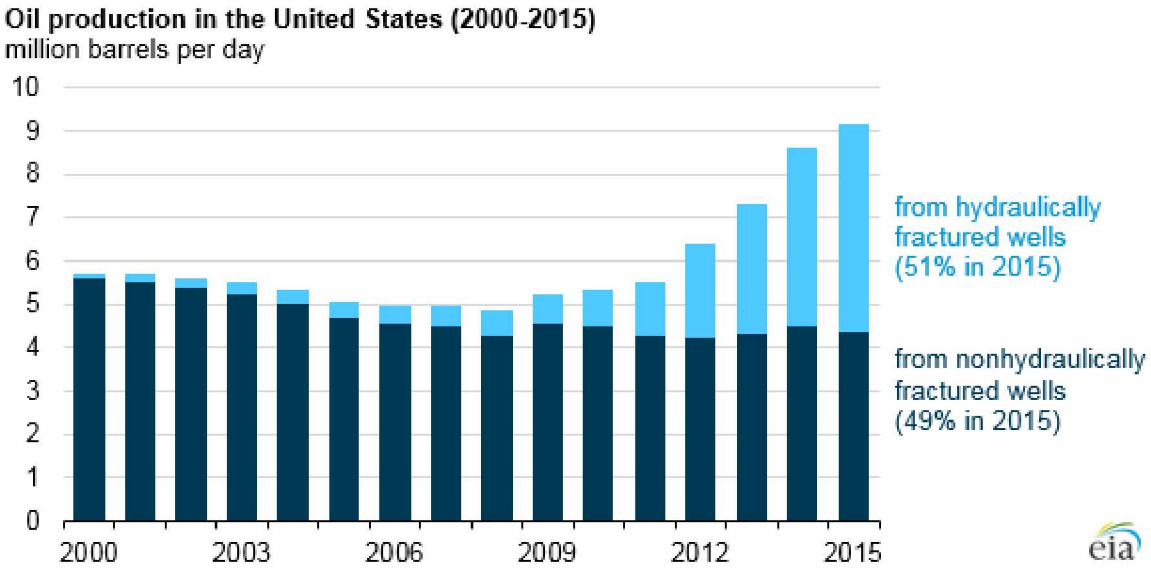

Figure 1-1 Oil production in the United States (5).

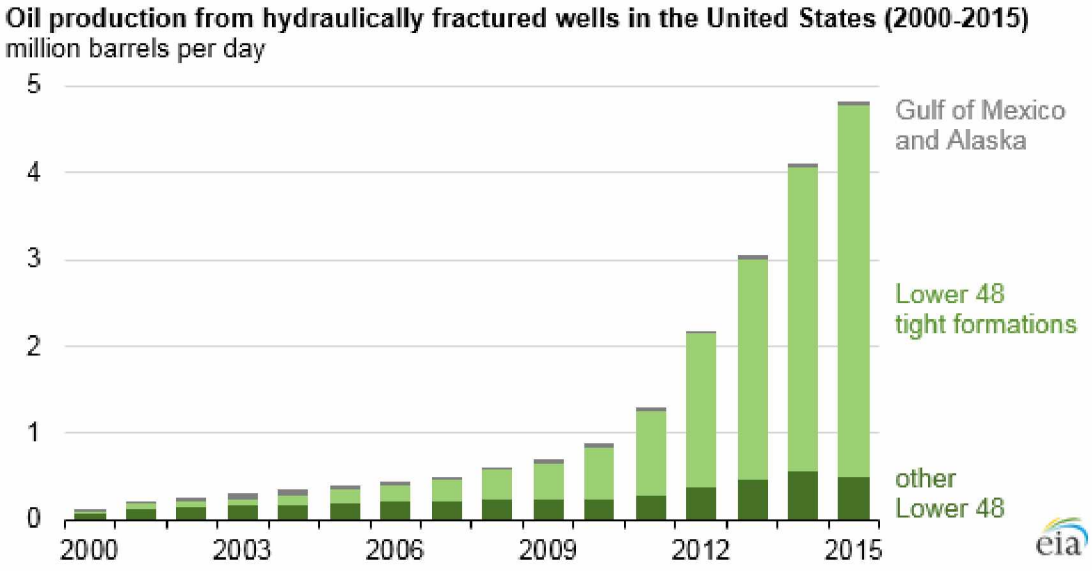

Figure 1-2 Growing trend in application of HF in the U.S. (5).

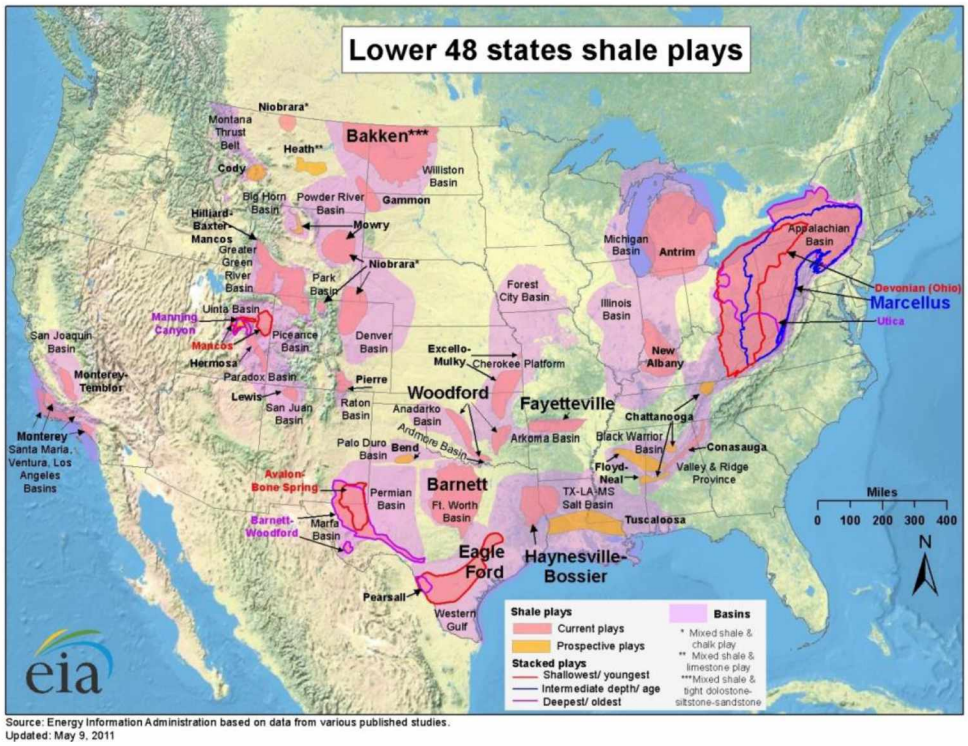

Figure 1-3 Shale formations in lower 48 states (6).

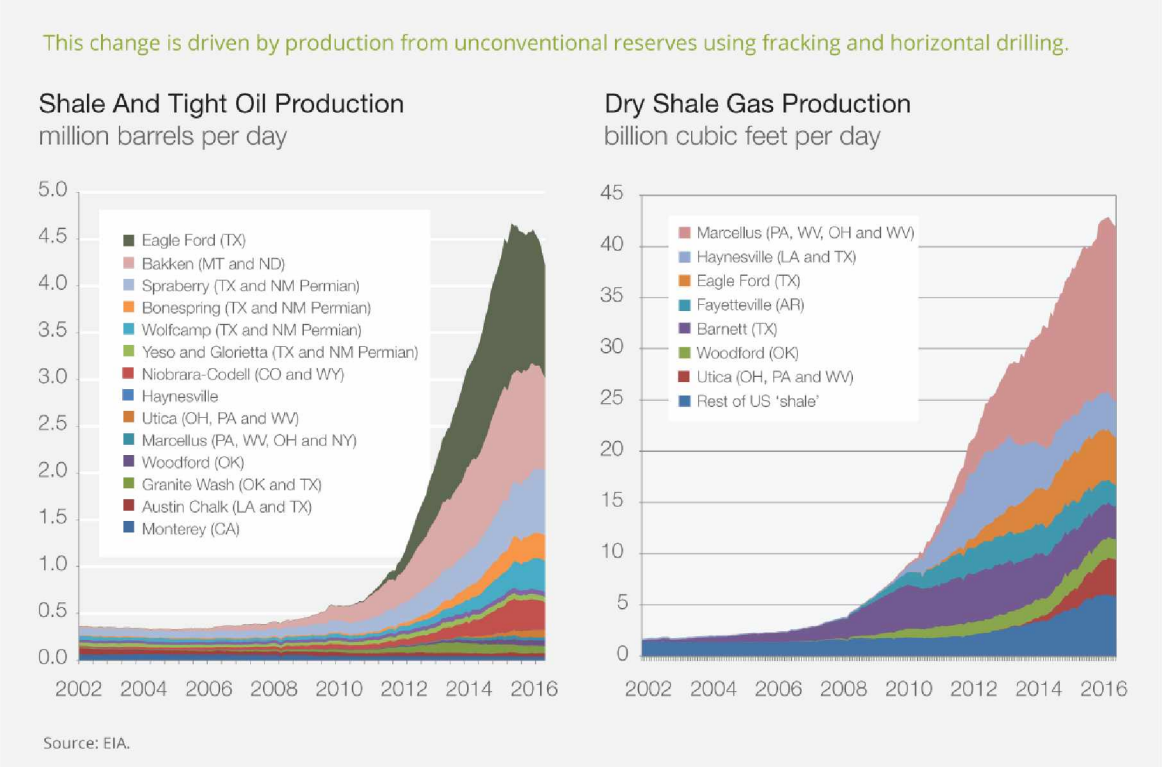

Figure 1-4 Oil and gas production history in billion cubic feet per day (8).

Based on a study by the Energy Information Administration (EIA), in 2015 the U.S. was ranked first in oil and natural gas production in the world due to extensive applications of the HF. Figure 1-5 shows the comparison of oil and gas production between the U.S. and its peers from 2008 to 2015. Figure 1-6 shows how oil imports in the U.S. decreased dramatically during 2007 to 2015. The U.S. is potentially ranked first in producing natural gas in the world (7).

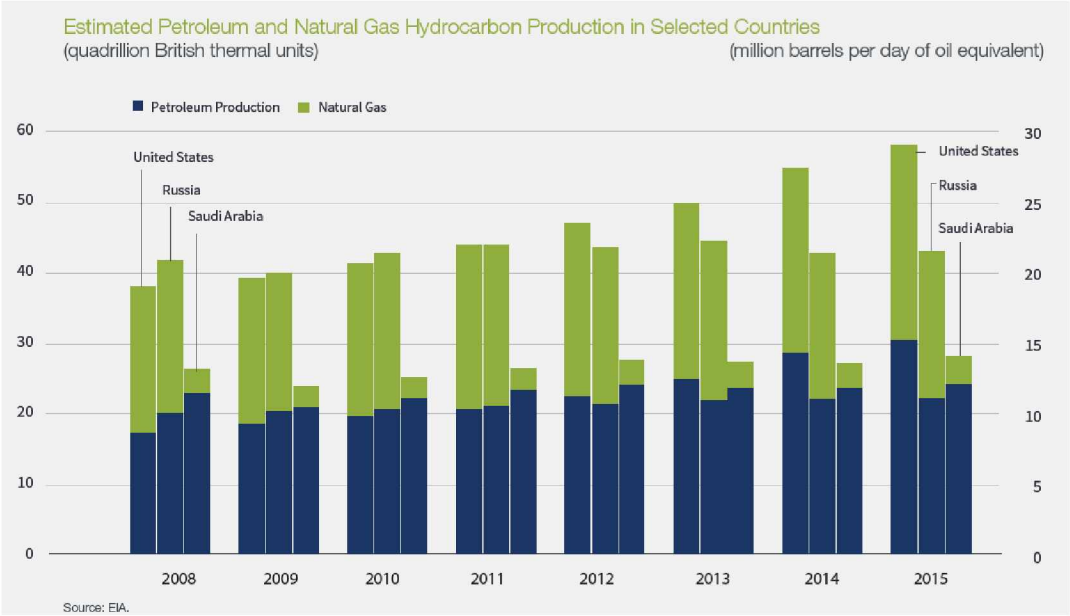

Figure 1-5 Comparison of oil and gas production by U.S., Russia, and Saudi Arabia (2008-2015) (7).

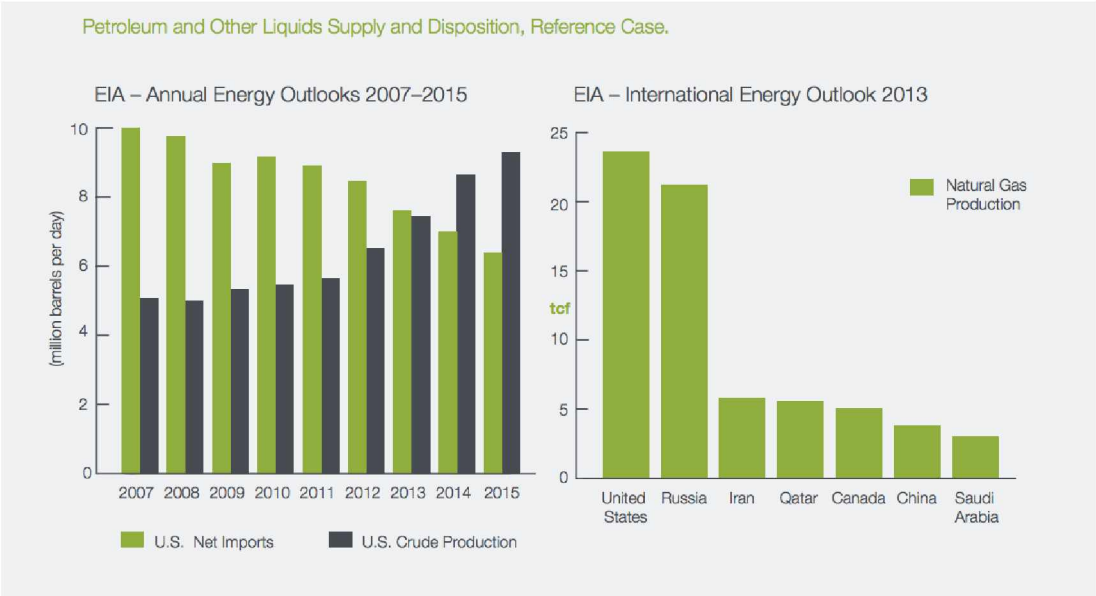

Figure 1-6 Dramatic lowering of oil imports by the U.S. (2008-2015) (7).

1.4 Oil and Gas in Alaska and Applications of HF

Most oil reserves in Alaska are conventional; however, almost all proved unconventional oil reserves are on the North Slope. Based on a U.S. Geological Survey (USGS) report, it is estimated that the North Slope contains up to 2 billion barrels of oil and 80 trillion cubic feet of natural gas in unconventional resources. The Great Bear shale formation south of Prudhoe Bay, is the only major unconventional oil field in Alaska (9). Using the HF technique in these formations can increase the oil and gas production in Alaska.

Figure 1-7 shows the comparison of oil production in Alaska and six of its peers in North America from 2008 to 2013. Oil production in Alaska decreased each year. Unlike Alaska, Alberta, Oklahoma, North Dakota, and Texas experienced a growing trend in oil production over these six years (10).

Figure 1-8 shows Alaska's oil production versus its international peers. Alaska and Australia have the lowest oil production from 2008 to 2013. Except Canada, oil production in other countries shown in the Figure 1-8 have declined each year (10).

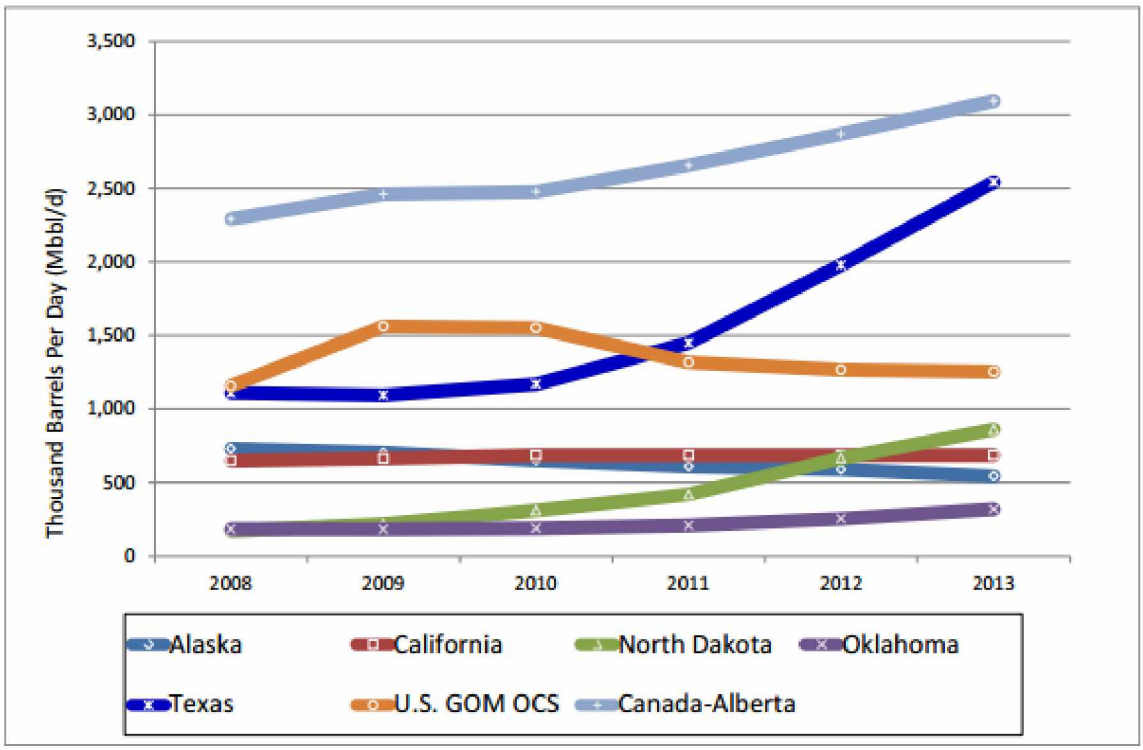

Figure 1-7 Comparison of oil production between Alaska and its North American peers (10).

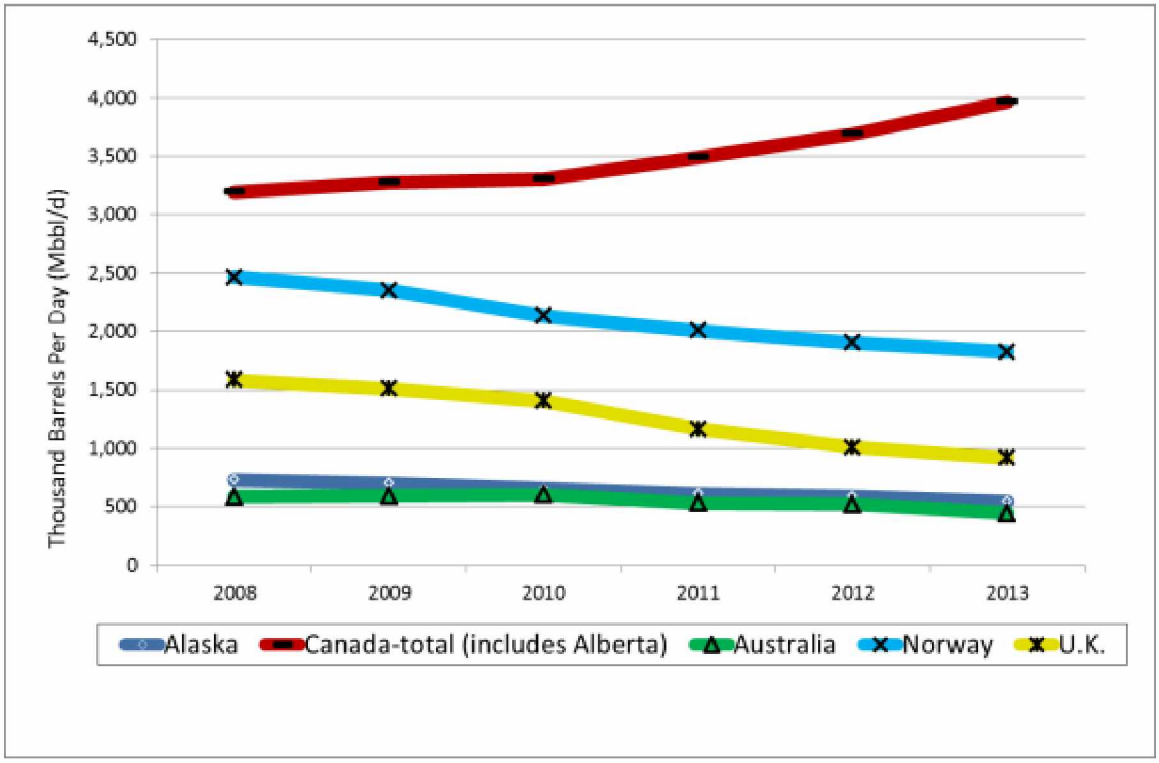

Figure 1-8 Comparison of oil production from Alaska and its international peers (10).

Figure 1-9 shows the history of natural gas production for Alaska and its peers in North America. Based on that, Alaska has almost the lowest gas production among its peers. There is a slightly decreasing trend of production over these six years. Texas is ranked first in gas production among these states because of taking advantage of the HF in tight shale formations (10).

Figure 1-10 shows the comparison of natural gas production from Alaska and its international peers. As can be seen, Alaska has the lowest gas production among its peers. The trend slightly declined over these six years (10).

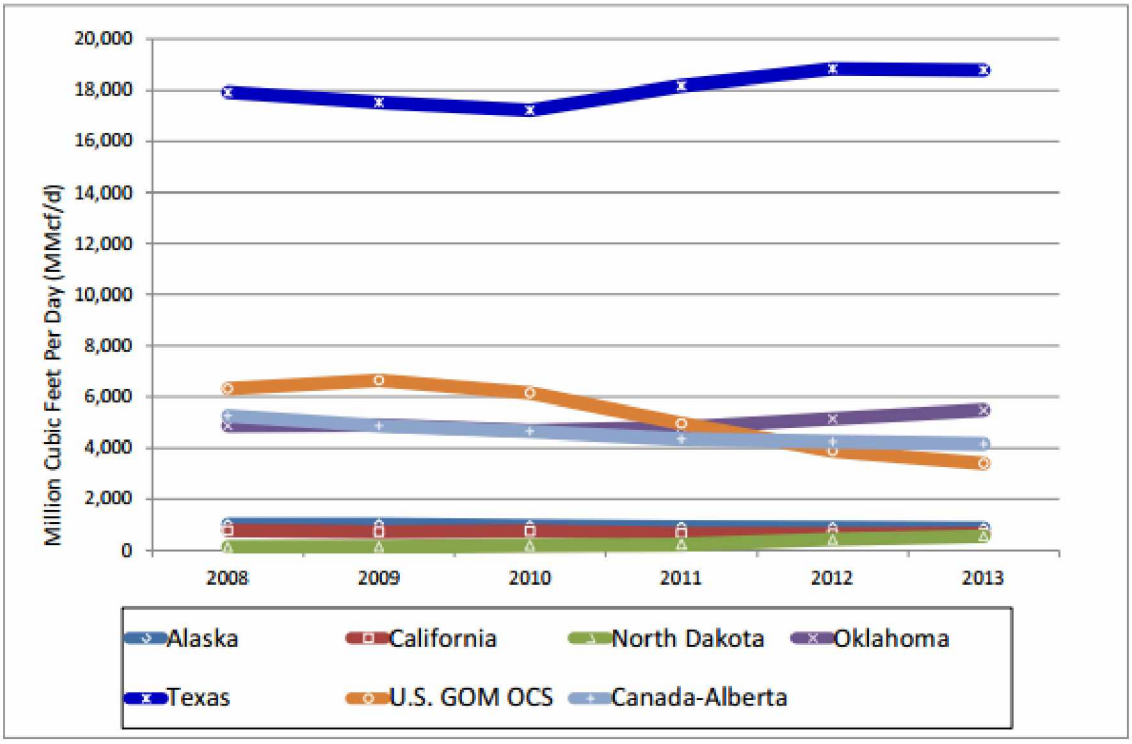

Figure 1-9 Comparison of natural gas production from Alaska and its North American peers (10).

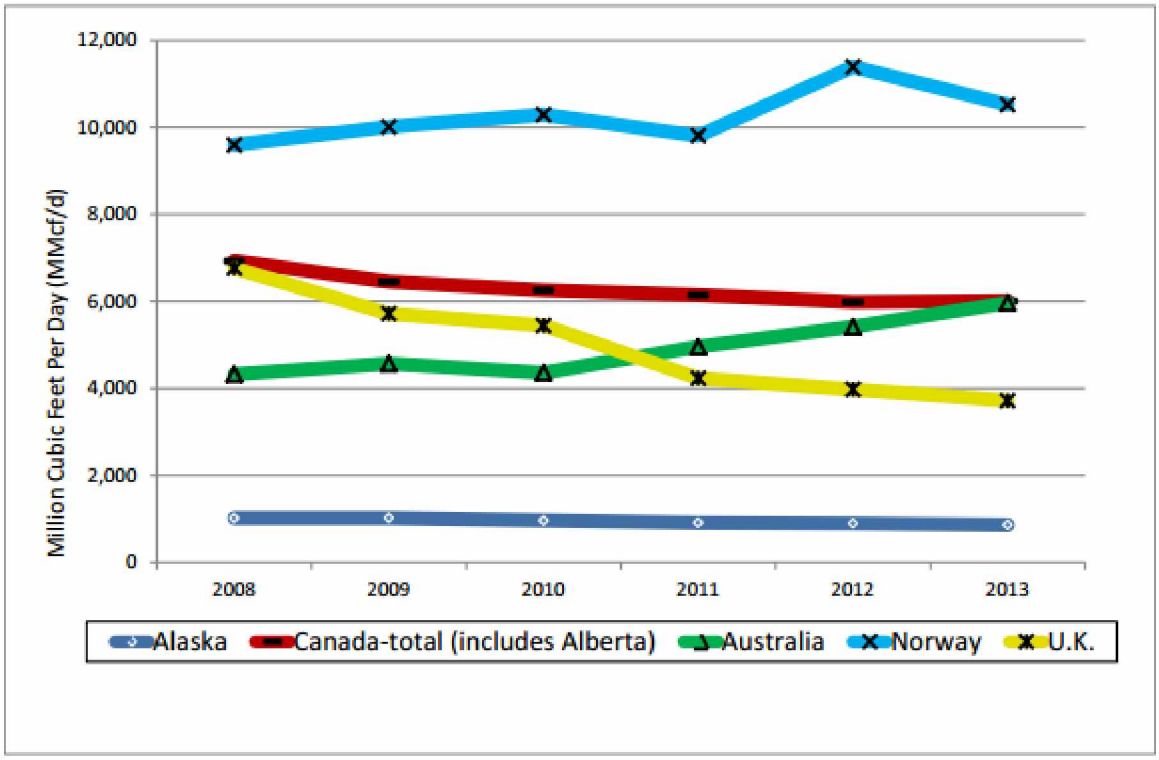

Figure 1-10 Comparison of natural gas production from Alaska and its international peers (10).

Figure 1-11 shows the comparison between proven reserves and undiscovered liquid hydrocarbons in Alaska and its peers in North America. The USGS estimates the potential of undiscovered resources in Alaska is relatively high compared to its peers (10).

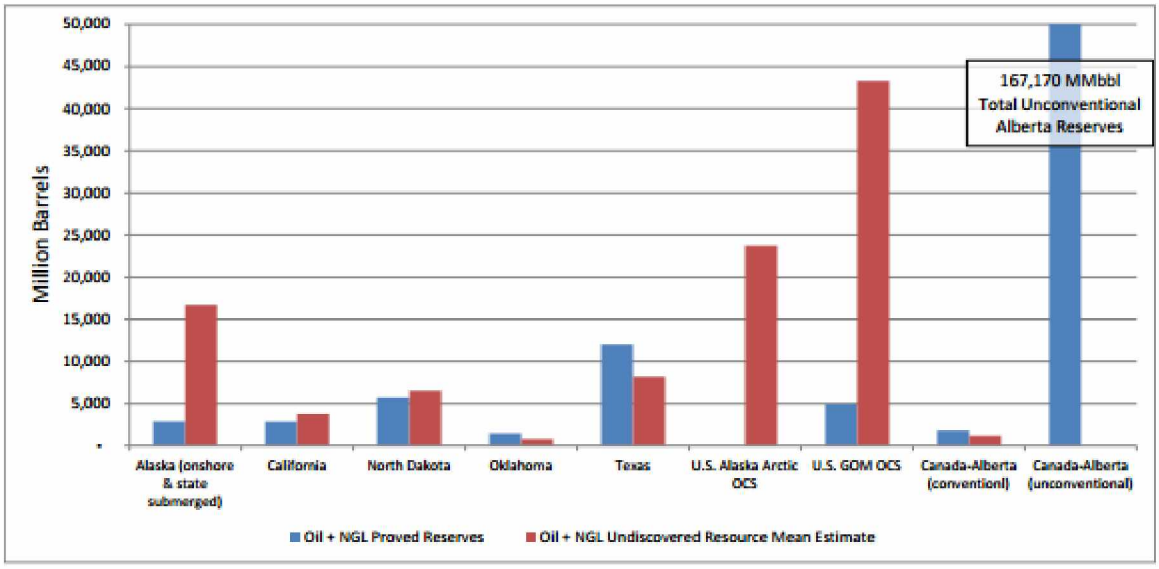

Figure 1-11 Proven reserves versus undiscovered liquid hydrocarbons (10).

Figure 1-12 shows the natural gas comparison of proven reserves and undiscovered resources in Alaska and its peers in North America. It can be stated that after the Gulf of Mexico (GOM), Alaska has the most undiscovered resources in North America. Figure 1-13 shows the comparison of proven reserves and undiscovered resources in Alaska and its international peers. After Norway, Alaska has the most undiscovered resources. It demonstrates the need for exploring these resources in Alaska (10).

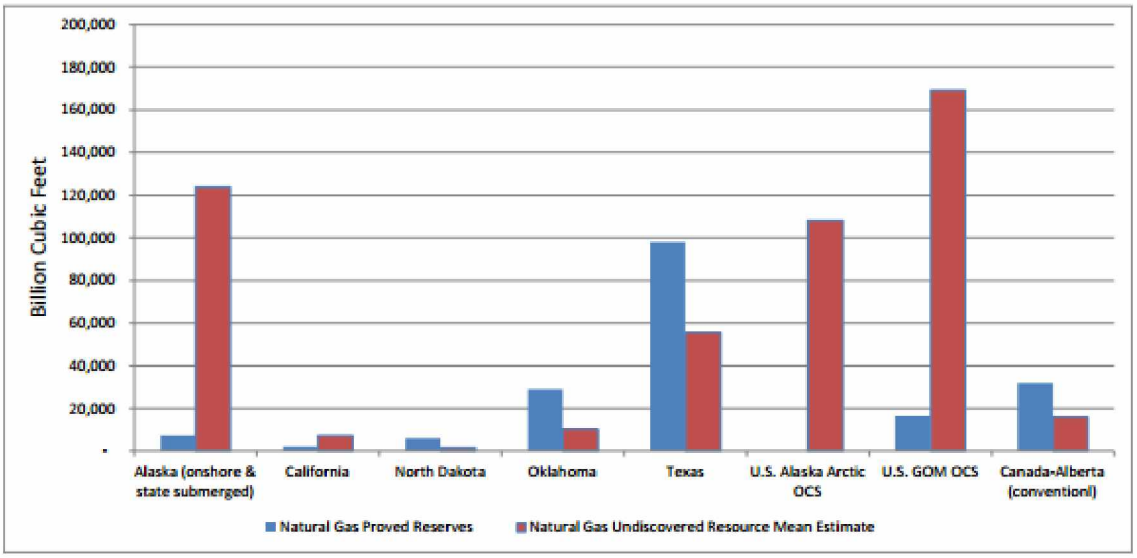

Figure 1-12 Proven reserves and undiscovered natural gas resources in Alaska and its North America peers (10).

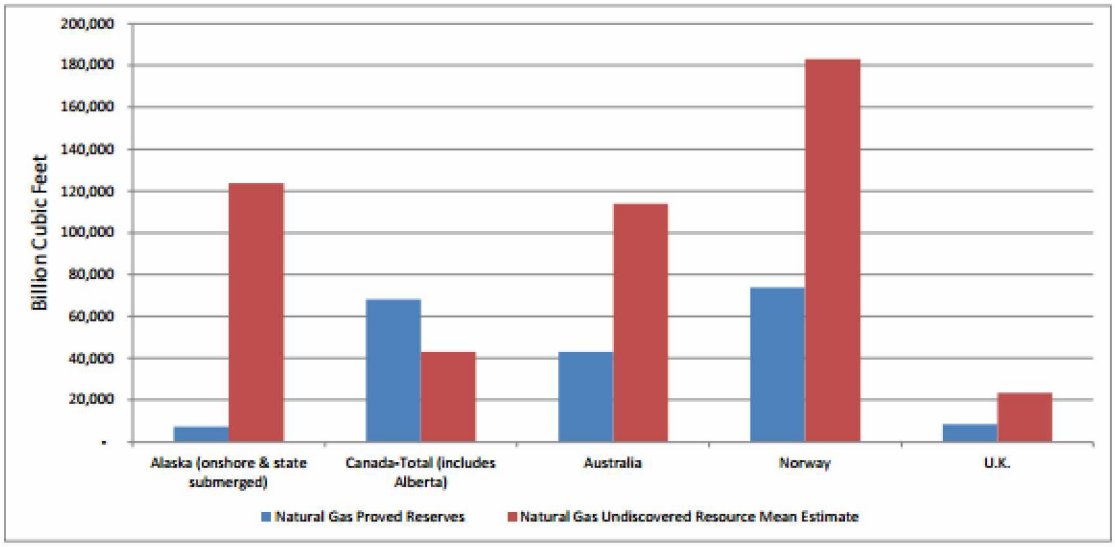

Figure 1-13 Proven reserves and undiscovered natural gas resources in Alaska and its international peers (10).

Based on a 2012 report by the USGS, it is estimated that undiscovered oil and gas from shale formations on the North Slope is almost the same as undiscovered oil and gas from the Eagle Ford shale formation. Figures 1-14 and 1-15 show the comparison of undiscovered oil and gas from several famous shale formations (11).

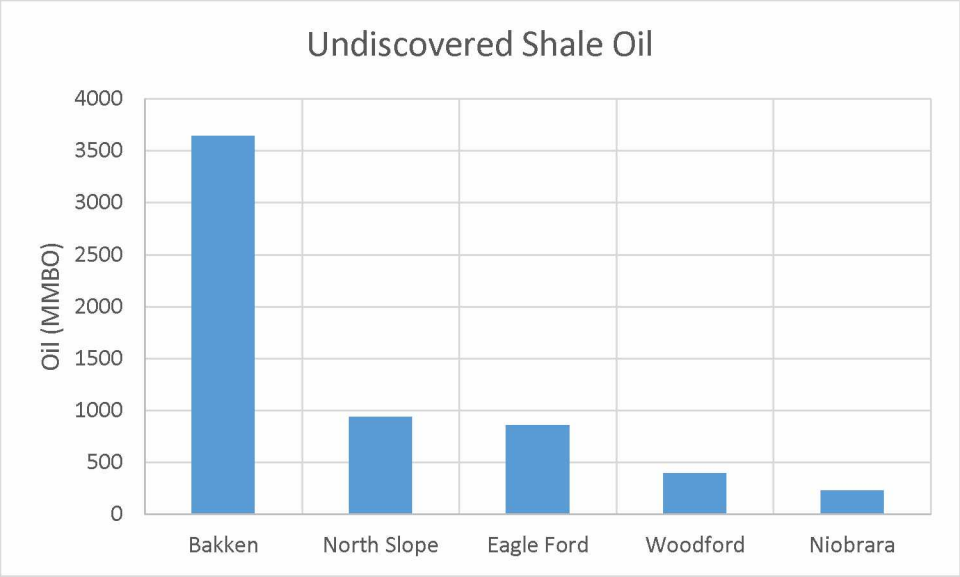

Figure 1-14 Comparison of undiscovered shale oil between famous formations (MMBO stands for Million Barrels of Oil (11).

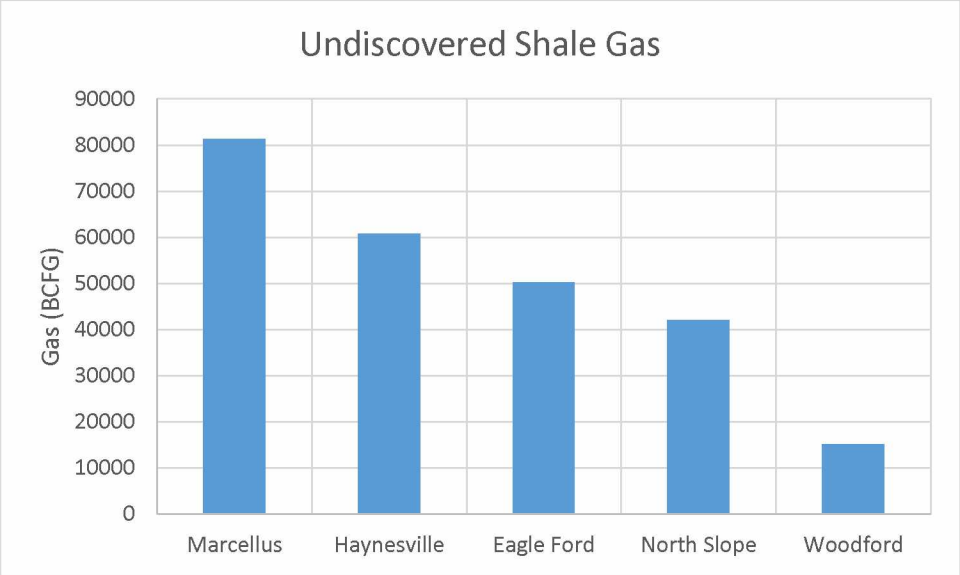

Figure 1-15 Comparison of undiscovered shale gas between famous formations (BCFG stands for Billion Cubic Feet of Gas) (11).

Figures 1-16 to 1-18 show the estimated undiscovered oil, gas, and natural gas liquid from three major shale formations in Alaska, respectively. In 2012, the USGS estimated that the Shublic shale formation has the highest potential among Alaska shale formations (11).

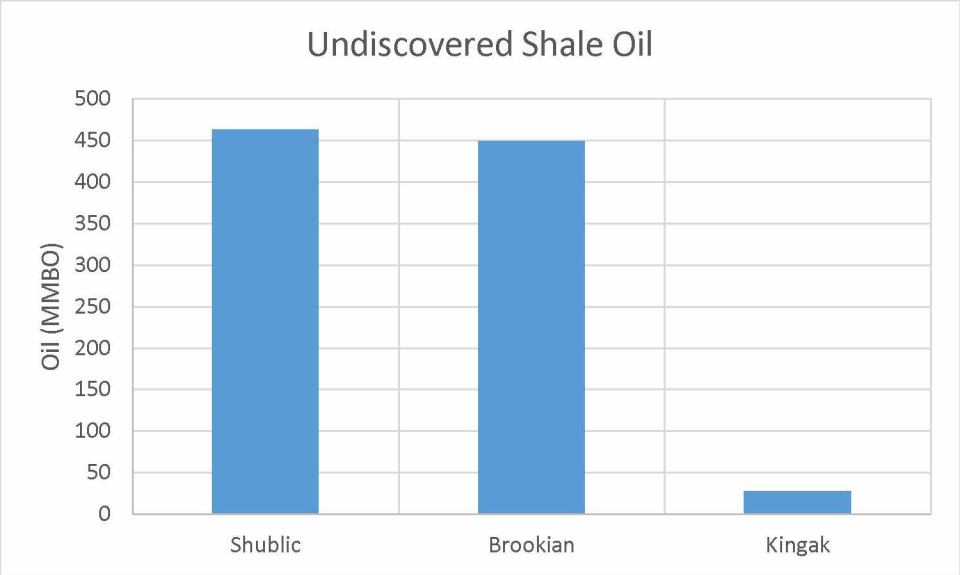

Figure 1-16 Comparison of undiscovered shale oil in Alaska (11).

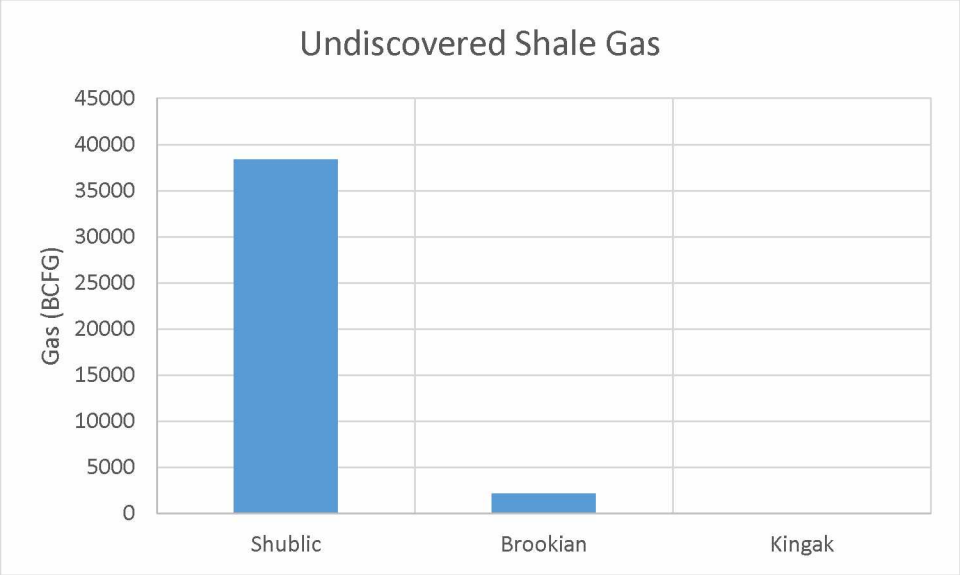

Figure 1-17 Comparison of undiscovered shale gas in Alaska (11).

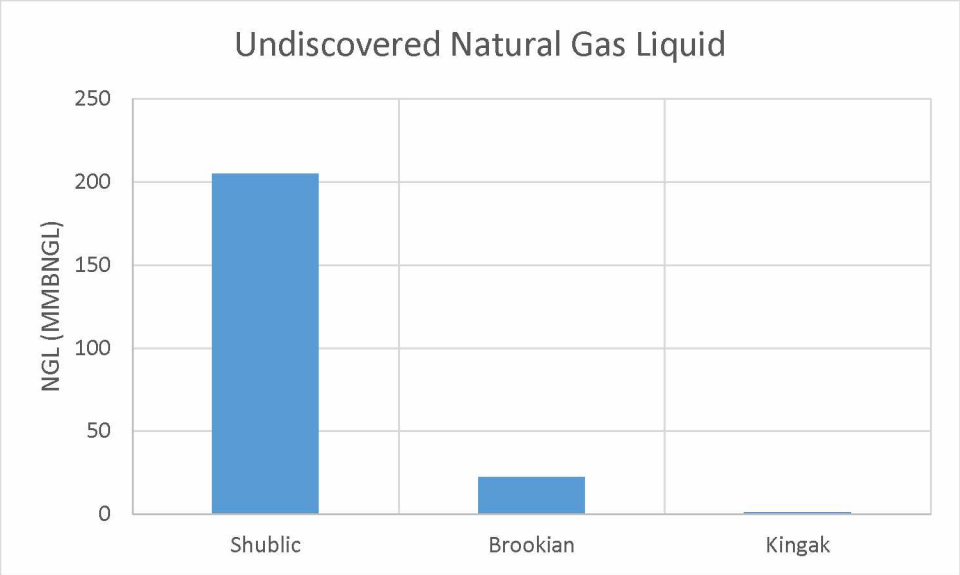

Figure 1-18 Comparison of undiscovered natural gas liquid in Alaska (MMBNGL stands for Million Barrels of Natural Gas Liquids) (11).

1.5 The Need for HF Studies and Simulations

As discussed in previous sections, HF is widely used in the oil and gas industry. There are many parameters that play roles in performing HF in the field. To investigate the effects of different parameters on HF, it is difficult to perform field tests. Thus, it is necessary to use different simulation methods like creating experimental and numerical models.

Based on a 2006 report by the National Science Foundation (NSF), there is enormous interest in simulations in engineering fields. Some reasons for growing interest in simulations are (12):

- Doing simulations is relatively cost effective.
- In many fields like military projects, simulations are much safer than real world experiments.
- Doing the simulation is usually quicker than conducting the real field work.
- Sometimes the results obtained by simulation are more realistic compared to field work.
- In some environmental sensitive projects, conducting simulations is more ethical.

Although many studies have been done in the area of HF, more are still necessary. Laboratory experiments and computer simulations of HF are useful. It is possible to simulate different conditions that a shale formation might feel in the real environment in a cost effective way. By

doing both experimental and numerical simulations, one can double check the findings and obtain reliable results.

1.6 Objectives of the Study

In order to better understand the HF technique better, both laboratory experiments and computer simulations are performed in this research to study the forming and development of HF under various field stress conditions. Therefore, the objective of this research are to:

1) Design and develop an experimental setup for performing HF experiments at a laboratory scale with controllable 3D stress conditions.
2) Conduct laboratory experiments to study the characteristics of HF under various stress conditions.
3) Develop a 3D numerical model and conduct computer simulations of HF in similar conditions as applied in the laboratory experiments. Compare the numerical simulation results with that of the laboratory experiments and further explore the characteristics of HF.

1.7 Outline of Subsequent Chapters

This thesis consists of six chapters. Following the introduction in Chapter One, Chapter Two is a literature review on experimental and numerical simulations of HF by previous researchers.

Chapter Three contains the laboratory tests that were performed on prepared cylindrical and disk specimens. These tests were performed to determine the strength and elastic characteristics of the material used in the subsequent HF experiments.

Chapter Four presents the design and development of laboratory HF experiments as well as the execution of the experiments and analysis of the results. Following thorough descriptions of specimen preparation and components of experimental setup, the procedure of experiment execution is illustrated. The results are presented and analyzed.

Chapter Five details the development of a 3D numerical model with ABAQUS, a commercially available Finite Element Analysis (FEA) software. Computer simulations are shown in the chapter. The results and the comparison with that from the laboratory experiments are discussed.

Chapter Six includes the conclusion of the study and the challenges encountered in both laboratory experiments and computer simulations. Recommendations for improving the setup to perform in further studies are also provided.

CHAPTER 2 LITERATURE REVIEW

HF is usually used to increase the permeability of a tight formation containing hydrocarbons. In this technique, high pressure fluid is pumped into a wellbore to create fractures in the formation. There are small solid particles in the fluid that remain inside fractures and keep them open after removing the fluid from the wellbore. Based on fracture mechanics theory, the hydraulic fracture would propagate along maximum horizontal stress.

HF is currently a hot topic for scientists, researchers, and practitioners in the industry. In this chapter some simulation studies by different researchers are reviewed.

2.1 Concepts of Fracture Mechanics in HF

In 1957, Irwin mentioned that there are three main modes of fracture propagation including: opening, sliding, and tearing. In the opening mode, two faces of the fracture tend to separate from each other due to tensile stress normal to the fracture plane. Hydraulic fractures are usually categorized in this mode. In the sliding mode, because of shear stress that is acting parallel to the plane of the fracture and perpendicular to the fracture front, two faces of the fracture slide over each other in the same plane but in the opposite direction. In the tearing mode, because of shear stress that is acting parallel to the plane of the fracture and parallel to the fracture front, the two faces of the fracture move to the side in opposite directions. These three modes of fracture extension can be seen in Figure 2-1 (13).

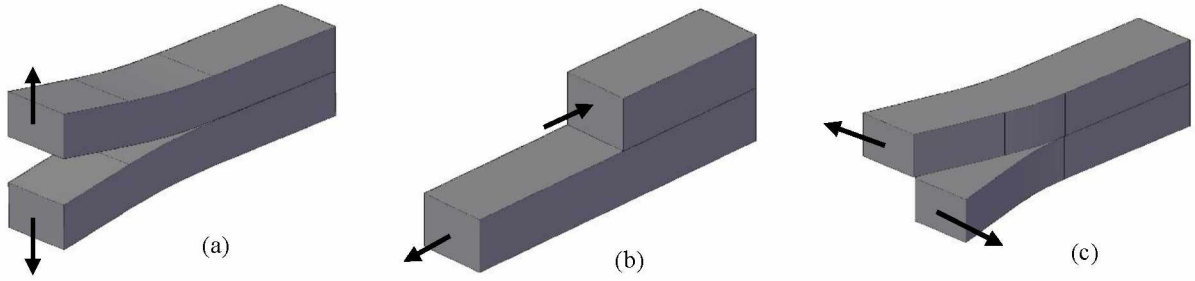

Figure 2-1. Basic fracturing modes, (a) opening, (b) sliding, (c) tearing by Irwin, 1957.

There are three more complex fracture modes. Mixed-mode fractures occur through a combination of tensile and shear forces. In fracture branching, the fracture occurs when it propagates along more than one path, where these paths have connection to each other. Finally, in multiple

fracturing, separate fractures are created at the wellbore and may grow out of each other's influence zone (14).

Sneddon and Sack (1946) assumed a hydraulic fracture process performed on an infinite elastic medium, where σ_v is the vertical stress, and σ_H and σ_h are the maximum and minimum horizontal stresses, respectively. All of these stresses are compressive. In the horizontal plane, σ_v is the stress component resisting a fracture from opening. Therefore, for keeping a hydraulic fracture open, the fracture fluid pressure should be at least equal to σ_v. Thus, to propagate a hydraulic fracture, the fluid pressure has to be larger than σ_v. The hydraulic fracture propagates in the path of least resistance. In an isotropic, homogeneous, elastic media, the direction of the growth path is perpendicular to the smallest principal stress. Sneddon and Sack found that the pressure of fluid needed for extending the fracture depends on the shape of it. Based on their studies, a penny-shaped crack needs the highest fluid pressure to grow. On the other hand, a Griffith crack requires the least fluid pressure to propagate. They presented Equations 2-1 and 2-2 to explain the fluid pressure needed for each type of fracture growth (15; 16):

$$P = \sigma_3 + \sqrt{\frac{\pi E \gamma}{2R(1-\nu^2)}} \ (\text{Penny} - \text{shaped crack}) \tag{2-1}$$

$$P = \sigma_3 + \sqrt{\frac{2E\gamma}{\pi l(1-\nu^2)}} \ (\text{Griffith crack}) \tag{2-2}$$

where P is the fluid pressure, σ_3 is the least principal stress, E is Young's modulus, ν is Poisson's ratio, R denotes the radius of the penny-shaped crack, l is the length of the Griffith crack, and γ is the specific energy of the material. From these equations, it can be concluded that regardless of the shape of fracture, as the hydraulic fracture grows larger, less fluid pressure is needed for its propagation.

Daneshy (2003) mentioned a new concept in fracturing, explaining that hydraulic fracture propagates in the local path of least resistance, not the global path. The conditions at the tip of the crack control the path of fracture propagation. Because of this, there is branching and off-balance fracture growth in many cases (14).

2.2 Experimental Modeling

Many people have tried to build physical models to study the effects of different parameters on the HF technique. Some of these models are discussed in this section.

Lamont and Jessen in 1963 performed the first laboratory HF experiments on cement blocks and natural rocks. Dimensions of blocks were 1.5×3.5×(4 to 8) in. First, a slot was created at the end face of each block along the longitudinal axis. Then the slot was filled with plastic aluminum. A borehole with 3/8 in. diameter was drilled at the center of the slot in the longitudinal axis (Figure 2-2) (17).

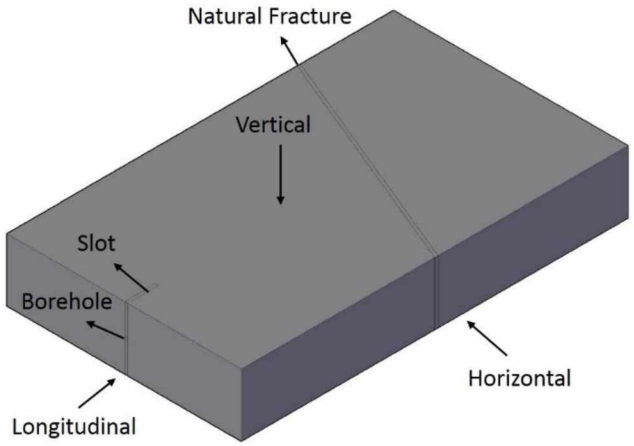

Figure 2-2 Sketch of designed block by Lamont & Jessen (1963).

For simulating the stress field, triaxial loading equipment, which uses mechanical loading and a combination of mechanical and hydraulic loading, was used for applying stresses on block samples. A manual hydraulic pump was used for injecting the fracturing fluid (i.e., water) (17).

Based on the experimental results, Lamont and Jessen stated that hydraulic fractures crossed the natural fractures at all different angles of approach. It was found that when a hydraulic fracture was approaching the interface, it reoriented and crossed the pre-existing fracture at right angles; this is consistent with theory that the path of a growing hydraulic fracture should be perpendicular to the least stress orientation. Also, it was observed that the hydraulic fracture departed from the interface, at right angles from a natural fracture. Another observation was regarding how a hydraulic fracture separates from an existing fracture. Tests on block samples indicated that the

location of this point is random and it is not related to the stress concentration. They mentioned that the offset between the locations of the entry and exit points are mainly due to small weakness planes in the rocks (17).

In 1974, Daneshy conducted some experiments and found that hydraulic fractures propagate through existing flaws in rocks or follow the path perpendicular to the least stress. He categorized material flaws into three groups based on their size: large (greater than several feet), medium (less than several feet), and small (less than several inches). Each discontinuity can be open or closed. Daneshy reported that at the field scale, effects of small and medium flaws are limited to local change in fracture growth (18).

Daneshy (1978) conducted some laboratory experiments to study the effects of different layers on hydraulic fracture growth. A block of a rock with dimensions of 6×12×2 in. was placed between two blocks of another rock with dimensions of 6×12×1 in. All faces of each block were ground and then cemented to each other. A borehole with 1 in. diameter and 4 in. length was drilled so that it extended through all three layers. The entire borehole was cased except for a 1 in. open-hole section at the center of the borehole to ensure that the fracture initiation in the center block. Different combinations of layers using various rocks were examined. It was found that when there was not any restriction for fractures to propagate, the fluid pressure decreased. In the case of different layers, however, when the hydraulic fracture reached the interface, the pressure of the fracturing fluid increased to cross the obstacle. It seemed that the strength of the interface is more important than the rock properties for propagating the hydraulic fracture from one layer to another layer. It showed that weak interfaces arrested fracture growth, while good bonded interfaces allowed fractures to cross them and propagate in the adjacent layer. Figure 2-3 shows the experimental setup used in this study. Load was applied on the sample only in one direction (19).

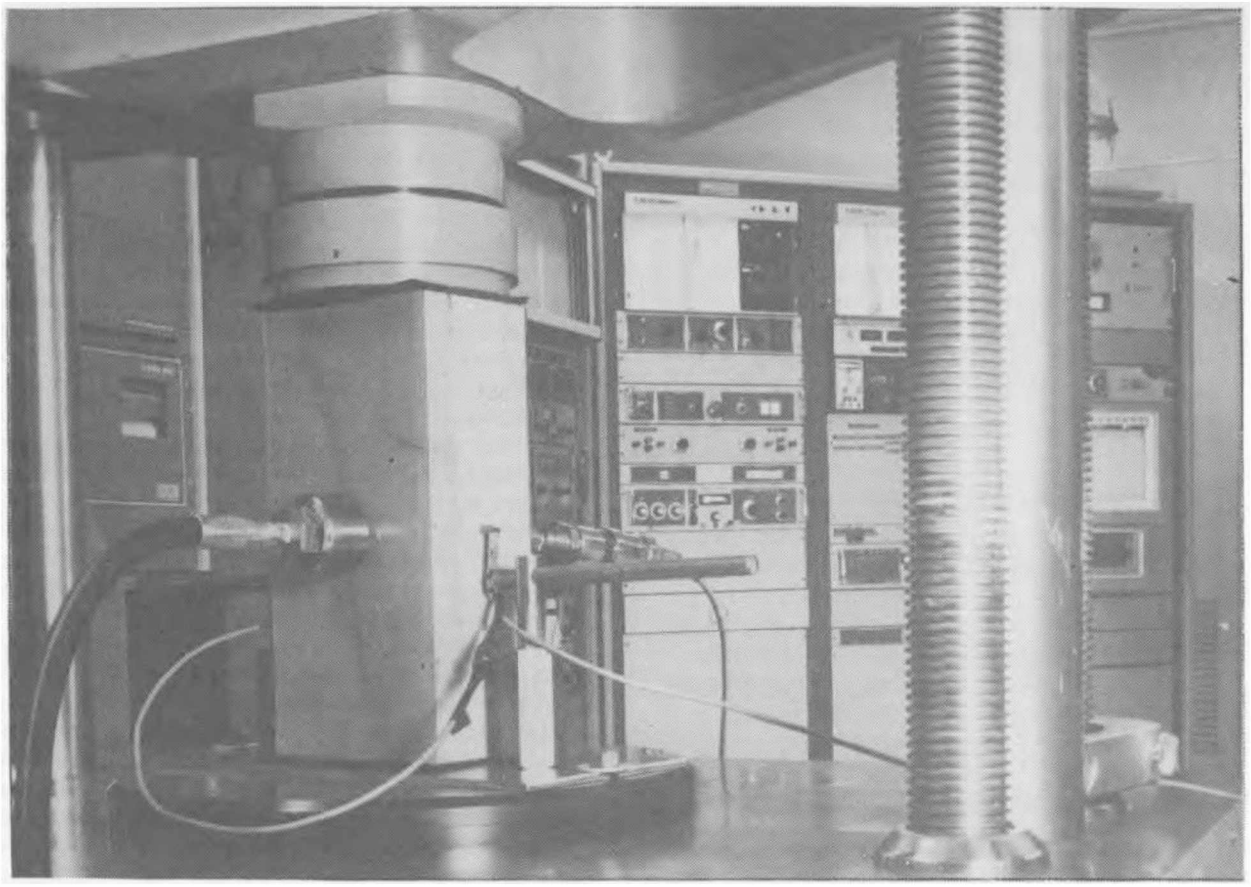

Figure 2-3 Experimental setup by Daneshy (19).

In order to study the effects of existing interfaces on hydraulic fracture propagation, Anderson, designed and performed some laboratory experiments on Indiana limestone and Nugget sandstone. The limestone was a homogeneous and isotropic rock and the sandstone had low porosity. Dimensions of block samples were varied from 2 to 4 in. on each side (20).

Medium-heavy oil (viscosity - 300 cp) was injected through a steel tube (0.25 in. diameter) which was bonded with epoxy to a 0.28 in. diameter borehole. There was a 0.5 in. long open-hole section at the bottom of the borehole, near the center of the block. After filling the borehole with oil, the average rate of pressurization of the fluid using a pressure intensifier was about 13.8 MPa/sec. Monitoring and recording the pressure of the oil were done using a pressure transducer (20).

At least two blocks, one of them containing the borehole and injection tube, were placed between platens of a 100 ton laboratory press. The interface surfaces were parallel to the platens. In addition to grinding the outer block faces that were in contact with the platens of the machine press, thin

(0.5-mm) Teflon sheets between the outer block faces and platens were used to reduce the friction and ensure the uniform distribution of load on the blocks. In this experiment, the block was under pressure just in one direction and other sides were unconfined (Figure 2-4) (20).

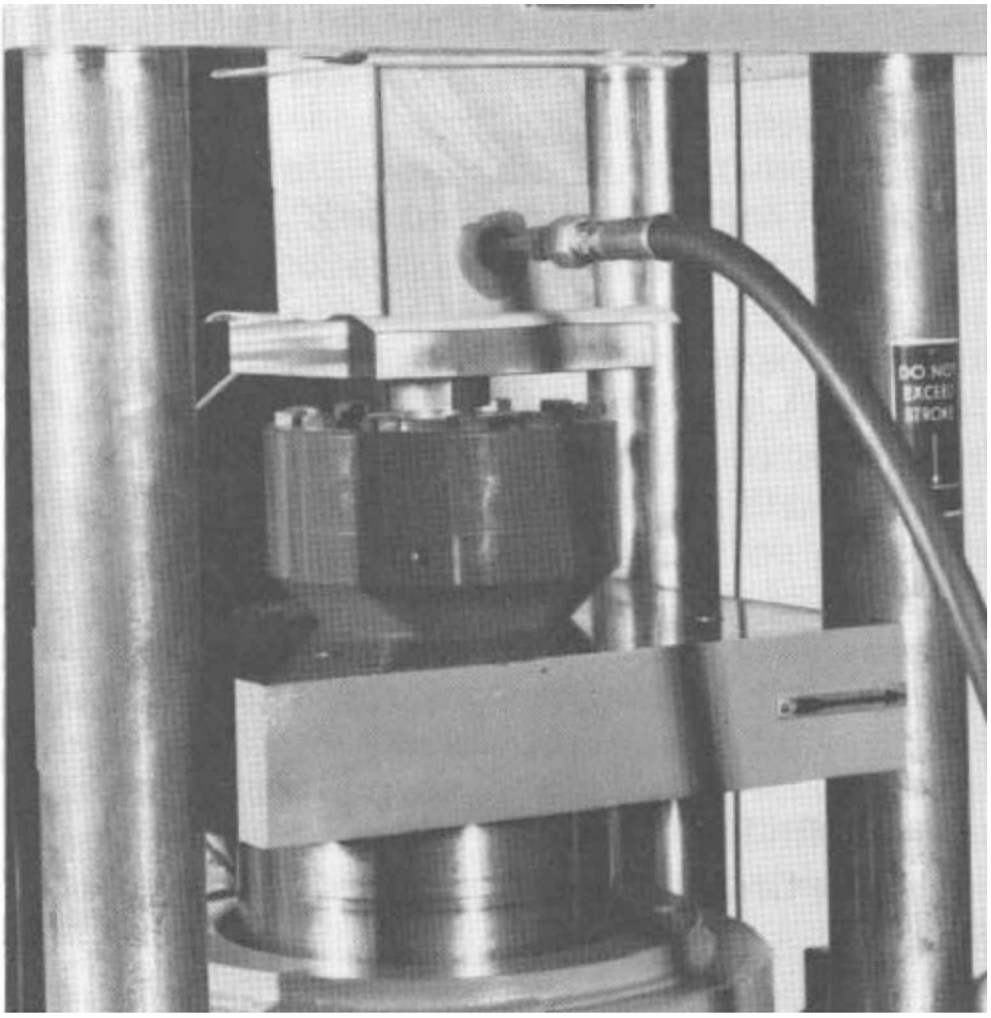

Figure 2-4 Experimental setup by Anderson (20).

The purpose of this study was to determine at which normal stress the hydraulic driven fracture that occurred in the block containing the tube crosses the unbonded interface and penetrates the adjacent block. This normal stress is called the threshold stress (σ_T). The value of the threshold stress was dependent on the interface preparation. Five methods of preparation were used for the interface between two blocks to produce different coefficients of friction. These were smooth dry, roughened dry, and three smooth dry surfaces lubricated with different fluids (water, C-100, and 630-AA) (20).

From the results, it was determined that when the interface was lubricated, in order for the hydraulic fracture to cross the interface and propagate into another block of the same material, the threshold normal stress should be increased. So it can be stated that frictional properties of discontinuities in shallow formations have a critical effect on hydraulic fracture growth (20).

Blanton in 1982, used a 500,000-lb triaxial load frame for loading the blocks of hydrostone and Devonian shale with dimensions of 12×12×15 in. The borehole diameter and length were 1/8 in. and 8 in., respectively. A 1 in. open-hole section in the borehole was maintained using steel tubing. In this study, two pairs of flatjacks were used for simulating the horizontal stresses on the block. Flatjacks were pressurized using a hydraulic pump. Figure 2-5 shows the experimental setup by Blanton (21).

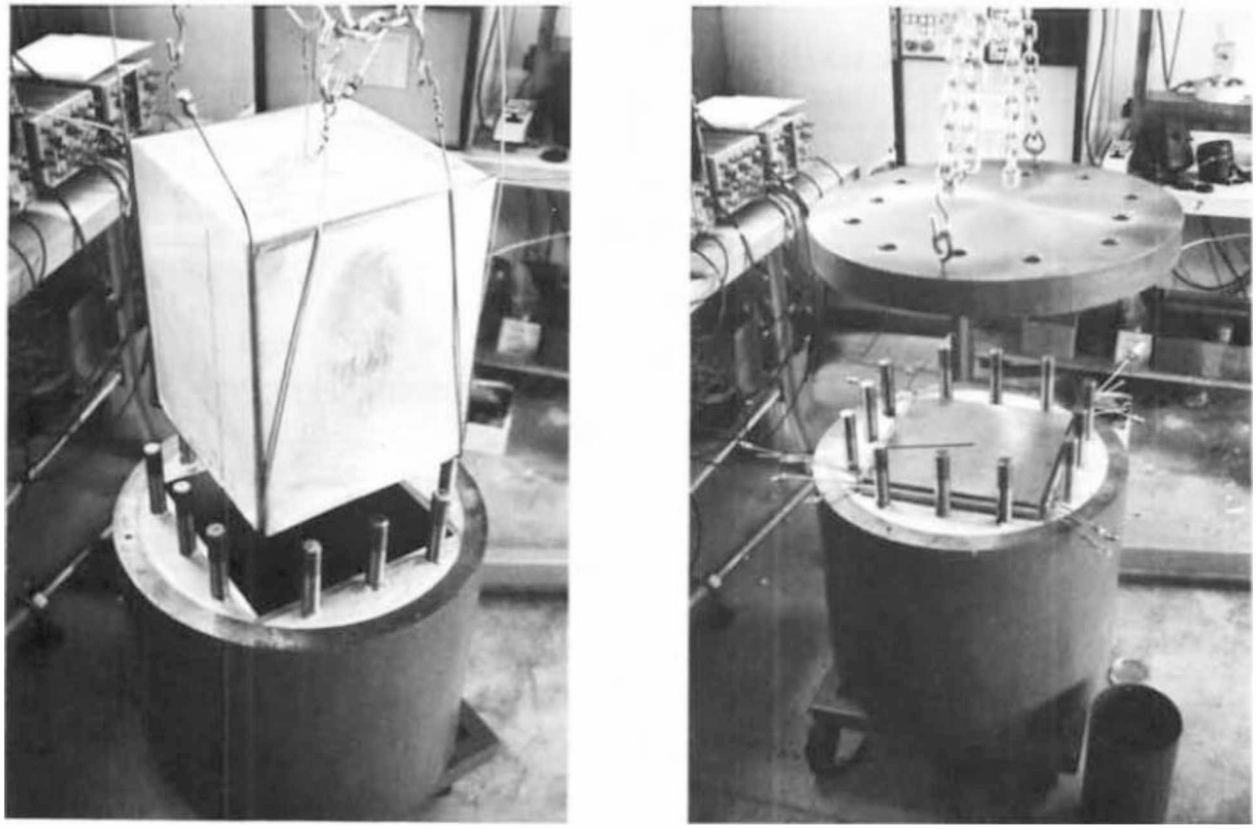

Figure 2-5 Experimental setup by Blanton (21).

From the results obtained from the test on the hydrostone block, it can be stated that hydraulic fractures crossed natural fractures at high differential stresses and high angles of approach. Opening pre-existing fractures by hydraulic fractures occurred at low differential stresses and low

angles of approach. Arresting hydraulic fractures by natural fractures occurred at intermediate values. At low angles of approach and low differential horizontal stress, the hydraulic fracture opened the pre-existing fracture and propagated across it (21).

Ahmed et al. conducted five different laboratory experiments on grout blocks with dimensions of 3.3×3.3×3.3 ft., to study the effects of distribution of stresses and perforation locations on fracture geometry. For loading the blocks, they used a polyaxial loading machine (Figure 2-6) (22).

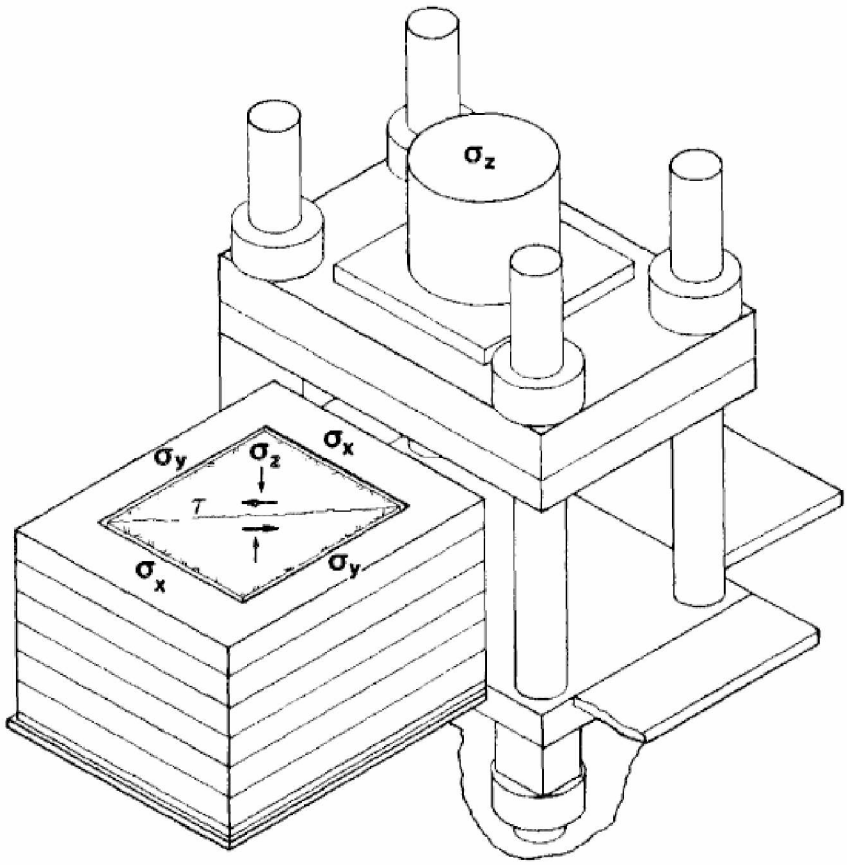

Figure 2-6 A sketch of experimental setup by Ahmed et al. (22).

For simulating the horizontal stresses, three flatjacks were used on each side of the block. Thus, a total of 12 flatjacks were placed and bonded around the sides of the blocks. Using this configuration, three different stresses could be applied in each horizontal direction. In fact, there were three layers in each block in which the stress distribution in each layer could be different from the others (Fig. 2-7). Table 2-1 summarizes the stress conditions of each test (22).

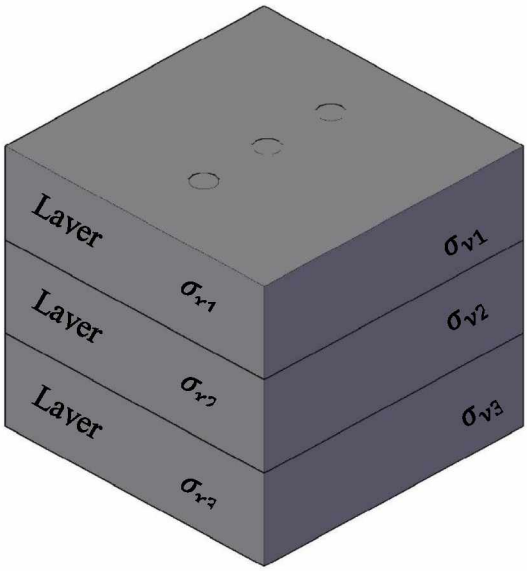

Figure 2-7 Three different stresses were applied in each horizontal direction by Ahmed et al.

In the first two tests, the vertical stress was 2000 psi. In order to study the effects of different horizontal stress distribution, two experiments with different combinations of stresses were performed on two blocks. It was observed that hydraulic fractures moved and propagated to the layer with lower stresses. In these two tests, the perforated part was placed in the middle of each block (in layer 2). In test 1, the hydraulic fractures did not propagate much to layers 1 and 3; but in test 2, since layer 3 had low stresses compared to layer 2, fractures propagated very well in layer 3 (22).

Table 2-1 Experimental conditions by Ahmed et al. (1983).

Test Number	Vertical Stress	Horizontal Stress in X Direction			Horizontal Stress in Y Direction		
	$\sigma_z\ (psi)$	$\sigma_{x_1}(psi)$	$\sigma_{x_2}(psi)$	$\sigma_{x_3}(psi)$	$\sigma_{y_1}(psi)$	$\sigma_{y_2}(psi)$	$\sigma_{y_3}(psi)$
1	2000	1200	700	1200	1900	1600	1900
2	2000	1900	900	900	1200	200	200
3	2300	500	1000	1500	1200	1700	2200
4	2300	500	1000	1500	1200	1700	2200
5	2300	500	1000	1500	1200	1700	2200

Three other tests were conducted to analyze the effects of location of perforation on the fracture propagation path. The purpose was to find the best place for the perforation section to have the largest area of fracture propagation in the middle layer. In these three tests, the vertical stress was 2300 psi and the minimum and maximum horizontal stresses in each layers were $\sigma_{x1} = 500$, $\sigma_{y1} = 1200$, $\sigma_{x2} = 1000$, $\sigma_{y2} = 1700$, $\sigma_{x3} = 1500$, and $\sigma_{y3} = 2200$. When half of the 6 in. perforation section was in the upper layer and half of it was in the middle layer, they observed that 35% of the created fracture area was in the upper layer, 38% of it was in the middle layer and 27% was in the lower layer. Other results are summarized in Table 2-2.

Table 2-2. Best location for perforation due to different horizontal stresses by Ahmed et al. (1983).

Test Number	Location of perforation	Fractured Area (%)		
		upper	middle	lower
3	Half in upper, half in middle	35	38	27
4	Whole in middle	33	48	19
5	Half in middle, half in lower	6	80	14

From the results, it can be concluded that when half of the perforation section was in the middle layer and half of it was in the lower layer, the maximum fracture area occurred in the target layer. From all of the experiments, they stated that hydraulic fracture tends to propagate from high stress regions to lower stress zones (22).

In 1984, Tuefel and Clark performed hydraulic fracture experiments on a block sample consisting of three layers with dimensions of 9.5×7.9×7.9 in. (24×20×20 cm). The length of each layer was 3.1 in. (8 cm). The diameter of the borehole at the center of the block was 0.27 in. (0.68 cm). A solid steel packer with diameter of 0.26 in. (0.65 cm) and length of 4.3 in. (11 cm) was cemented using epoxy at the end of the borehole. A hollow steel packer with the same dimensions was used at the other end of the borehole. An injection hole with diameter of 0.09 in. (0.22 cm) was located at the center of the hollow packer. With these arrangements, there was a 0.8 in. (2 cm) open-hole section in the center of the middle layer. Fracturing fluid (40 weight oil) was injected into the

open-hole section. In this study, they applied load on the sample only in the vertical direction and there was no confining stress (23).

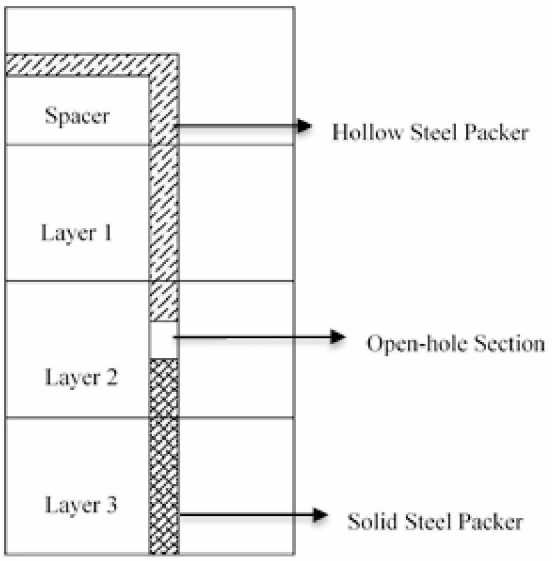

Figure 2-8 Schematic of specimen designed by Tuefel and Clark (1984).

When all the layers were from one type of rock, there was a direct relation between tensile strength of rock and the applied normal stress for fractures propagating fracture across the interface. As the surface roughness of the interface (the shear strength of the interfacial) increased, the applied normal stress (required for fracture growth across the interface of the layer) decreased (23).

In 1984, Shaffer et al. conducted sixteen experiments on a physical model containing Hydrostone cement and a mixture of hydrostone (70%) and sand (30%) with dimensions of 14×14×14 in. The borehole diameter was 0.2 in (0.5 cm) and the length was 0.6 in (1.5 cm). Distance between the borehole and interface was about 1.5 in (3.8 cm). Medium weight oil was used as the injecting fluid. In low differential stress, the hydraulic fracture was arrested by the interface. In most other cases, the hydraulic fracture crossed the interface. In these tests, the horizontal stress was applied in one direction, meaning one side of the block was free during the experiment. Figure 2-9 shows the schematic of the experimental setup (24).

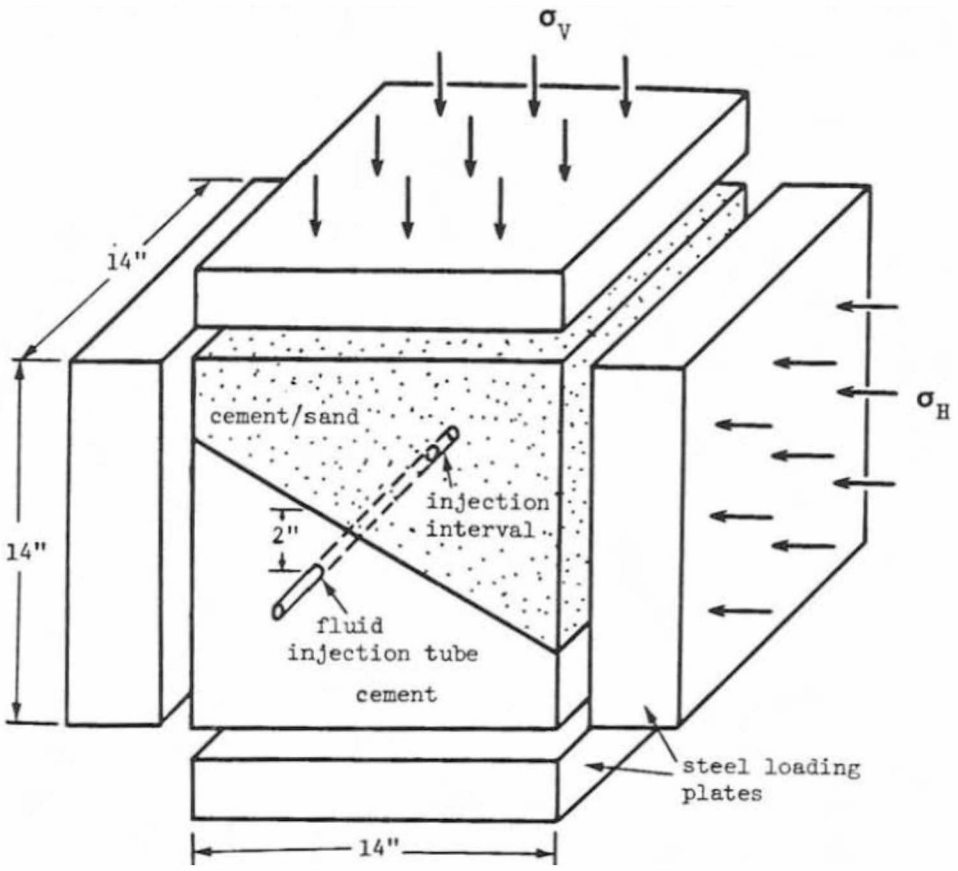

Figure 2-9 Schematic of experimental setup by Shafter et al. (1984).

In 1986, Blanton designed some laboratory experiments on Hydrostone blocks with dimensions of 12×12×15 in. Differential stress between maximum and minimum horizontal stress, $(\sigma_H - \sigma_h)$, and angle of approach or the angle between the existing fractures and the maximum horizontal stress, (α), were two parameters that changed in the experiments (25).

From the experimental results, it can be suggested that crossing occurred at high angles of approach and high differential stresses, while opening occurred at low differential stresses and low angles. It was found that material properties played the main role in controlling the fracture propagation path at low differential stresses. Because of this, both opening and crossing occurred at low differential stresses (25).

Warpinski and Teufel in 1987 reported some observations in mineback experiments at the U.S. DOE Nevada Test Site. Based on their observations, geological discontinuities, including joints, faults, and bedding planes, have some effect on hydraulic fracture growth. Some of them diverged

when intersected with joints; some terminated when crossing the faults. In the intersection of hydraulic fractures with bedding planes, it was observed that the fractures propagated to 1 to 2 in. across the planes of discontinuities (26).

In the next phase, they conducted some laboratory experiments on Coconino sandstone specimens with dimensions of 8×6×6 in. (20.3×15.24×15.24 cm). For simulating the in situ stress conditions, a triaxial load frame was used. Flatjacks were used for producing horizontal stresses (26).

They concluded that at high horizontal differential stress and angles of approach between hydraulic fracture and natural fracture in the block equal or greater than 60°, the hydraulic fracture crossed the natural one. The same occurred when the horizontal differential stress was medium and the angle of approach was 90°. The hydraulic fracture was arrested by the pre-existing fracture when the differential stress was high and the angle of approach was 30°. In other combinations of horizontal differential stress and angle of approach, the hydraulic fractures diverted along the joints and opened them (26).

Blair et al. in 1989 performed some laboratory experiments on three blocks of gypsum cement. They used sandstone lenses (Tablets) as the interface in designing the blocks. The dimensions of the blocks were 11.5×11.5×18 in. (29.2×29.2×45.7 cm) and were tested under triaxial loading conditions. For applying confining pressure to the blocks, flatjacks were used. In this study, they used wire mesh embedded in the gypsum block, to track the path of fracture growth after injecting the fluid into the borehole. The wire mesh was located close to the top and bottom of the Gypsum block. In this series of experiments, the stress conditions were $\sigma_1 = 1500\ psi\ (10.3\ MPa), \sigma_2 = 1000\ psi\ (6.2\ MPa), \sigma_3 = 300\ psi\ (2.1\ MPa)$, where, σ_1 was perpendicular to the sandstone tablets, σ_2 was vertical parallel, and σ_3 was horizontal parallel to the lenses (Figure 2-10). Further investigation on the cut blocks demonstrated that when hydraulic fractures intersected the sandstone tablet, they propagated through that discontinuity (27).

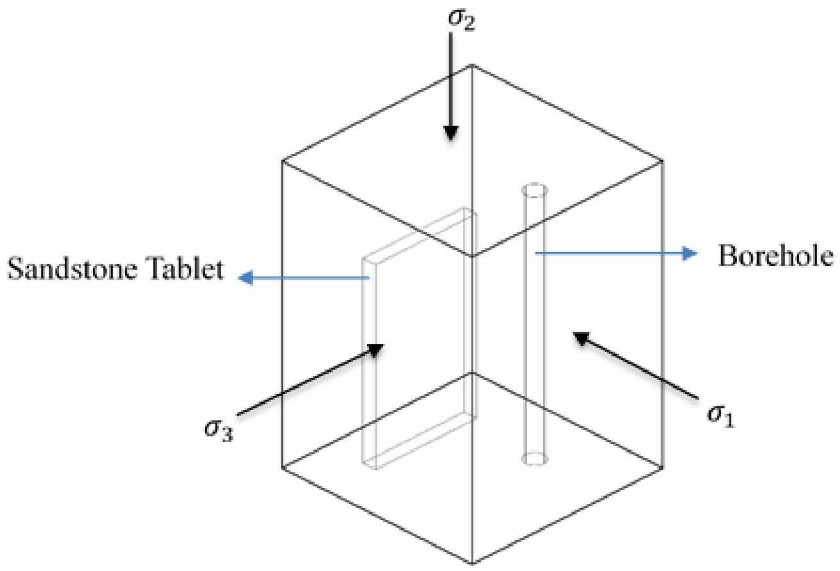

Figure 2-10 Gypsum cement block designed by Blair et al. (1989).

In 2005, hydraulic fracture experiments were performed on a Portland cement block with dimensions of 11.8×11.8×11.8 in. The experiments were performed in a true triaxial pressure machine capable of simulating in situ stress conditions. In order to prevent shear stress, a thin Teflon sheet was inserted with Vaseline between the block and platen of pressure. Acoustic transducers were used in direct contact with the block for monitoring propagation of hydraulic fractures (Figure 2-11). Viscasil with a viscosity of 100 Pa·s was used as the fracturing fluid in this study (28; 29).

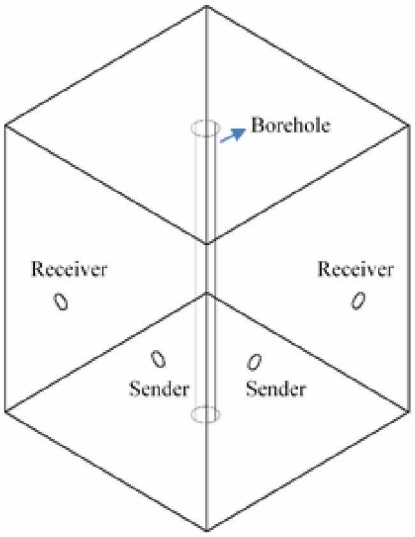

Figure 2-11 Acoustic transducers attached to the block by De Pater and Beugelsdijk (2005).

De Pater and Beugelsdijk concluded that when the flow rate is low, the natural fractures that were existed in the block would become opened; but, when the flow rate was high, new fractures in the block could be propagated. Furthermore, they observed that when the differential horizontal stress was high, existing fractures in the rocks could not change the hydraulic fracture propagation path; but when it was low, the pre-existing fractures had great influence on the hydraulic fracture growth path (28; 29).

Casas et al. conducted an experimental study to determine the effects of discontinuities on hydraulic fracture growth. They used a block of Colton sandstone with low permeability with dimensions of 2.5×2.5×3 ft. A central borehole with diameter of 1.5 inch was drilled along the entire length of the block using a servo-controlled drill rig. The entire borehole was cased with steel, except a central 12 in. of the borehole. Newtonian silicon-based filled (viscosity of 586800 cP) was used as the injection fluid in this study (30).

They concluded that under high confining stress, fractures propagate planar. They used two different materials for each filler of artificial joints. When hydraulic fractures reached the epoxy-filled joint, fractures arrested because of viscoelastic behavior of the epoxy. When hydraulic fracture reach the grout-filled joint, fractures were not arrested by the joint because of different stiffness between the grout and Colton sandstone (30).

In 2011, Zhou and Xue used a triaxial machine (the sketch of the setup shown in Figure 2-12), and block samples with dimensions of 11.8×11.8×11.8 in. to study the effects of random natural fractures on hydraulic fractures. For simulating a naturally fractured reservoir, after preparing blocks of cement and sand, they put blocks into an oven and heated them for three hours at 400° C. Because of dehydration and shrinkage of cement, random fractures occurred in the blocks. A borehole with diameter of 0.24 in. and length of 5.5 in. was drilled in the center of block. A steel tube of 5.1 in. length was used in the hole, leaving a 0.4 in. open-hole section in the wellbore in the center of the block for initiating the HF. For categorizing the effects of horizontal stresses on the propagation of hydraulic fractures in a simulated naturally fractured reservoir, they presented a dimensionless factor of differential stress (K_h) (31):

$$K_h = \frac{\sigma_H - \sigma_h}{\sigma_h} \tag{2-3}$$

They observed that both differential stress and existing natural fractures influenced the hydraulic fracture propagation path. They reported that when the value of K_h was less than 1.5, there were random radial fractures in the blocks, indicating that the impact of random fractures in the block was more important than the impact of differential stress. When K_h was between 1.5 and 2.5, hydraulic fractures tended to be vertical with random branches; and when the value of K_h was larger than 2.5 the effects of random natural fractures were minimum, and differential stress controlled the hydraulic fracture propagation. In this case, bi-wing hydraulic fractures occurred in the blocks (31).

Athavale et al. performed laboratory HF tests on homogenous and laminated blocks. In situ stresses were simulated using high pressure flatjacks. A borehole with diameter of 1 in. and length of 15 in. was drilled for injecting high viscosity (100,000 cP) fracturing fluid. A steel tube was inserted at 5 in. at top and bottom of the borehole, so there was a 5 in. open-hole section for fracture initiation. Performing HF tests on two 11×11×15 in. blocks showed that for the homogenous cement block, planar bi-wing penny shaped fracture growth occurred, but for the laminated block, complex and branching fracture growth was observed. Figure 2-13 shows the TerraTek stress frame used in this study (32).

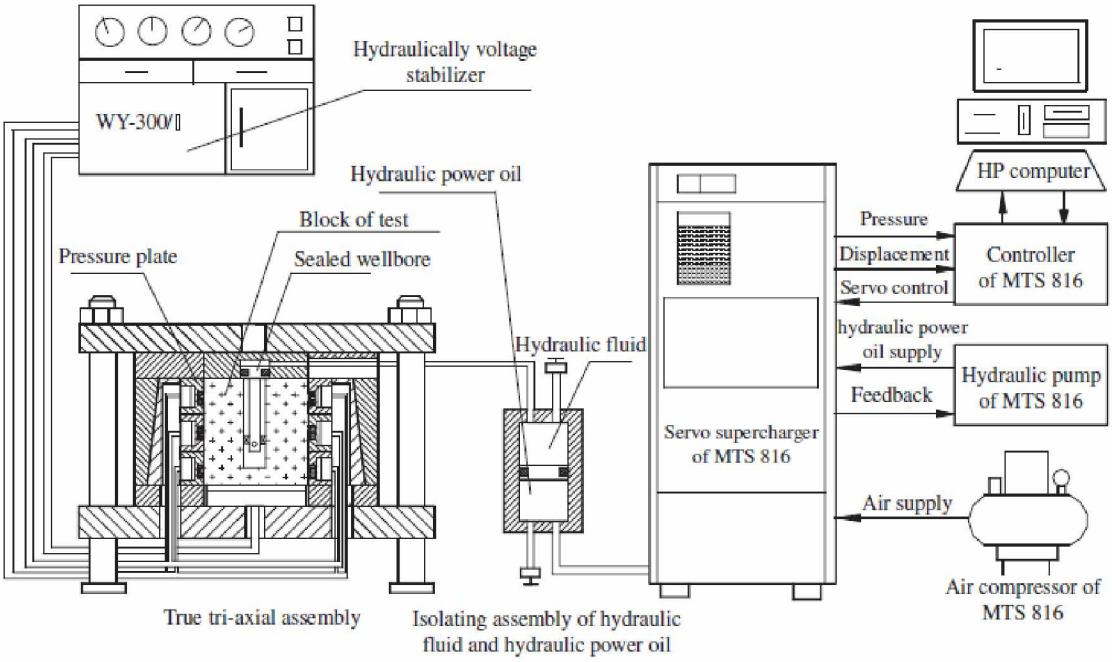

Figure 2-12 Schematic of the triaxial HF setup used by Zhou and Xue (2011).

Figure 2-13 TerraTek stress frame used by Athavale et al. (32).

There are some stimulation techniques for increasing production from oil and gas wells. Some of the techniques are conventional HF, high-strain-rate fracturing, shear stimulation, acid stimulation, and thermal stimulation. Frash et al. conducted mechanical impulse HF (MIHF) stimulation method on two granite specimens with dimensions of 11.8×11.8×9.45 in., and 11.8×11.8×11.8 in. MIHF is a type of high strain rate fracturing (HSRF) stimulation method. The basic idea of HSRF comes from dynamic failure phenomena, which states that by increasing loading rates, brittle behavior and the number of fractures increase. Compared to conventional HF, using HSRF, multiple fractures with different orientations can occur. In the MIHF simulation method, a source of mechanical energy is used for generating a dynamic high pressure hydraulic impulse in a wellbore. For generating impulses some equipment such as accumulators, hammers, and high-velocity pistons can be used. By performing the experiment on two granite specimens, one in an unconfined condition and the other in a heated true-triaxial confinement situation, it was shown that MIHF increased well production significantly (33).

Bing et al. in 2014 conducted some hydraulic fracture tests on four shale blocks with dimensions of 15.75×15.75×15.75 in. In this study using an acoustic emission (AE) system, the interaction between hydraulic fractures and natural fractures in the blocks were observed. The diameter of the drilled borehole and length were 0.75 in. and 5.5 in., respectively. There was a 2.36 in. open-hole section in the borehole. A triaxial loading machine was used for simulating the in situ stress conditions on the block samples. Slick water was injected as the fracturing fluid in these experiments. For monitoring the natural fractures in the block, six AE probes were used. On each side of the block, one AE probe was attached. From the observations of this study, they concluded that small natural fractures did not have great impact on the hydraulic fracture propagation path. These small fractures could just affect the hydraulic fracture in a local zone. Natural fractures with big aperture or low bonding strength could divert the path of the hydraulic fracture growth (34).

2.3 Numerical Modeling

Sneddon and Elliot's work is one of the main principals for many HF simulations. Their work was focused on opening of fractures for 2D simulation and for circular, penny-shaped cracks (35). Perkins and Nordgren improved their work to develop the Perkins-Kern-Nordgren (PKN) model. In the PKN model, the influence of fluid loss is included. This model works well for fractures with a high ratio of length to height (36; 37).

The Khristianovic-Geertsma-de Klerk (KGD) plane strain model was first proposed by Khristianovic and Zheltv and then improved by Geertsma and de Klerk. In the KGD model, a hydraulic fracture is assumed as one single planar crack that starts from the well and propagates through the formation. This model is usually appropriate for fractures with a small ratio of length to height (38; 39). Figure 2-14 shows geometry of cracks in the Sneddon, PKN, and KGD models (40).

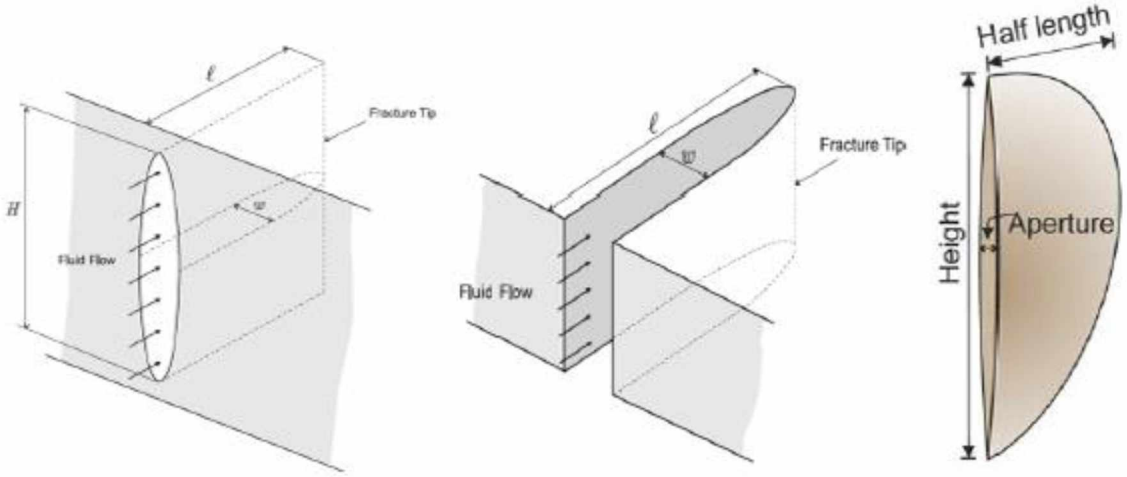

Figure 2-14 Geometry of crack proposed by PKN (left), KGD (center), and Penny-shaped models (40).

The pseudo three dimensional (P3D) model and the planar three dimensional (PL3D) model were developed based on the three previously discussed models. In these two models, there is no limitation for the height of fracture. Basically, the P3D model is the improved form of the PKN model. In the PL3D model, the geometry of the crack can be irregular and propagation of the crack is restrained by the tensile strength of the material (41).

The Finite Element Method (FEM) is based on discretization of the whole domain into finite subdomains. This is done by meshing the domain. Then for each element the solution is described by a combination of shape functions. FEM is very powerful for simulating fracture propagation, and it is able to simulate complex 3D shapes. There is a developed version of FEM called XFEM (extended finite element method) for simulating very complex geometries. This method is highly effective to model HF (42).

The Boundary Element Method (BEM) can be used for simulating HF when the system is small. The domain includes two sections. One part is the fracture and the other part is surrounding rock. A boundary is defined at the intersection of the fracture wall with rock (43).

The Discrete Element Method (DEM) is another useful method for simulating HF. In this method, discrete elements are defined. In this approach for simulating the failure of elements and interactions between them, Newton's motion equations are used. Unlike FEM, simulation of complex fracture geometry is almost impossible (44). Today many people are using commercial software generated based on the above methods for modeling HF. Some of these methods are explained in the following paragraphs.

In 2016, Zou et al. used cohesive zone theory to simulate HF in 3D. In the cohesive zone, the propagation of crack can be controlled. Also, using this method, one is able to explain characteristics of fluid migrating from the crack space into the adjacent rock. In this study, a vertical fracture was modeled, which passes through created layers. Figure 2-15 shows the 3D HF model developed by Zou et al. (45).

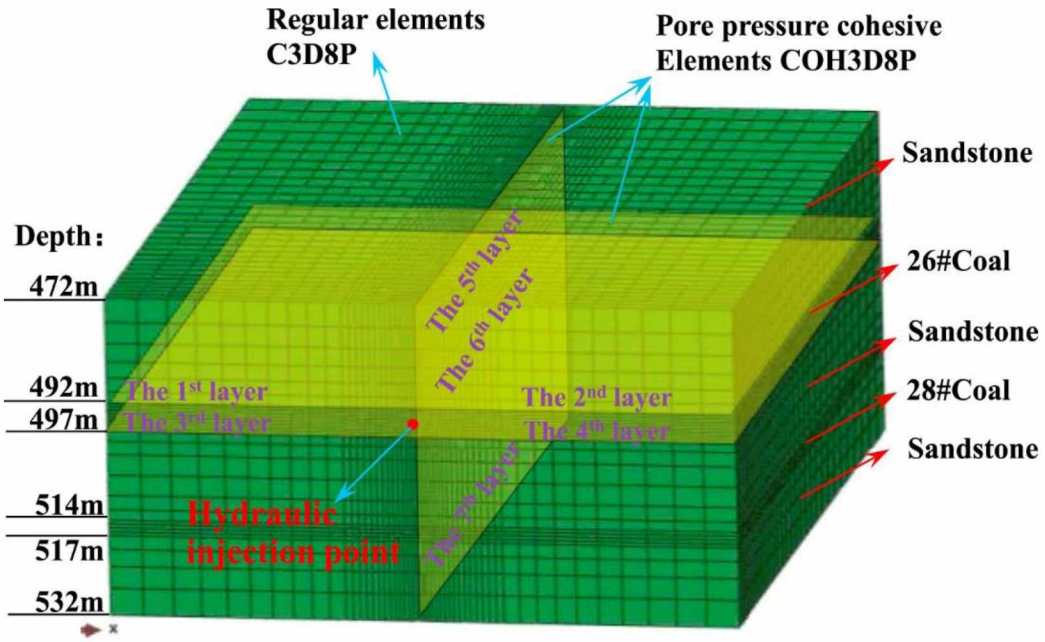

Figure 2-15 3D HF model by Zou et al. (2017).

Bao et al. simulated the hydraulic fracture tip by considering two different cases for injecting fluid. They assumed injection without lag, and also investigated the effect of fluid lag. Their results

matched well with analytical solutions. Figure 2-16 shows simulation of the hydraulic fracture with and without fluid lag (46).

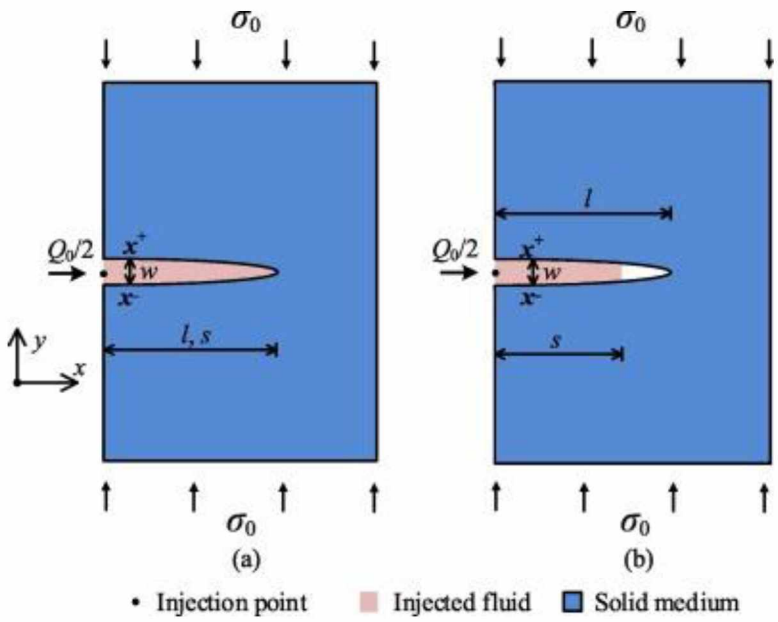

Figure 2-16 Hydraulic fractures in half space: (a) without fluid lag; (b) with fluid lag by Bao et al. (2016).

Feng et al. studied the heat migration from hydraulic fractures to the adjacent formation and vice versa. They applied the created heat module in FLAC3D and found that the temperature at the crack tip increased during injection. Also, they reported that cooling of hydraulic fluid can create additional tensile stress in the formation. Figure 2-17 shows the geometric model of the tight gas reservoir by Feng et al. (47).

Wang et al. simulated a coal seam using 2D particle flow code (PFC2D). They stated natural fractures have great impacts on the hydraulic fractures propagation path (three main interaction types between hydraulic fractures and natural fractures are crossing, opening, and arresting). They were not able to categorize interaction type based on different conditions (48).

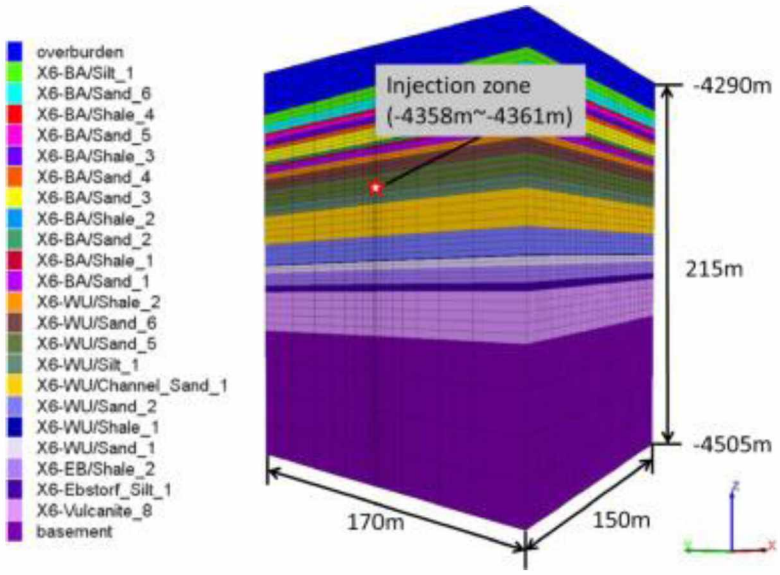

Figure 2-17 Graphic presentation of the stratigraphy and the geometric model of the tight gas reservoir by Feng et al. (2016).

CHA]'TER 3 LABORATORY TESTS TO DETERMINE PROPERTIES OF MATERIAL USED FOR HF EXPERIMENTS

In preparation for the laboratory HF experiments, it is necessary to know the elastic and strength properties of material to be used as the samples. In this research, plaster was used as the material for laboratory HF experiments.

Several standard rock mechanics tests were performed on prepared cylindrical and disk samples to find out the strength and elastic properties of the plaster. The following tests were performed and are explained in the next sections:

- Uniaxial Compressive Strength (UCS) Test
- Deformability Test
- Brazil Test
- Triaxial Compressive Strength Test

3.1 Specimen Preparation

After mixing plaster powder with water, several cylindrical plastic molds (2 in. diameter and 4 in. length) were used to construct the specimens (Figure 3-1). The molds were submerged under hot water to loosen the plaster from the mold walls. After removing from water, an air pump was used to blow compressed air from the hole that was created at the bottom of the mold to take out the prepared specimens.

Figure 3-1 Plastic cylindrical molds.

The cutting machine was used to cut both ends of specimens as flat as possible. Then the specimens were ground with a grinding machine to make a very smooth surface on both ends of the samples. Figures 3-2 and 3-3 show the cutting machine and the grinding machine, respectively.

Figure 3-2 Cutting machine.

Figure 3-3 Grinding machine.

Ideally, these samples should be completely flat and squared off at the edges so the loading machine can apply the load to the entire cross-sectional area equally. Flatness and squareness

devices were used to check how flat and smooth the ends of specimens were. These instruments are shown in Figures 3-4 and 3-5, respectively. The length and diameter of specimens were recorded and are shown in Table 3-1.

Figure 3-4 Flatness device.

Figure 3-5 Squareness device.

Table 3-1 Dimensions of prepared specimens.

Sample Number	Type	Test	Diameter (in)	Length (in)
1	Cylindrical	UCS	2.007	3.535
2	Cylindrical	Deformability	2.005	3.712
3	Disk	Brazil	2.007	1.056
4	Disk	Brazil	2.012	1.034
5	Disk	Brazil	2.001	1.053
6	Cylindrical	UCS & Deformability	2.006	3.594
7	Cylindrical	Triaxial	2.007	3.439
8	Cylindrical	Triaxial	2.013	3.683

3.2 TerraTek Hydraulic Press Machine

For performing rock mechanics tests, the largest hydraulic press machine in Alaska was used. This machine was built by the Terratek Company in Salt Lake City, UT. It can apply axial load up to 330,000 pounds. There is a refrigerator attached to the main chamber that can simulate Arctic conditions, with temperatures as low as -60° Fahrenheit. Operating the machine mostly is done using a computer (TerraTest software) connected to it. All data is stored as an Excel file for further processing. Figure 3-6 shows the hydraulic press machine.

Figure 3-6 TerraTek hydraulic press machine.

3.3 Uniaxial Compressive Strength Test

Uniaxial compressive strength (UCS) is one important measurement needed to properly assess the strength properties of a rock or any other material. In this test, the specimen whose length is almost twice its diameter is loaded axially. Axial load is increased continuously up to failure of the specimen. Two steel bearing blocks are used at the top of the specimen under the piston in this test. One of the blocks should be spherically seated and the other is a plain rigid block (49). Load in pounds and displacement of the piston in mil is recorded at each second and stored as an Excel file. Two tests were done on specimens No. 1 and No. 6. Figure 3-7 shows the uniaxial test setup for specimen No. 1.

Figure 3-7 Uniaxial compressive test setup.

Compressive strength of the specimen is calculated using Equation 3-1:

$$\sigma_c = \frac{P}{A} \tag{3-1}$$

where P is the peak load (pounds), A is the cross-sectional area of the specimen (in^2), and σ_c is UCS of the specimen (psi).

Loading rate in each test was calculated from Equation 3-2:

$$Loading\ rate = \frac{P}{t} \tag{3-2}$$

where t is the time that the specimen breaks (seconds).

Figures 3-8 and 3-9 show load (lb) vs displacement (mil) for specimens No. 1 and 6, respectively.

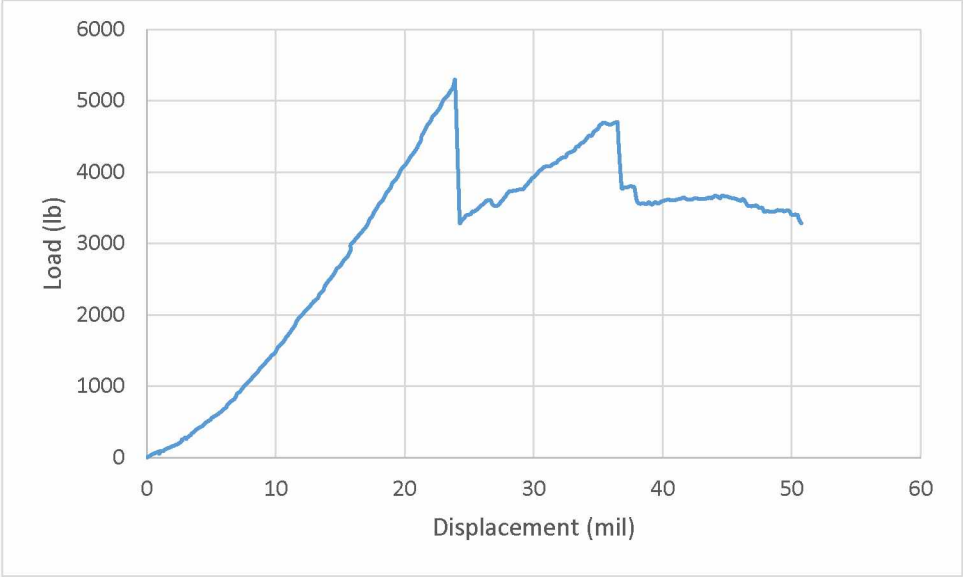

Figure 3-8 Load (lb) vs. displacement (mil) – Sample No. 1.

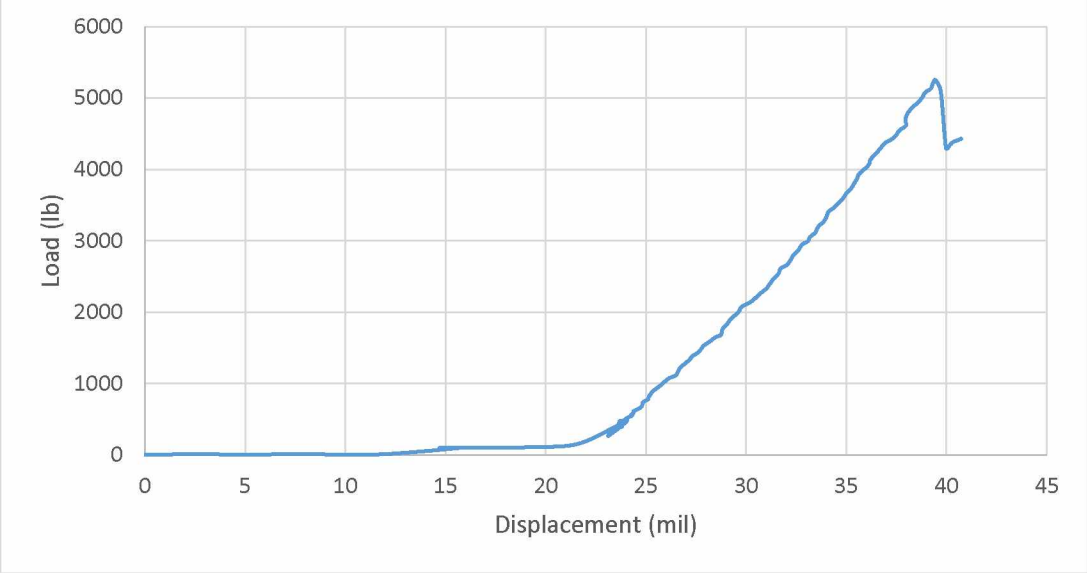

Figure 3-9 Load (lb) vs. displacement (mil) – Sample No. 6.

After breaking the sample, the breaking angle was recorded. The internal friction angle can be estimated using Equation 3-3:

$$\varphi_{Break} = 2\beta - 90 \tag{3-3}$$

where β is breaking angle, and φ_{Break} is the internal friction angle. The tool used for measuring the breaking angle is shown in Figure 3-10 and the results are summarized in Table 3-2.

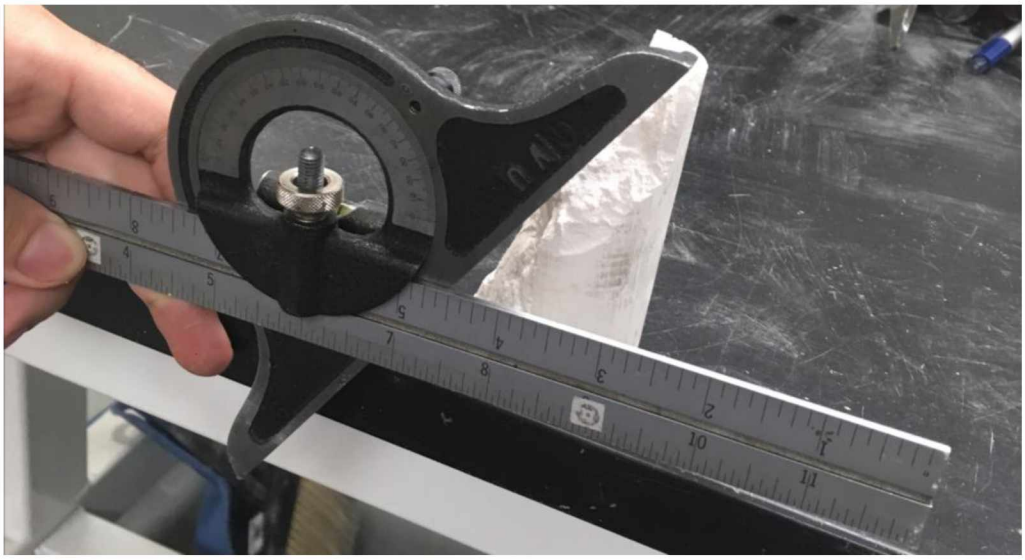

Figure 3-10 The tool used for measuring breaking angle.

Table 3-2 Uniaxial compressive strength tests results.

Sample	Max Load (lb)	σ_c (psi)	Loading Rate (lb/s)	β (degree)	φ_{Break} $(degree)$
1	5289.612	1672.011	41.47	72	54
6	5246.445	1660.02	41.068	63	36
Average	**5268.028**	**1666.015**	**41.27**	**66.5**	**43**

3.4 Deformability of Material in Uniaxial Compression

The purpose of this test was to find the Young's Modulus and Poisson Ratio of the plaster specimens. The Shear Modulus and Bulk Modulus were found as well. This was done using data obtained with the hydraulic press machine, as well as the set of Linear Variable Differential

Transformers (LVDTs) and a Transverse Deformation Jacket. LVDTs are used for measuring axial deformation and the deformation jacket is used for measuring transverse (diametric) deformation. Figure 3-11 shows the deformability test setup for specimen No. 6.

Figure 3-11 Deformability test setup.

The Young's Modulus and Poisson Ratio of a sample are very important, as they determine how much load that sample can bear before it deforms permanently. These values are only valid within the elastic range for the sample, as they are based off of Hooke's Law. Because of this, these samples also can be used in further tests. The Young's Modulus relates to how much a rock can deform until the deformations become permanent under normal stress. The Poisson Ratio is used to relate the Young's Modulus across different planes within a rock. These two values are important as they determine how much load can be applied to a rock without it permanently deforming. The Shear Modulus is like the Young's Modulus, but it deals with strain due to shear

stress. The Bulk Modulus pertains to the change in volume of the rock due to loading. These values relate to the rock's overall strength (50).

Stress is calculated using Equation 3-1. Axial and transverse strain are calculated using the stored data after each test and Equations 3-4 and 3-5 (50):

$$\varepsilon_a = \frac{\Delta L'}{L'} \tag{3-4}$$

$$\varepsilon_t = \frac{\Delta D}{D} \tag{3-5}$$

where ε_a is axial strain, L' is undeformed distance between anchor points for LVDTs (in), $\Delta L'$ is change in distance between anchor points for LVDTs (in), ε_t is transverse strain, D is the diameter of specimen (in), and ΔD is change in diameter of the specimen (in). For specimens No. 2 and 6, axial stress versus both axial and transverse strain was plotted in Figures 3-12 and 3-13, respectively.

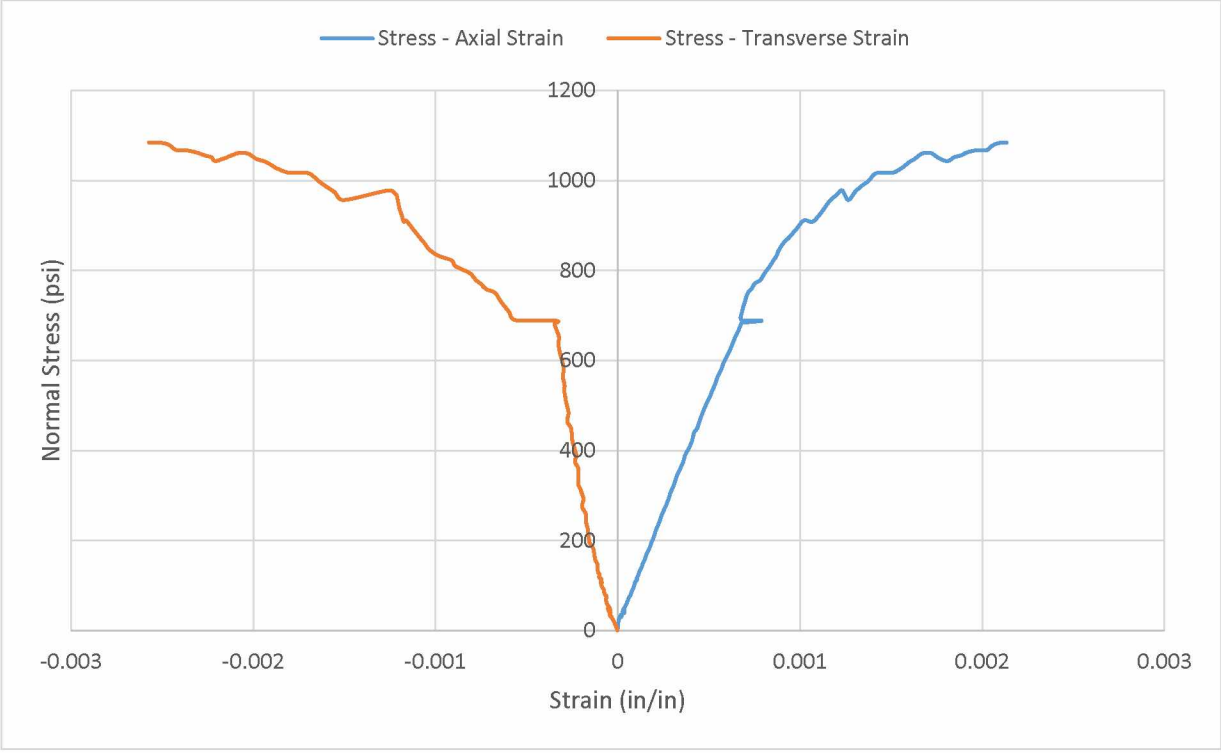

Figure 3-12 Normal stress vs. strain – sample No. 2.

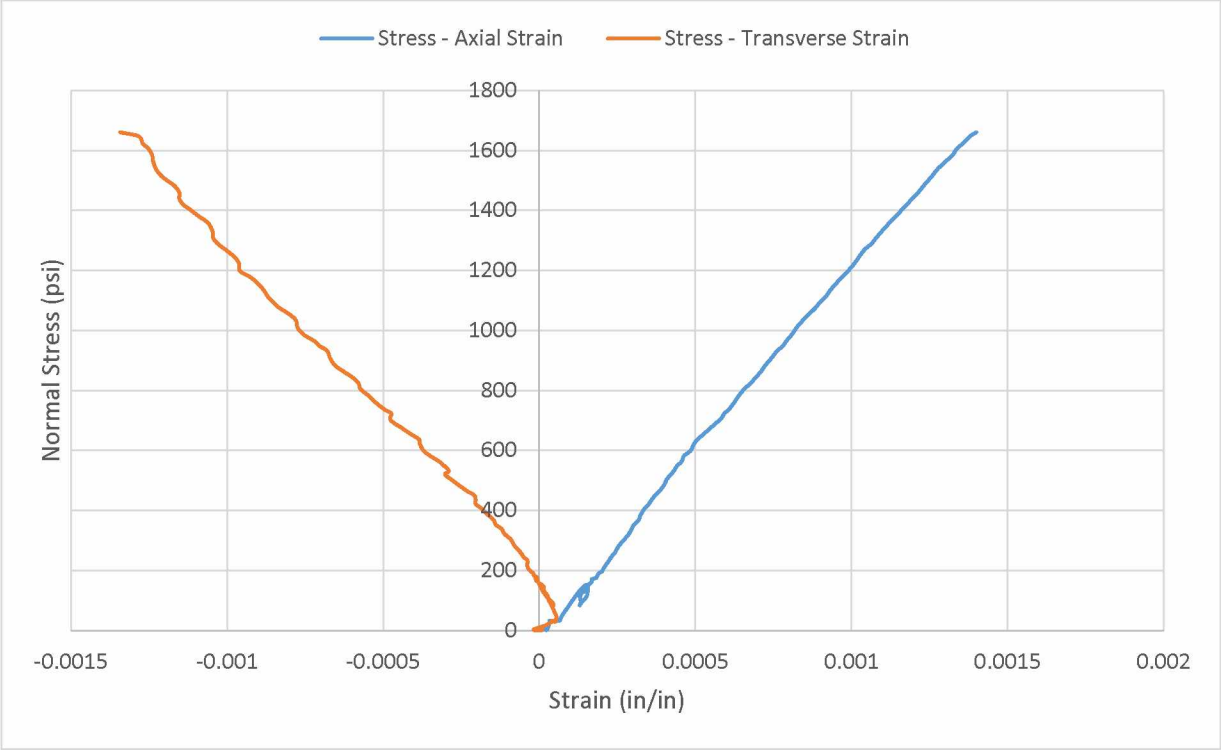

Figure 3-13 Normal stress vs. strain – sample No. 6.

To calculate Young's Modulus (E), the average method was used. The slope of the linear portion of stress vs. axial strain is the Young's Modulus. After finding a straight line along the axial stress vs. axial strain curve, Young's Modulus is estimated using Equation 3-6 (50):

$$E = \frac{\Delta\sigma}{\Delta\varepsilon_a} \tag{3-6}$$

Poisson Ratio (ν), is the change in transverse strain compared to the change in axial strain at the same range of axial stress used for calculating E (50):

$$\nu = -\frac{\Delta\varepsilon_t}{\Delta\varepsilon_a} = -\frac{Slope\ of\ axial\ stress - strain\ curve}{Slope\ of\ transverse\ stress - strain\ curve} = -\frac{E}{Slope\ of\ transverse\ curve} \tag{3-7}$$

Both the Shear Modulus (G), and the Bulk Modulus (K) are found using the Young's Modulus and Poisson Ratio. The Shear Modulus and the Bulk Modulus are found using Equation 3-8 and 3-9, respectively (51).

$$G = \frac{E}{2(1+\nu)} \tag{3-8}$$

$$K = \frac{E}{3(1-2\nu)} \tag{3-9}$$

Figure 3-14 shows load (lb) vs displacement (mil) for specimen No. 2, and the results are summarized in Table 3-3.

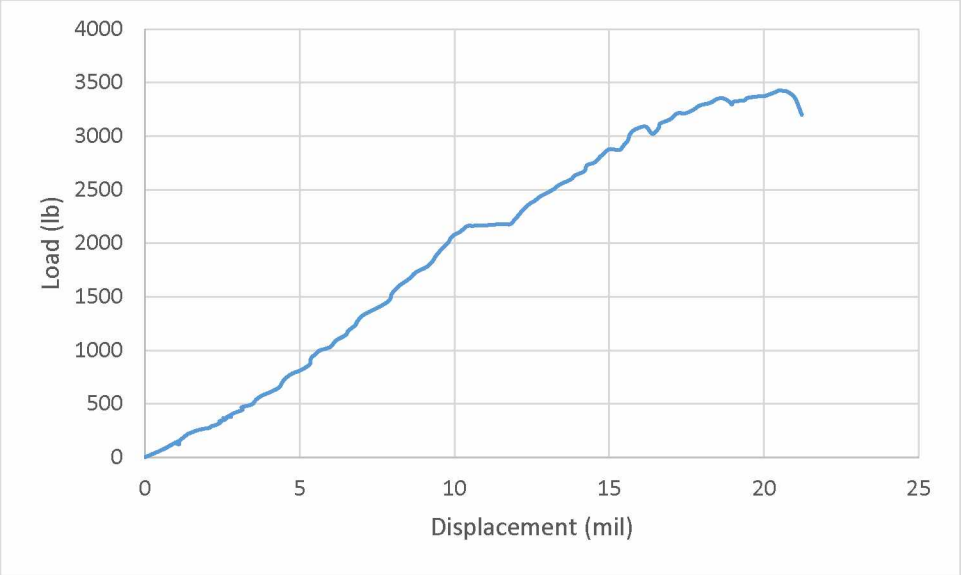

Figure 3-14 Load (lb) vs. displacement (mil) – Sample No. 2.

Table 3-3 Elastic properties of the used plaster.

Sample	Loading rate (lb/s)	E (psi)	ν	G (psi)	K (psi)
2	29.366	985,014	0.469	335,120	5,408,269
6	41.068	866,469	0.463	296,019	3,960,196
Average	**32.217**	**925,741**	**0.466**	**315,569**	**4,684,232**

3.5 Brazil Test for Indirect Tensile Strength of Material

The purpose of this test was to find the tensile strength of the plaster. This was done using data obtained with the hydraulic press machine, as well as the set of steel loading jaws. The steel loading jaws were used to distribute the hydraulic press load over the rounded section of the disk sample.

Tensile strength is the measure of how well a material can resist being pulled apart. The tensile strength of some materials like rock is very low, especially when compared to its compressive strength. This means that when designing anything involving rock, tensile stresses should be minimized to help increase the longevity of the rock.

The Brazil test for indirectly determining tensile strength of a rock was developed as an alternative to the more difficult direct method of measurement. This method presents an acceptable alternative based on numerous experiments which have proven that a majority of rocks in biaxial stress fields fail in tension (52).

Duct tape was applied to the samples so that the loading jaws would contact the samples with a greater surface area and the load would be distributed about the tape instead of applying a point load. Figure 3-15 shows the Brazil test setup for specimen No. 3.

Figure 3-15 Brazil test setup.

The loading rate for this test is much lower than that for compressive strength tests. The tensile strength, σ_t, was found using the Equation 3-10 (52):

$$\sigma_t = \frac{2P}{\pi D t} \tag{3-10}$$

where P is the peak load (lb), D is the diameter (in), and T is the thickness of disk sample (in). Figures 3-16 to 3-18 show load (lb) vs displacement (mil) for specimens No. 3, 4, and 5, respectively. The results are summarized in Table 3-4.

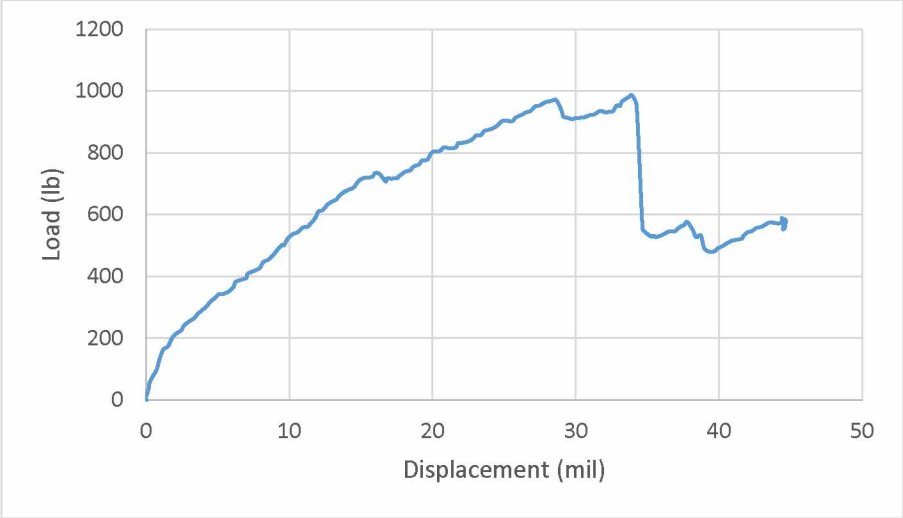

Figure 3-16 Load (lb) vs. displacement (mil) – Sample No. 3.

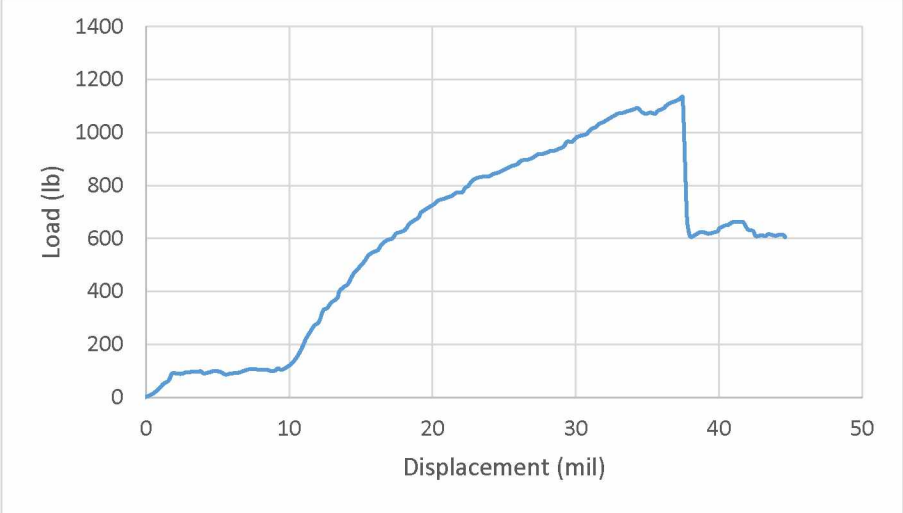

Figure 3-17 Load (lb) vs. displacement (mil) – Sample No. 4.

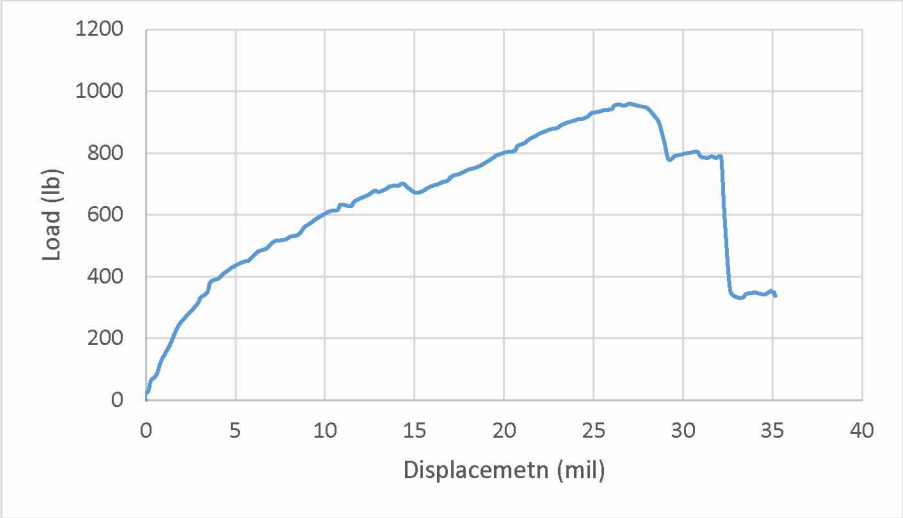

Figure 3-18 Load (lb) vs. displacement (mil) – Sample No. 5.

Table 3-4 Tensile strength tests results.

Sample	Max Load (lb)	Loading Rate (lb/s)	$\sigma_t\ (psi)$
3	986.373	8.398	296.285
4	1133.141	9.065	346.749
5	958.314	10.304	289.542
Average	**1025.943**	**9.255**	**310.858**

3.6 Triaxial Compressive Strength Test

The purpose of this test was to find the strength properties of the plaster. These properties include the triaxial factor, cohesion, and angle of internal friction. The Mohr-Coulomb Criterion was used to find these properties using the confining stress and axial stress used to break the samples at several confining stress levels. This step was done using data obtained with the hydraulic press machine, as well as the triaxial (Hoek) cell.

The body of the triaxial cell has an air bleeder connection and a connection for hydraulic fluid. Inside the cell, there is a flexible jacket of appropriate material to prevent the contact of hydraulic fluid with specimen. There is a hydraulic pump, capable of maintaining constant confining pressure within 2% of the desired value, connected to the hydraulic press machine. After placing

the sample inside the cell and connecting air and hydraulic cables to the triaxial cell, the pump is turned on to make sure that there is no air inside the cell. By removing the air from the cell, the space between the inner surface of the cell and membrane is fully filled with hydraulic fluid. Next, axial load is applied to the sample inside cell to a certain amount (for example 500 psi), then stopped. After that, confining pressure is applied up to that same amount (500 psi) and maintained until the end of the test. Then axial load is again applied until the sample breaks (53). Figure 3-19 shows the triaxial test setup for specimen No. 7.

Figure 3-19 Triaxial compressive test setup.

For each test, σ_1 is calculated using Equation 3-1. Table 3-5 shows the σ_1 vs. σ_3 values. Figure 3-20 shows the plot of σ_1 vs. σ_3. The Mohr-Coulomb relationship is a linear relationship, although the data in reality is not linear. The R^2 value of 0.88 means that this graph is fairly close to linear. The equation of the trend line also reveals important information about the plaster specimen. The slope is the triaxial factor ($\tan\psi$), and the y-intercept is the uniaxial compressive strength (σ_c). These values then relate to the cohesion (c), and the internal friction angle (φ) of the specimen.

Table 3-5 σ_1 vs. σ_3.

Sample Number	$\sigma_3\ (psi)$	$\sigma_1\ (psi)$
Avg. (1 & 6)	0	1666.015
7	200	2883.166
8	500	3381.052

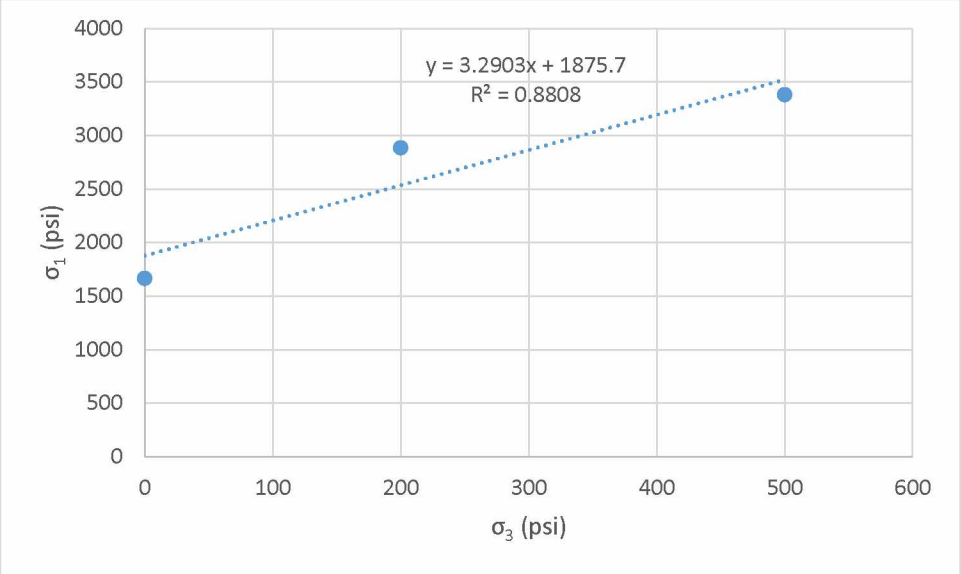

Figure 3-20 σ_1 vs. σ_3 (Mohr-Coulomb).

The internal friction angle was found two ways. The theoretical value was found by relating φ to tanψ (Equation 3-11). The break value, or experimental value, was found by measuring the breaking angle (β), and then finding φ (Equation 3-3).

$$tan\Psi = \frac{1+sin\varphi}{1-sin\varphi} \rightarrow \varphi_{theory} = Arcsin(\frac{tan\Psi - 1}{tan\Psi + 1}) \tag{3-11}$$

C can be calculated using Equation 3-12.

$$\sigma_c = \frac{2Ccos\varphi}{1-sin\varphi} \rightarrow C = \frac{\sigma_c \times (1-sin\varphi)}{2cos\varphi} \tag{3-12}$$

The resulting Mohr-Coulomb criterion for the used plaster is:

$$\sigma_1 = \sigma_c + \sigma_3 tan\Psi \rightarrow \sigma_1 = 1875.7 + \sigma_3(3.2903) \quad (3\text{-}13)$$

Figures 3-21 and 3-22 show load (lb) vs. displacement (mil) for specimen No. 7 and 8, respectively, and the results are summarized in Tables 3-6 and 3-7.

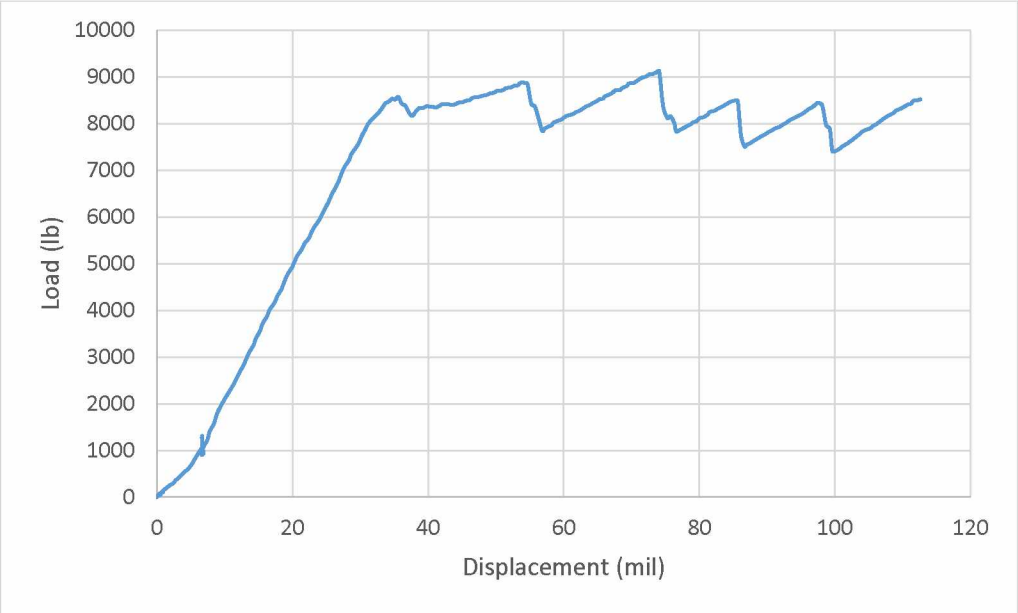

Figure 3-21 Load (lb) vs. displacement (mil) – Sample No. 7.

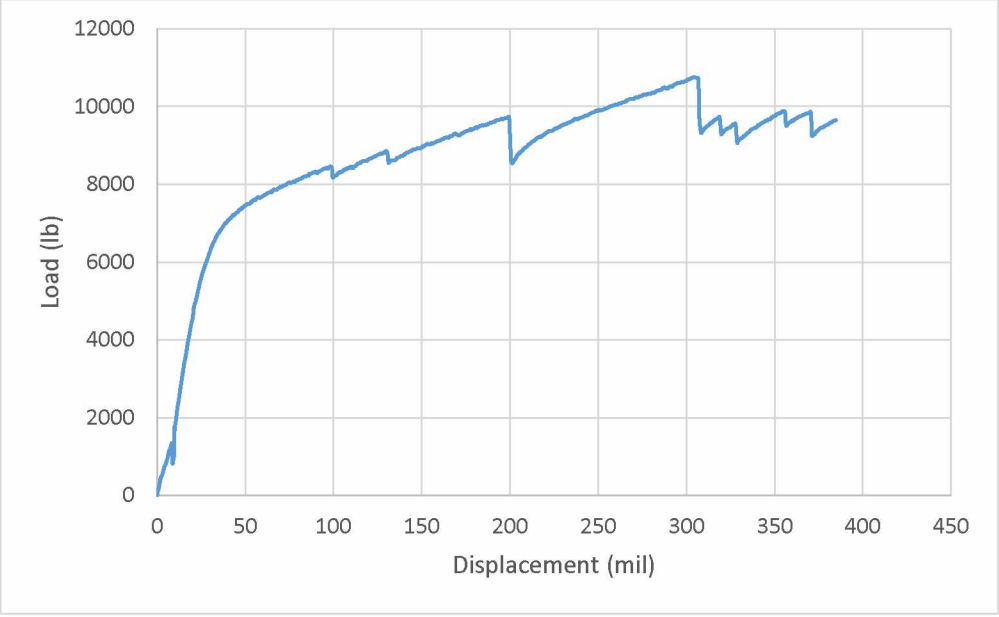

Figure 3-22 Load (lb) vs. displacement (mil) – Sample No. 8.

Table 3-6 Triaxial compressive tests results.

Sample	$\sigma_3\ (psi)$	Max Load (lb)	$\sigma_1\ (psi)$	Loading rate (lb/s)	β	$\varphi_{Break}\ (degree)$
Avg. (1 & 6)	0	5268.028	1666.015	41.27	66.5	43
7	200	9121.248	2883.166	45.663	62	34
8	500	10749.73	3382.052	16.646	58	26

Table 3-7 Strength properties of the used plaster.

$\sigma_c\ (psi) - Curve$	Cohesion (psi)	tanψ	$\varphi_{Test}\ (degree)$	$\varphi_{Break}\ (degree)$
1875.7	**517.03**	3.2903	**32.265**	34.3

3.7 Material Properties Summary

Based on the results, it can be stated that the used plaster is weak compared to typical rocks. Poisson's ratio of plaster is higher than most of rocks. All other elastic properties are relatively lower than rocks. The ratio between compressive strength to tensile strength for typical rocks is about 10 to 20. However, this ratio for the used plaster is about 5. Elastic and strength properties of plaster and typical shale are summarized in Table 3-8.

Table 3-8 Summarized properties of the plaster.

	Parameter	Plaster	Shale
Strength Properties	σ_c (psi)	1666.015	1400 – 14,000
	σ_t (psi)	310.858	280 - 1400
	C (psi)	517.03	400 – 4300
	φ (degree)	33.3	15 – 33
Elastic Properties	E (psi)	925,741	$(1.5 – 5)\times10^6$
	ν	0.466	0.3 – 0.35

Table 3-9 Summarized properties of the plaster (continued).

	Parameter	Plaster	Shale
Elastic Properties	G (psi)	315,569	$(0.6 - 1.8) \times 10^6$
	K (psi)	4,684,232	$(1.2 - 5.5) \times 10^6$

CHAPTER 4 LABORATORY EXPERIMENTAL STUDIES OF HYDRAULIC FRACTURING

4.1 HF Experiments

To conduct HF experiments in the rock mechanics lab, a rock box was designed and built. A hydraulic loading frame manufactured by TerraTek was used to apply vertical stress and two flat-jacks were built for applying horizontal stresses. Based on the dimension of the rock box, cubic samples made of plaster with dimensions of 5.7×5.7×6 in. (height is 6 in.) were molded. A top spacer was designed for injecting hydraulic fluid into a hole inside the prepared specimen. These procedures are explained thoroughly in this chapter.

4.1.1 The HF Experiment Apparatus

To conduct HF experiments, two different horizontal stresses must be applied in addition to the vertical stress. It was decided to use the TerraTek hydraulic loading frame as one of the major elements in the laboratory experiments and a rock box was fabricated to apply horizontal stresses. The experiment apparatus is illustrated in Figure 4-1. Each component of the apparatus is explained in detail in the next sections.

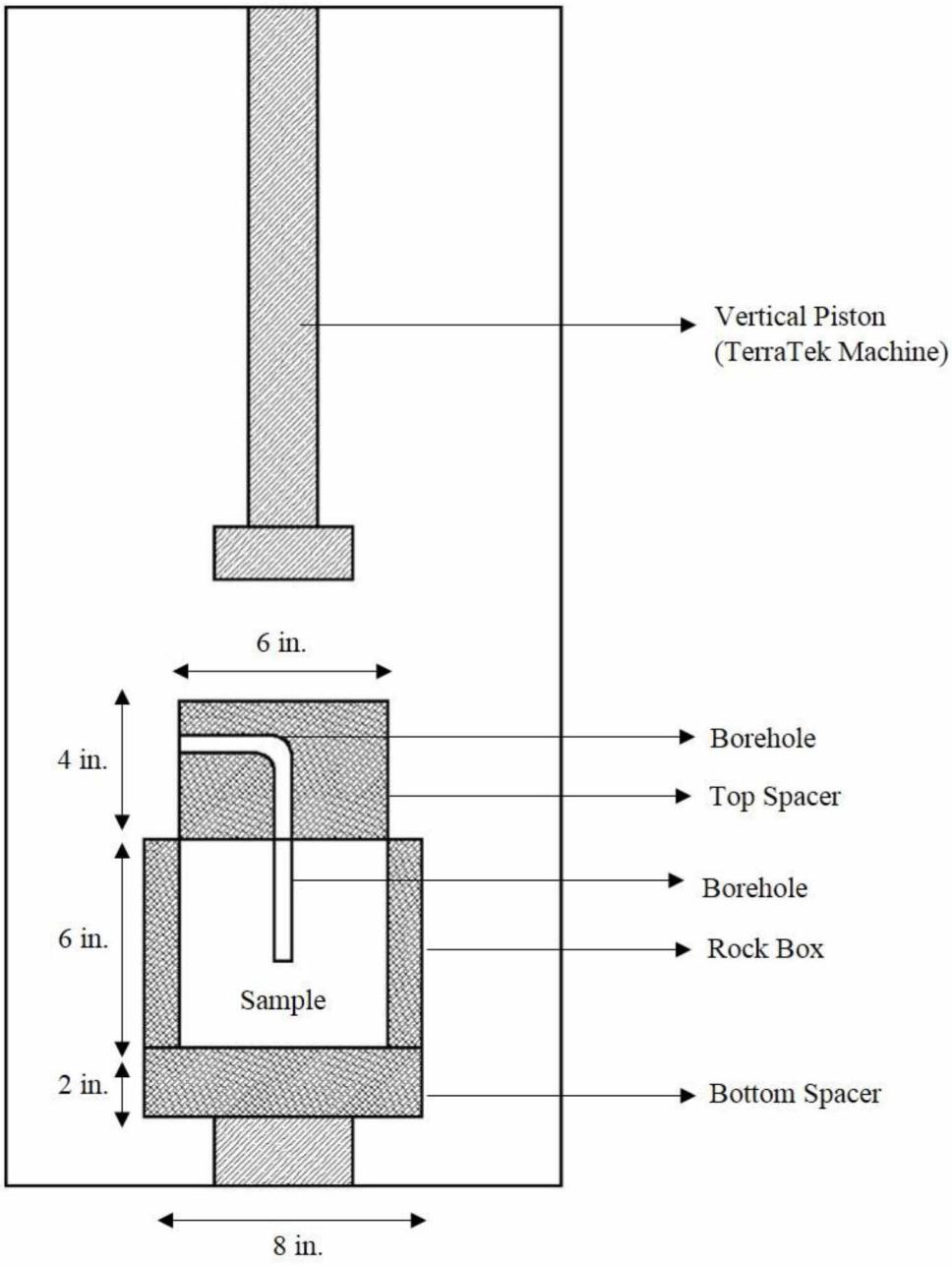

Figure 4-1 A sketch of cross-section view of the experiment apparatus.

4.1.2 Specimen Preparation

A cubic mold was built using wood boards. To avoid sticking plaster to the mold, first two vertical boards were nailed to the bottom board, but the other two vertical boards were pushed between these fixed boards. Next, it was painted and waxed. The built mold is shown in Figure 4-2.

Figure 4-2 The built wooden mold.

Two clamps were used to hold the vertical boards in place. Then prepared plaster was poured into the mold and after a few hours, the clamps were unlocked and the sample was removed from the mold. Figure 4-3 shows plaster in the mold.

Figure 4-3 Clamps used for holding faces of the mold.

After removing the specimen from the mold, the top face of the specimen was ground to have a smooth surface. With the specimen placed in a clamp, all imperfections were removed using a file (Figure 4-4).

Figure 4-4 The file used for trimming the faces of the specimen.

A borehole with a diameter of 0.5 in. and length of 4 in. was drilled in the center of the prepared specimen. Then the top 3 in. of the hole was drilled again with a larger bit (diameter of 0.68 in.). The prepared specimen is shown in Figure 4-5.

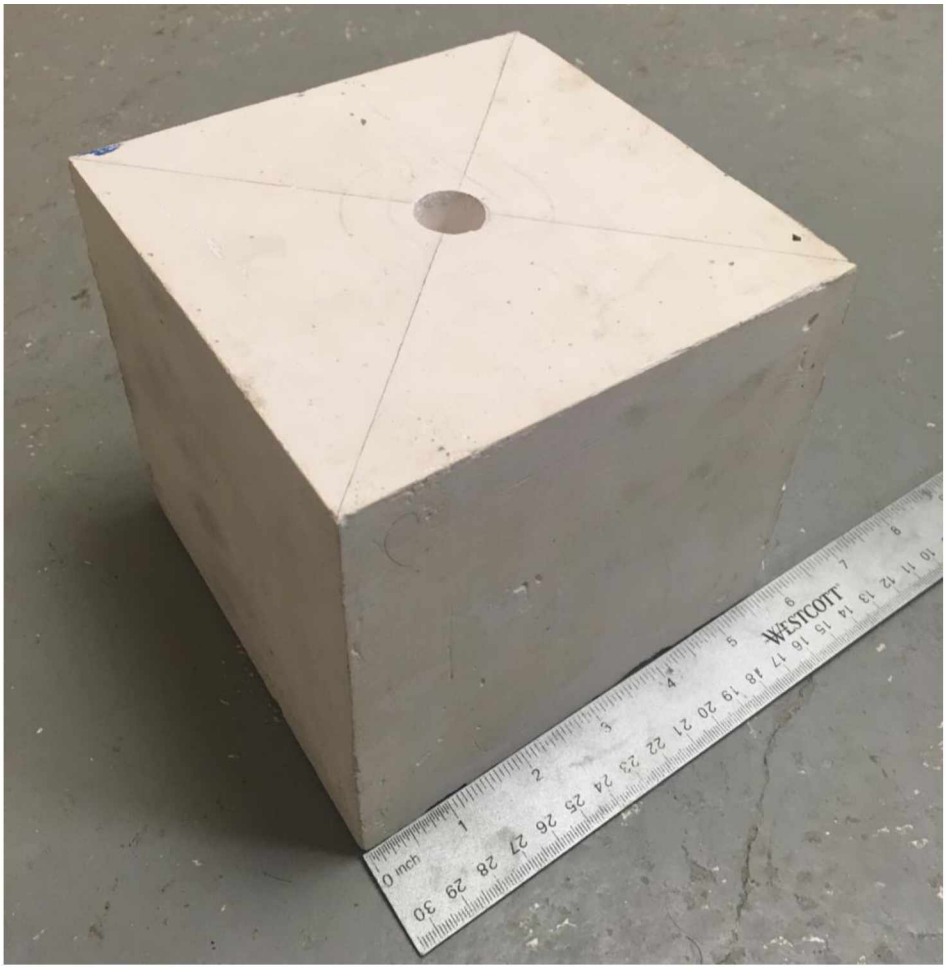

Figure 4-5 The prepared specimen.

4.1.3 Experimental Setup

4.1.3.1 TerraTek Machine

To use the TerraTek loading frame and TerraTest software for the planned HF experiments, the environmental chamber was removed from the loading frame to have more space for placing components of the experiment apparatus under the loading piston as shown in Figure 4-6 (without the environmental chamber).

Figure 4-6 TerraTek loading frame after removing the chamber.

4.1.3.2 Fabrication of Experiment Rock Box

A cubical frame (the rock box) was fabricated out of steel with an outside length by width of 8 by 8 in., and a height of 6 in. The thickness of steel plate forming the rock box was 1 in. A 2-in. thick bottom spacer was welded to the side frames of the rock box. The dimensions of the inside of the rock box was 6×6×6 in. Figure 4-7 shows the rock box.

Figure 4-7 Steel rock box.

4.1.3.3 Flat-jacks

In order to apply horizontal stresses on the sample, two flat-jacks were built. The size of each flat-jack was 5.7×5.7 in. and its thickness was 0.3 in. The space inside the flat-jack was filled with hydraulic fluid. Two tubes were attached to each of the flat-jacks. One of them was connected to a pump for injection of hydraulic oil. Another one was used as the exit tube to bleed the air from the flat-jack. After pumping oil into the flat-jack and bleeding air out from the exit tube, the exit tube was sealed. The flat-jacks were placed between the sample and the inner faces of the rock box. Figure 4-8 shows a constructed flat-jack.

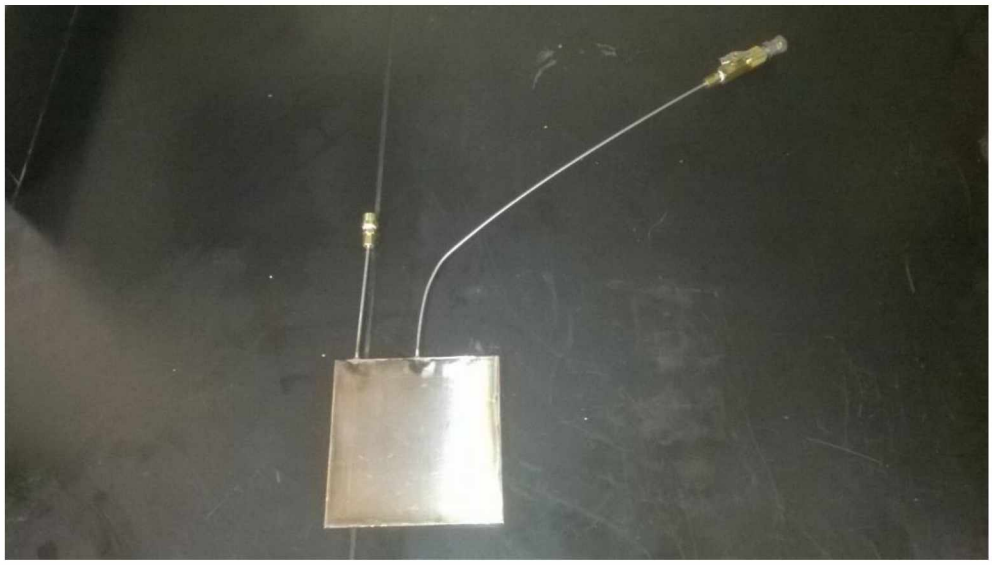

Figure 4-8 Flat-jack.

4.1.3.4 Top Spacer

For carrying out the HF experiments, it was necessary to inject fluid into the borehole drilled at the center of the sample and, at the same time, transfer vertical stress to the sample. To do that, a steel top spacer with a dimension of 5.7×5.7×4 in. was built. A hole with a diameter of 0.5 in. was drilled inside the spacer for the injection of fluid. The top spacer is shown in Figure 4-9.

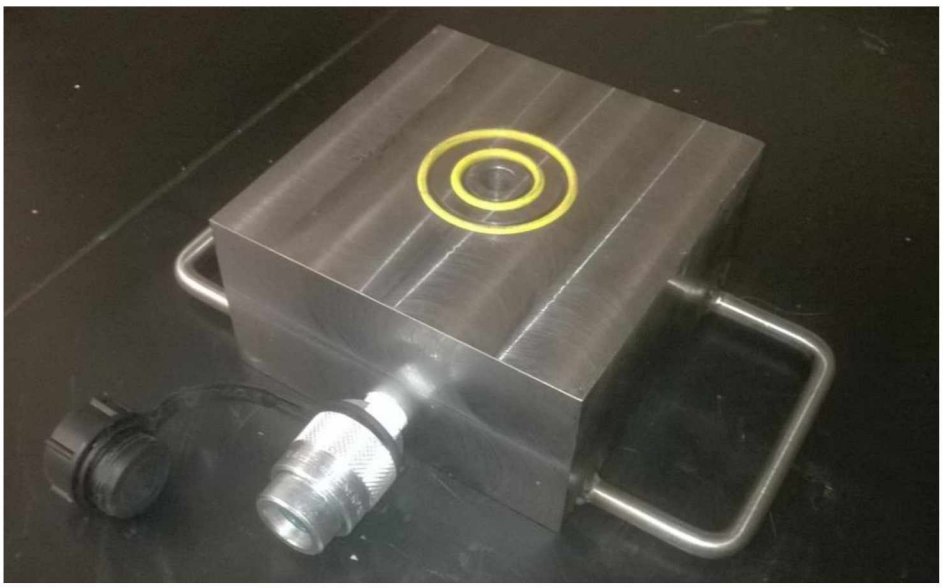

Figure 4-9 Top spacer.

4.1.3.5 Casing

A hollow steel tube was prepared with a length of 3 in. and outer and inner diameters of 0.68 and 0.5 in., respectively, to simulate the casing of a well. It leaves an open-hole section of 1 in. at the bottom of the borehole without steel casing. Figure 4-10 shows the casing. The prepared specimen with casing inside the borehole is shown in Figure 4-11.

Figure 4-10 Steel casing.

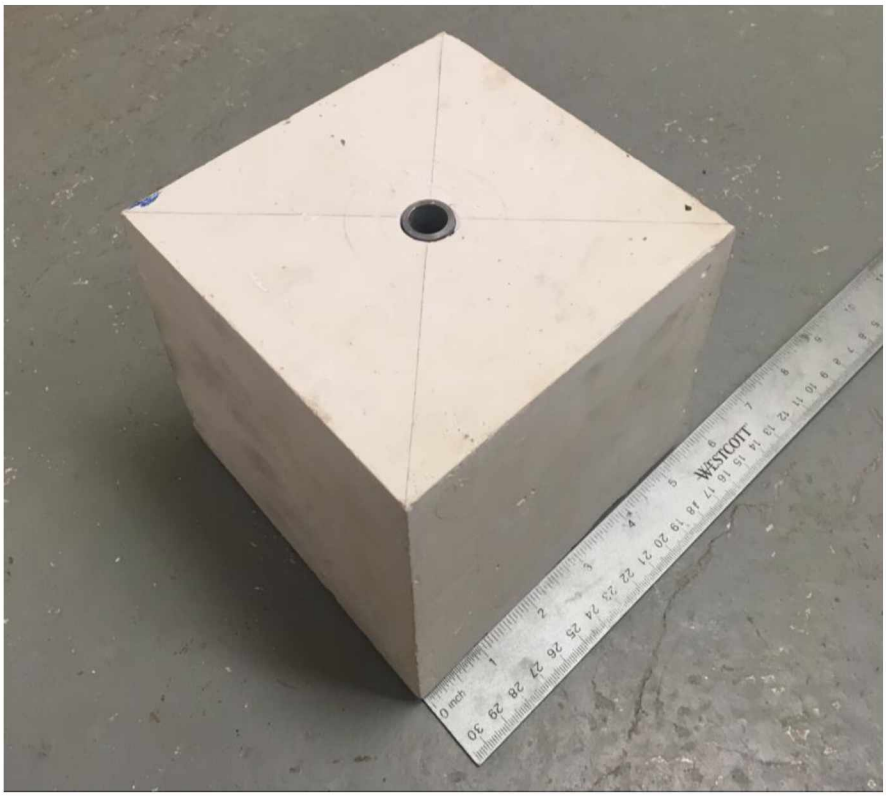

Figure 4-11 Casing placed inside drilled hole in center of specimen.

4.1.3.6 Test Procedure

- First place the two flat-jacks and specimen inside the rock box (Figure 4-12).

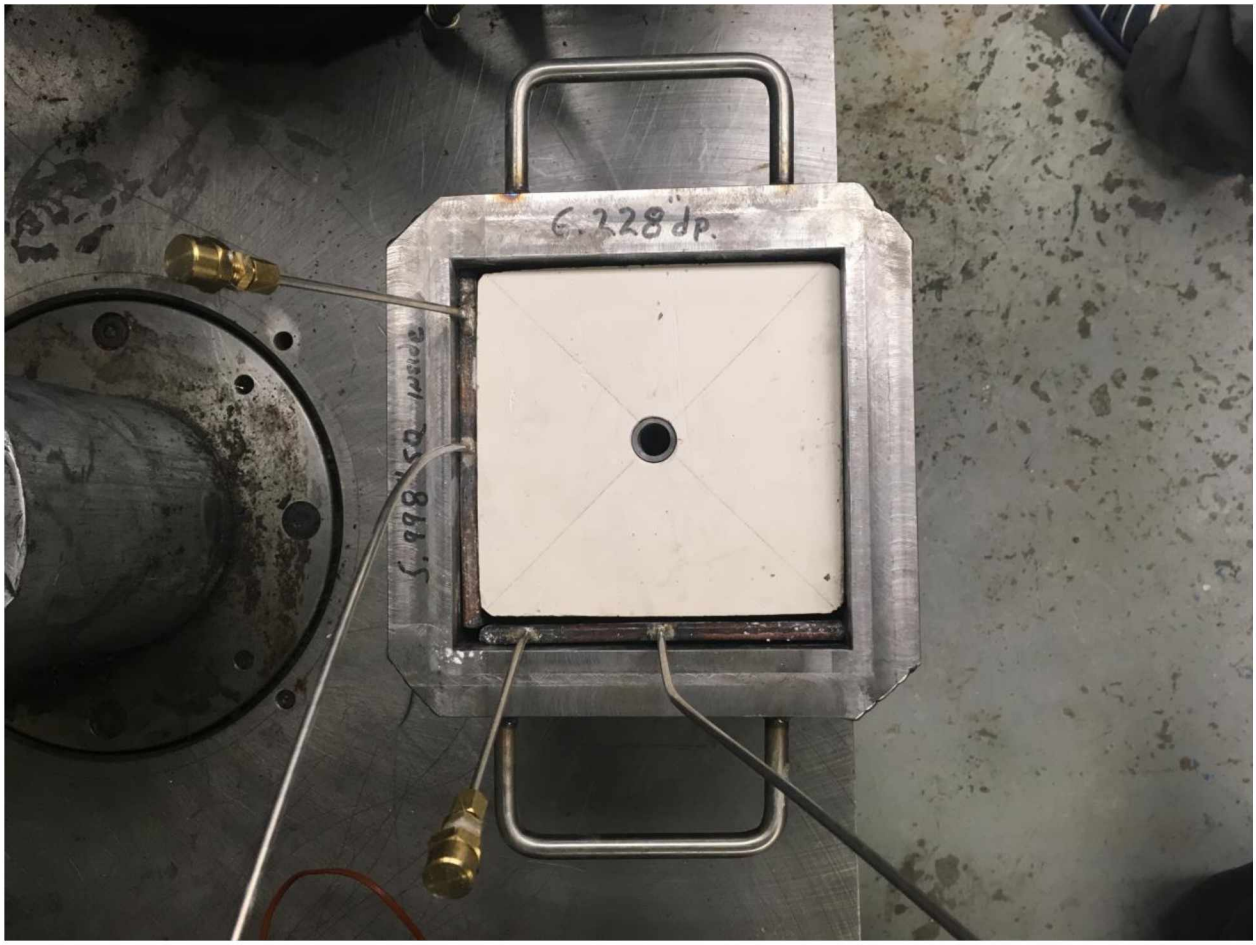

Figure 4-12 Specimen and flat-jacks placed inside the rock box.

- Place the rock box under the vertical piston. Put the top spacer on the specimen. Two steel bearing blocks are placed on top of the top spacer, as shown in Figure 4-13.

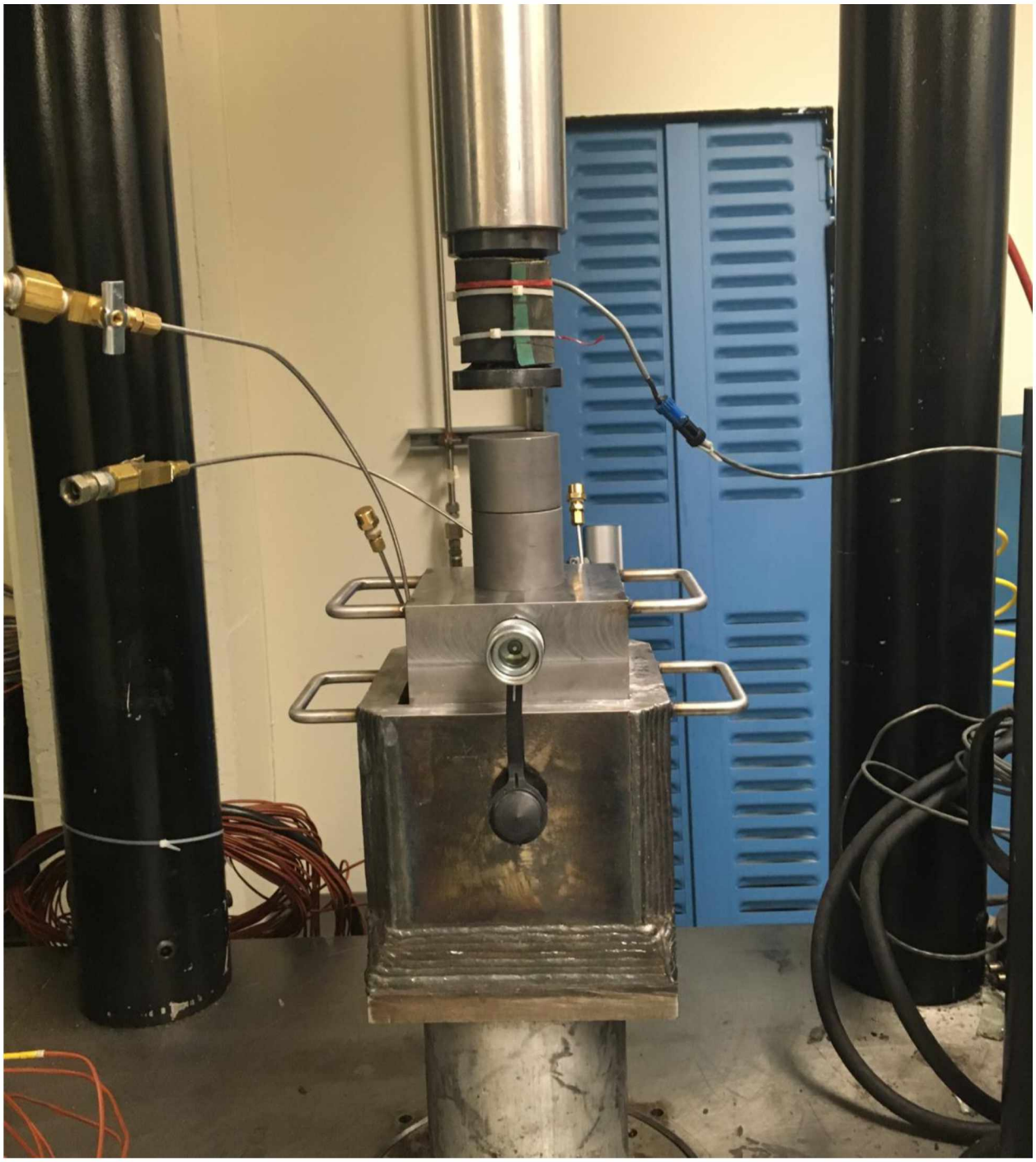

Figure 4-13 Placing the setup under the TerraTek load frame.

- Two pumps are connected to the side flat-jacks to apply different levels of horizontal stresses to the sample. Another pump is connected to the top spacer to inject fluid into the

borehole drilled inside the sample. Figure 4-14 shows connections of pumps to the flat-jacks and top spacer.

Figure 4-14 Pumps connected to flat-jacks and top spacer.

- Move the vertical piston down to touch the two bearing blocks using manual controller of the TerraTek load frame (Figure 4-15).

Figure 4-15 Using manual controller to make contact between piston and the bearing blocks.

- Apply vertical stress using manual controller of TerraTek load frame and TerraTest software to the bearing blocks. The vertical stress is maintained constant until the end of test, which is done by TerraTest control software.
- Apply horizontal stresses by pumping hydraulic fluid into flat-jacks. These pressures are maintained at a pre-determined constant level until the end of the test.
- Start injecting hydraulic fluid into the borehole, until a hydraulic fracture occurs. The pressure gauge should be monitored carefully. When the pressure suddenly drops, it means the hydraulic fracture initiates inside the specimen. The highest pressure is recorded.
- Retract vertical piston, release the vertical stress, and release the pumps connected to the flat-jacks and top spacer.
- Remove the specimen, and inspect the propagation path of the hydraulic fracture. Figure 4-16 shows one of the specimens after the test.

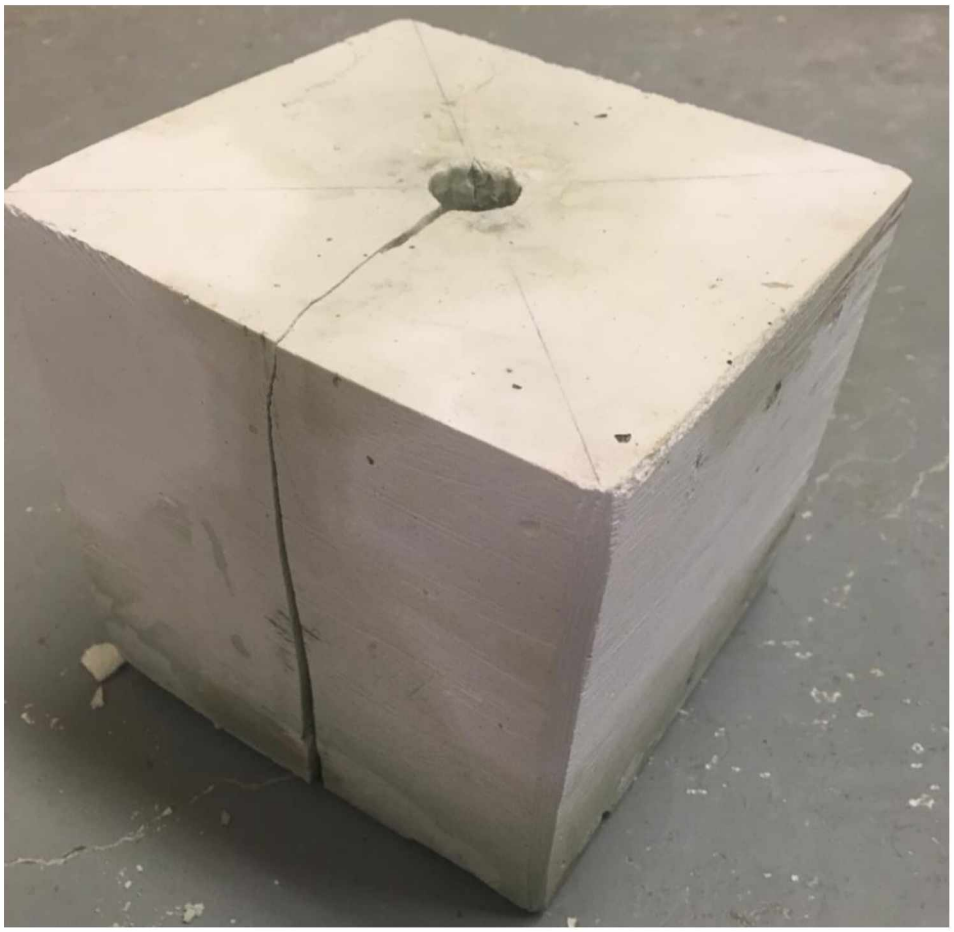

Figure 4-16 Specimen No. 2 after performing the test.

4.2 Results and Discussion

Five tests were performed. Characteristics of all tests are summarized in Table 4-1. Figures 4-17 to 4-21 show the propagation of hydraulic fracture along the maximum horizontal stress and perpendicular to the minimum horizontal stress for tests No. 1 to 5.

For test No. 2 and 4, the injection of fluid continued after the hydraulic fracture occurred and, therefore, the fracture propagated throughout the specimen. As injection continued, the injection pressure did not go beyond the peak pressure, which was recorded and caused failure.

For specimens No. 1, 3, and 5, after fractures occurred (the pressure suddenly dropped), the injection of fluid stopped. Then by using a saw each specimen was cut open into two halves.

In all the cases, the applied pressure to initiate the fracture was recorded. As can be seen in Table 4-1, by increasing differential horizontal stress, the required pressure (P_{HF}) for creating hydraulic fracture decreases. In fact, each 100 psi increase of differential horizontal stress, results in a 100 psi decrease in the required pressure to create hydraulic fracture.

Table 4-1 Conditions of applied stresses during each test.

Test #	$\sigma_v\ (psi)$	$\sigma_h\ (psi)$	$\sigma_H\ (psi)$	T (psi)	$\sigma_H - \sigma_h\ (psi)$	$P_{HF}(psi)$
1	1000	100	200	310	100	416
2	1000	100	300	310	200	320
3	1000	100	400	310	300	215
4	1000	100	500	310	400	118
5	1000	100	600	310	500	16

Figure 4-17 Specimen No. 1

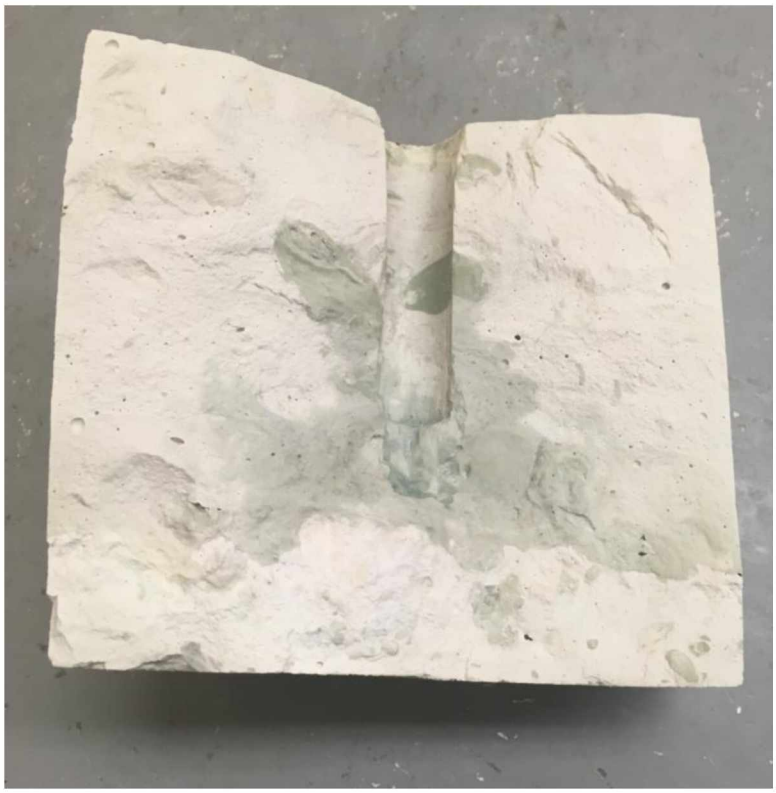

Figure 4-18 Specimen No. 2

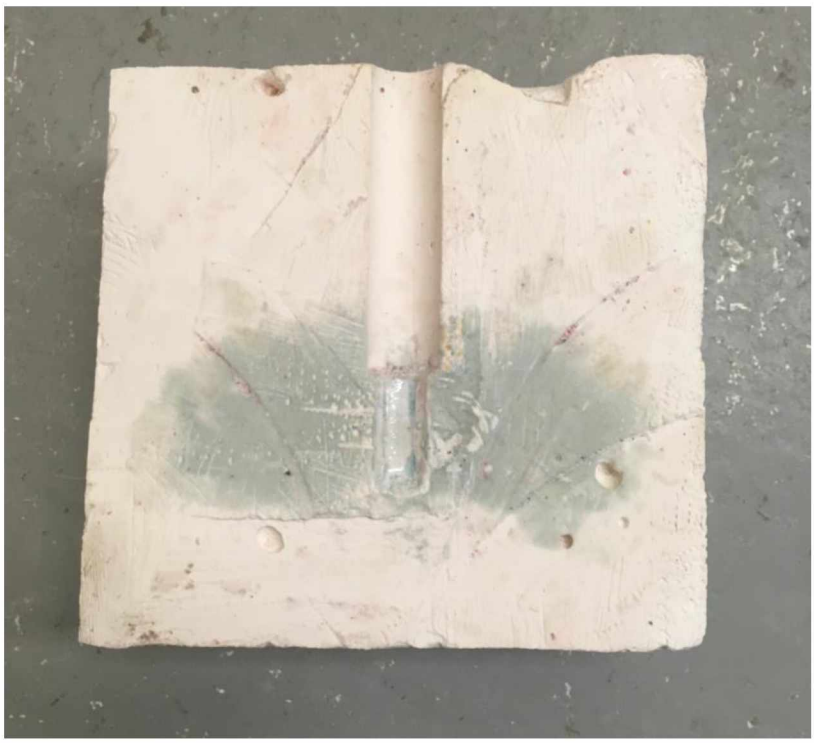

Figure 4-19 Specimen No. 3

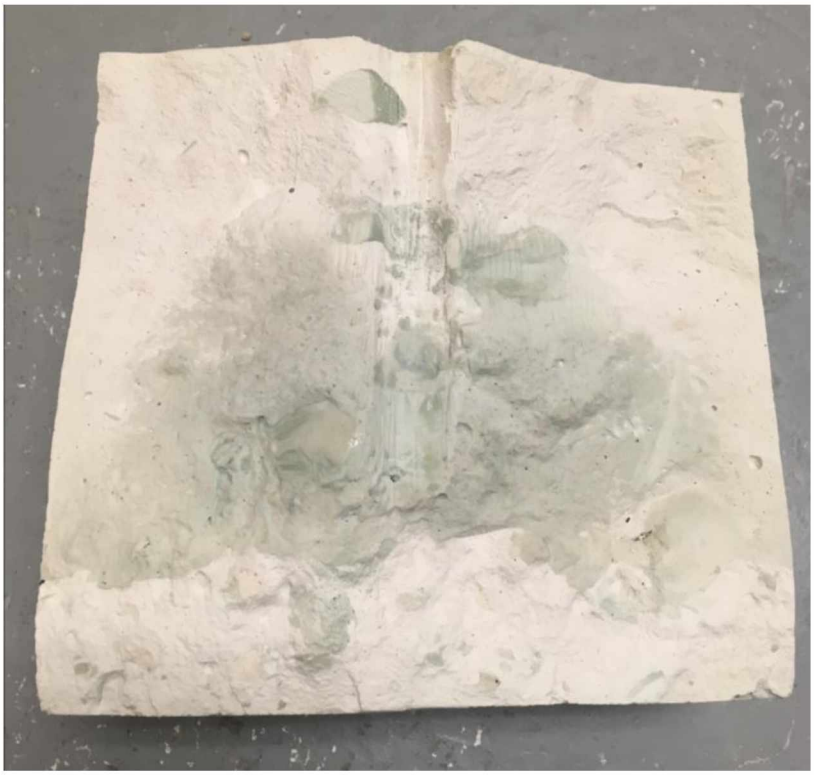

Figure 4-20 Specimen No. 4

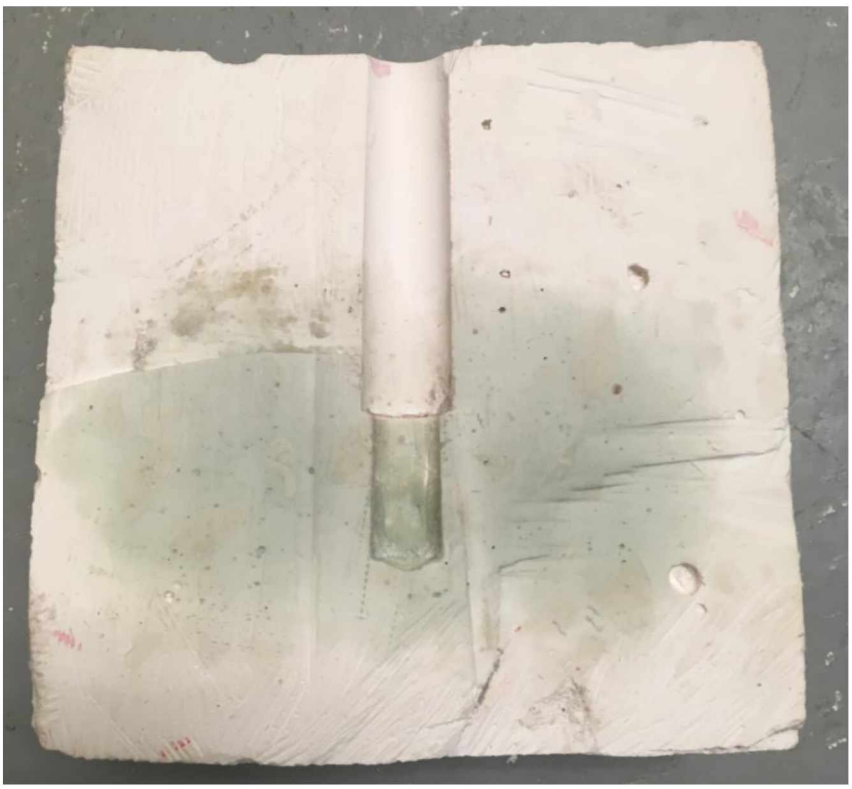

Figure 4-21 Specimen No. 5

In all the performed tests, the vertical stress and minimum horizontal stress were kept constant, to see the effect of differential horizontal stress on the required pressure for creating hydraulic fracture. In the next chapter, these tests were validated using computer modeling and more scenarios were simulated.

In all tests, vertical hydraulic fracture was created and propagated along maximum horizontal stress, which agrees well with theory of propagation of hydraulic fracture. It shows the efficiency of the experimental setup. Based on the developed theory, hydraulic fracture would propagate perpendicular to the minimum principal stress (54).

Kirsch in 1898 generated Equations 4-1 and 4-2 to determine the stress distribution around an underground circular opening. Figure 4-22 shows the stress distribution around a circular opening in a biaxial field (51).

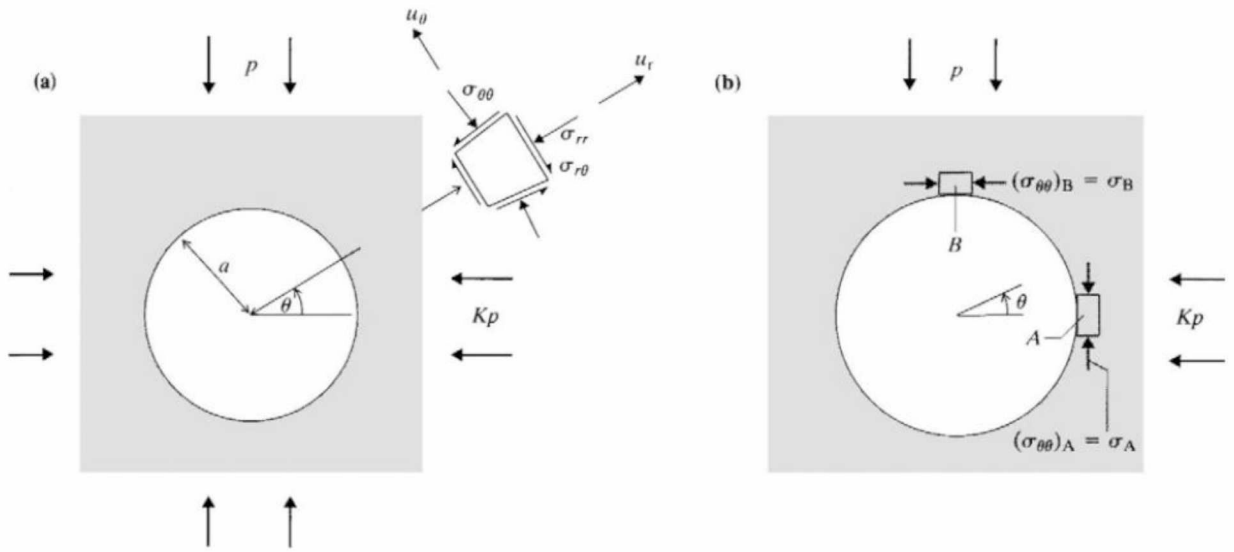

Figure 4-22 Stress distribution around a circular opening in a biaxial stress field (51).

$$\sigma_{rr} = \frac{P}{2}\left[(1+K)\left(1-\frac{a^2}{r^2}\right) - (1-K)\left(1-4\frac{a^2}{r^2}+3\frac{a^4}{r^4}\right)cos2\theta\right] \quad (4\text{-}1)$$

$$\sigma_{\theta\theta} = \frac{P}{2}\left[(1+K)\left(1+\frac{a^2}{r^2}\right) + (1-K)\left(1+3\frac{a^4}{r^4}\right)cos2\theta\right] \quad (4\text{-}2)$$

where σ_{rr} and $\sigma_{\Theta\Theta}$ are the radial and tangential stresses, respectively, P and KP are the horizontal stresses around the opening (Figure 4-22), K is constant, a is the radius of opening, and r is the distance from the center of opening. Zobac in 2007 showed the 2D failure criterion of HF along maximum horizontal stress direction (Equation 4-3), which is developed from Kirsch Equations (55):

$$P_{HF} = 3\sigma_h - \sigma_H - P_p + T \quad (4\text{-}3)$$

where P_p is the pore pressure.

In the performed experiments in the lab, the specimens were almost dry before conducting the test. Therefore, it was assumed that pore pressure was zero. Equation 4-3 was used to estimate pressure required to initiate HF in all five performed tests. The theoretical results are compared with experimental results in Figure 4-23. As can be seen the values obtained from the experiments are very close to those estimated from Equation 4-3. The experimental values are slightly higher than the mathematical approach. The small differences could be because the equation does not consider

vertical stress. In the next chapter, the experiments are simulated numerically in a 3D environment to investigate the effect of the vertical stress.

Figure 4-23 Comparison of experimental simulations versus the theoretical approach.

CHAPTER 5 THREE DIMENSIONAL NUMERICAL SIMULATION OF HYDRAULIC FRACTURING

In this research, a numerical simulation software package ABAQUS was used for 3D modeling of HF. ABAQUS is a commercially available Finite Element Analysis software. The first version of this software was released in 1978. This software has been a popular tool among researchers in different engineering disciplines.

The objective of this chapter is to conduct 3D modeling of HF and compare the numerical results with the laboratory experiments. With the verification of the model, further exploration of HF are conducted by varying the vertical stress and the minimum horizontal stress levels to investigate the effect of these stress components on HF, which was not performed in the laboratory experiments.

5.1 Model Design

To simulate the 3D specimen used in the laboratory experiment, a solid and deformable cube was modeled. By using the "cut extrude" feature, the borehole was modeled. The size of cube and borehole was the same as the laboratory specimen (cube size and diameter of borehole were 5.7×5.7×6 in. (height is 6 in.) and 0.5 in., respectively). The model is shown in Figure 5-1. The material properties obtained in Chapter 3 (Table 3-8) were imported into the software. As in the experimental setup, the three faces were fixed (Figure 5-2).

Three steps were defined. The first step was applying vertical stress. This stress propagated through the next steps. The second step was applying the horizontal stresses. This step propagated through the third step too. The third step was applying pressure at the 1 in. open-hole section at the bottom of the borehole.

Vertical stress was applied on the top face (XZ plane). Then horizontal stresses were applied on the other faces. The maximum horizontal stress was applied along the YZ plane (perpendicular to the YX plane). The minimum horizontal stress was applied along the YX plane (perpendicular to the YZ plane). Figure 5-3 shows stresses that were applied on three faces of the specimen.

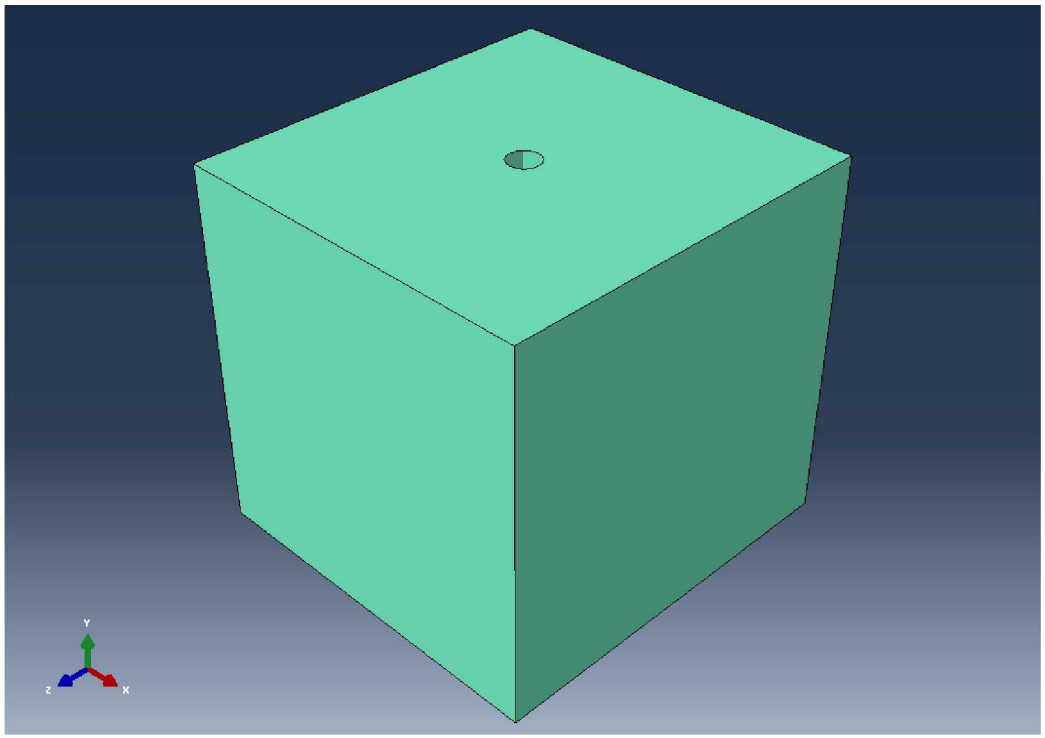

Figure 5-1 The geometry of specimen.

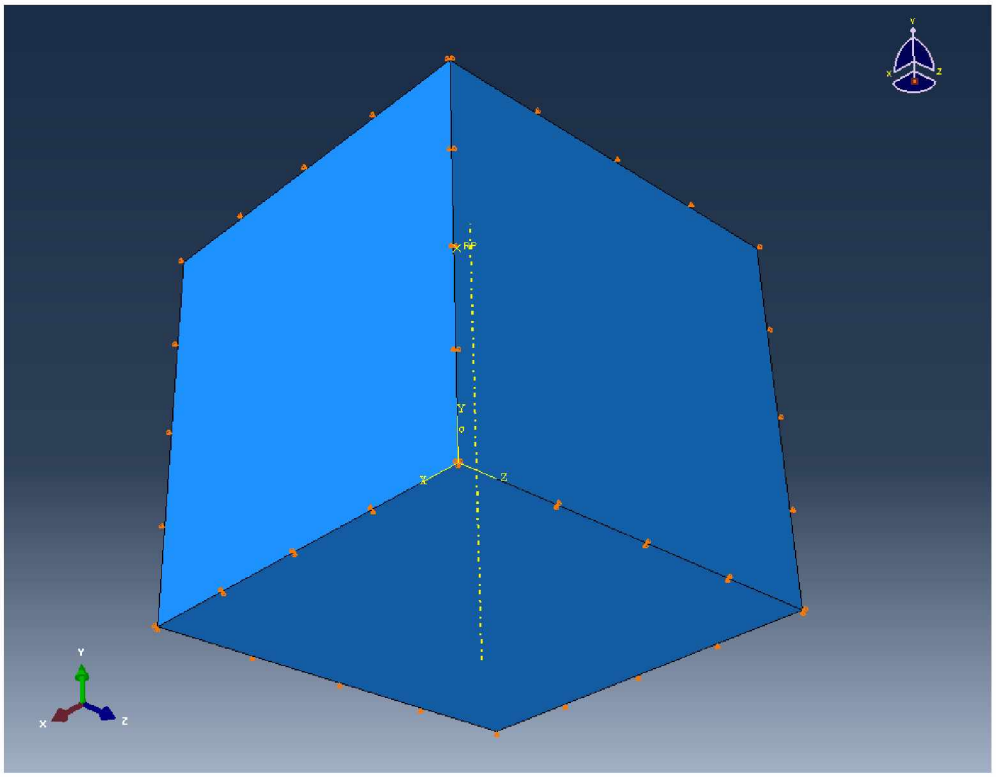

Figure 5-2 Applying fixed boundary conditions on three faces of sample.

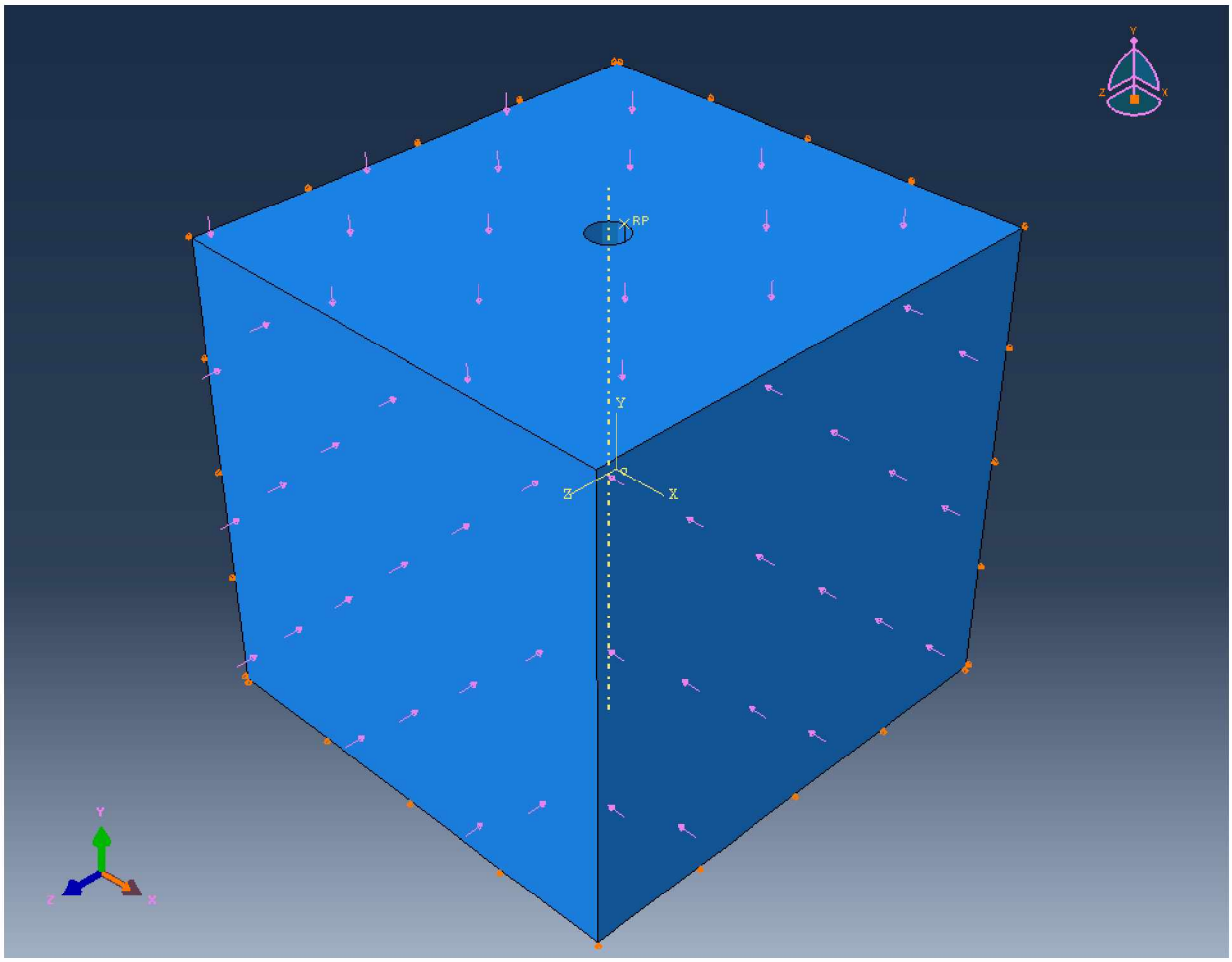

Figure 5-3 Applying stresses on three faces of sample.

To apply recorded pressure from experiments to the bottom of the borehole, the borehole was partitioned into two sections. Then the pressure was applied to the bottom 1 in. of the borehole (Figure 5-4).

For meshing the sample, standard analysis with linear geometric order was used. The element type selected was C3D4, a 4 node linear element, free meshing technique using tetrahedron shapes was applied to the model. Figure 5-5 shows the meshed specimen. There were 11,701 nodes and 62,371 elements in this model.

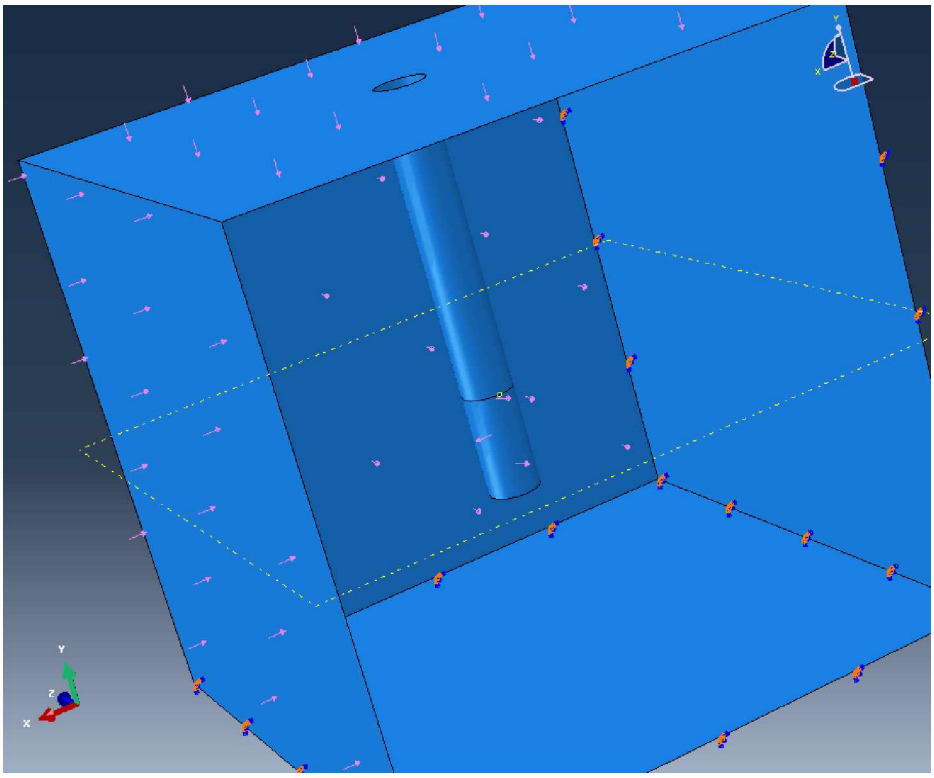

Figure 5-4 Applying pressure at the bottom 1 in. of the borehole.

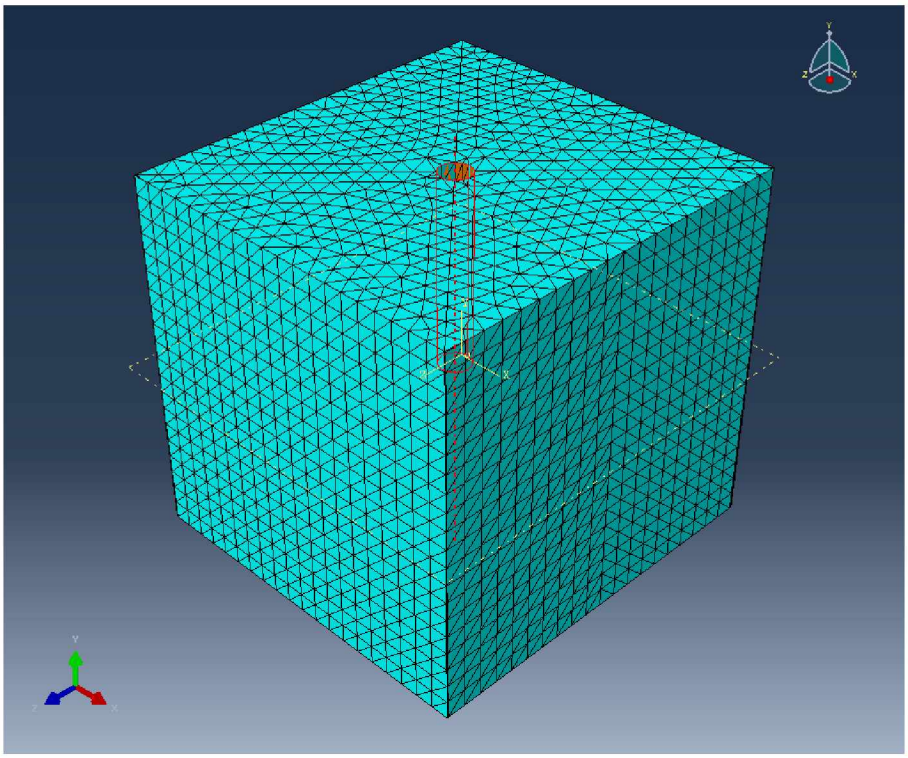

Figure 5-5 Meshed sample.

5.2 Results and Discussion

The deformed and undeformed shapes of the sample provided by ABAQUS are shown in Figure 5-6. The transparent shape represents undeformed shape when there is no stress applied on the sample. The green shape is the deformed shape after all stresses applied on the sample.

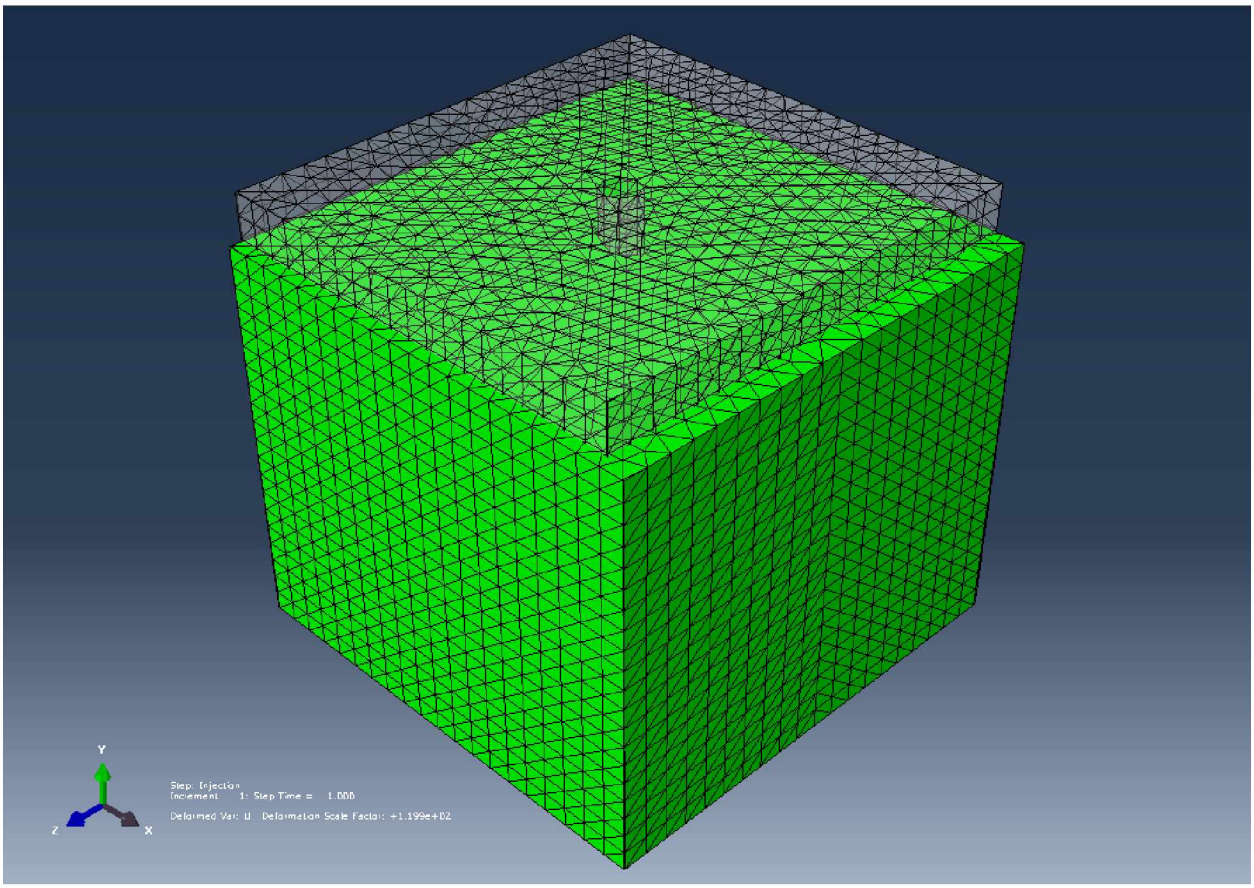

Figure 5-6 Undeformed and deformed shapes of the sample.

Fjaer et al. explained the theory of HF in their book. For a circular well, they proved that hydraulic fracture would propagate along maximum horizontal stress. They showed that the maximum and minimum tangential stress on the borehole wall can be calculated from Equations 5-1 and 5-2 (56):

$$\sigma_{\theta,max} = 3\sigma_H - \sigma_h \quad (5\text{-}4)$$

$$\sigma_{\theta,min} = 3\sigma_h - \sigma_H \quad (5\text{-}5)$$

where, $\sigma_{\theta,max}$ and $\sigma_{\theta,min}$ are the maximum and minimum tangential stresses, respectively, and σ_H and σ_h are the maximum and minimum horizontal stresses, respectively (56). The maximum

tangential stress occurs in the minimum horizontal stress direction, while the minimum tangential stress takes place in the direction of maximum horizontal stress (56).

It was proven that when a well is drilled along vertical stress, hydraulic fracture occurs where σ_θ is smallest. Equation 5-3 shows the condition that fracture starts to propagate along maximum horizontal stress direction (56):

$$P_{HF} = \sigma_{\theta,min} + T \tag{5-3}$$

$$P_{HF} = P_{gauge} + \gamma_{fluid} \times h \tag{5-4}$$

where T is tensile strength of the formation rock, P_{gauge} is the pressure reading when fractures initiate, γ_{fluid} is the unit weight of drilling fluid, and h is the depth of injection. In the experiment, since the depth of borehole was only 4 in., it was assumed that $P_{HF} = P_{gauge}$.

In the numerical model, maximum and minimum horizontal stresses were applied along YZ and YX planes, respectively. The plots of principal stress along the YZ plane and the YX plane for test No. 2 are shown in Figures 5-7 and 5-8, respectively. At the wall of an underground opening there are two principal stresses, σ_r (radial stress) and σ_θ (tangential stress). Based on Kirsch's equation for a circular opening, radial stress is always zero at the wall. So in fact the plot of principal stress at the wall of the opening provided by the software is the tangential stress. In the YZ plane, Equation 5-3 was met for all the experiments. Also, for the YX plane, it was verified that no fracture occurs. For example, in test No. 2, when the maximum horizontal stress was 300 psi, the minimum horizontal stress was 100 psi. Based on Equation 5-2, the tangential stress at the wall of the borehole should be zero in the direction of maximum horizontal stress. In ABAQUS, for each element within the bottom 1 in. of the borehole, the value of principal stress was a very small negative or positive number. This is because ABAQUS shows the principal stress for an element. Note that in this model the element had a tetrahedron shape with four nodes. In the finite element method, the requested output was estimated at each node and then the average was attributed to the element. It was possible to find two elements in the YZ direction with principal stress values of 24 and -14. The total principal stress for these two elements is 10. From Table 4-1, for test No. 2 ($P_{HF} = P_{gauge} = 320\ psi$) the tensile strength of the plaster was about 310 psi, so Equation 5-3 was met for these elements along the YZ plane. The principal stress along the YX plane was

checked for the elements in the bottom 1 in. of the hole to make sure that no element met Equation 5-3. Therefore, it can be concluded that the hydraulic fracture initiates along the maximum horizontal direction.

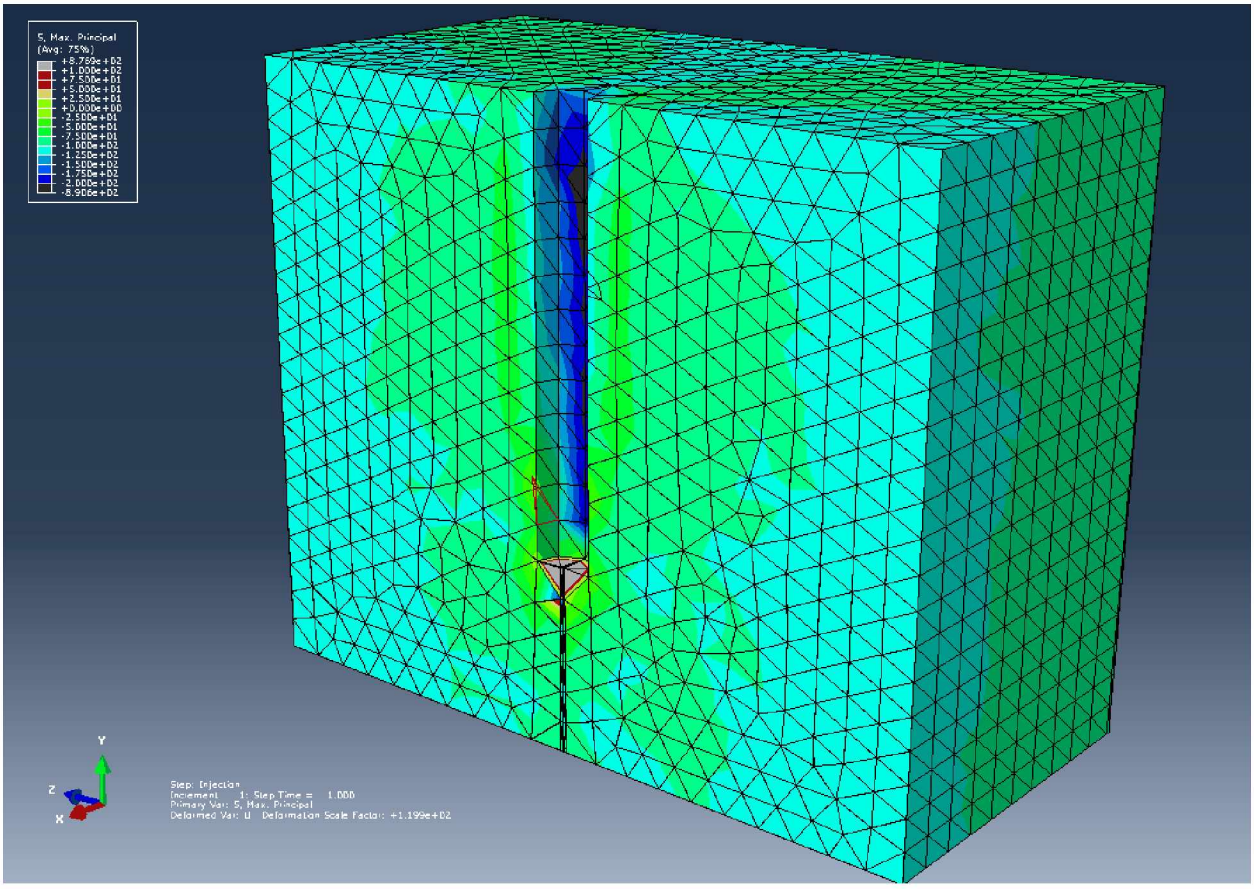

Figure 5-7 Principal stress plot along YZ plane (test No. 2).

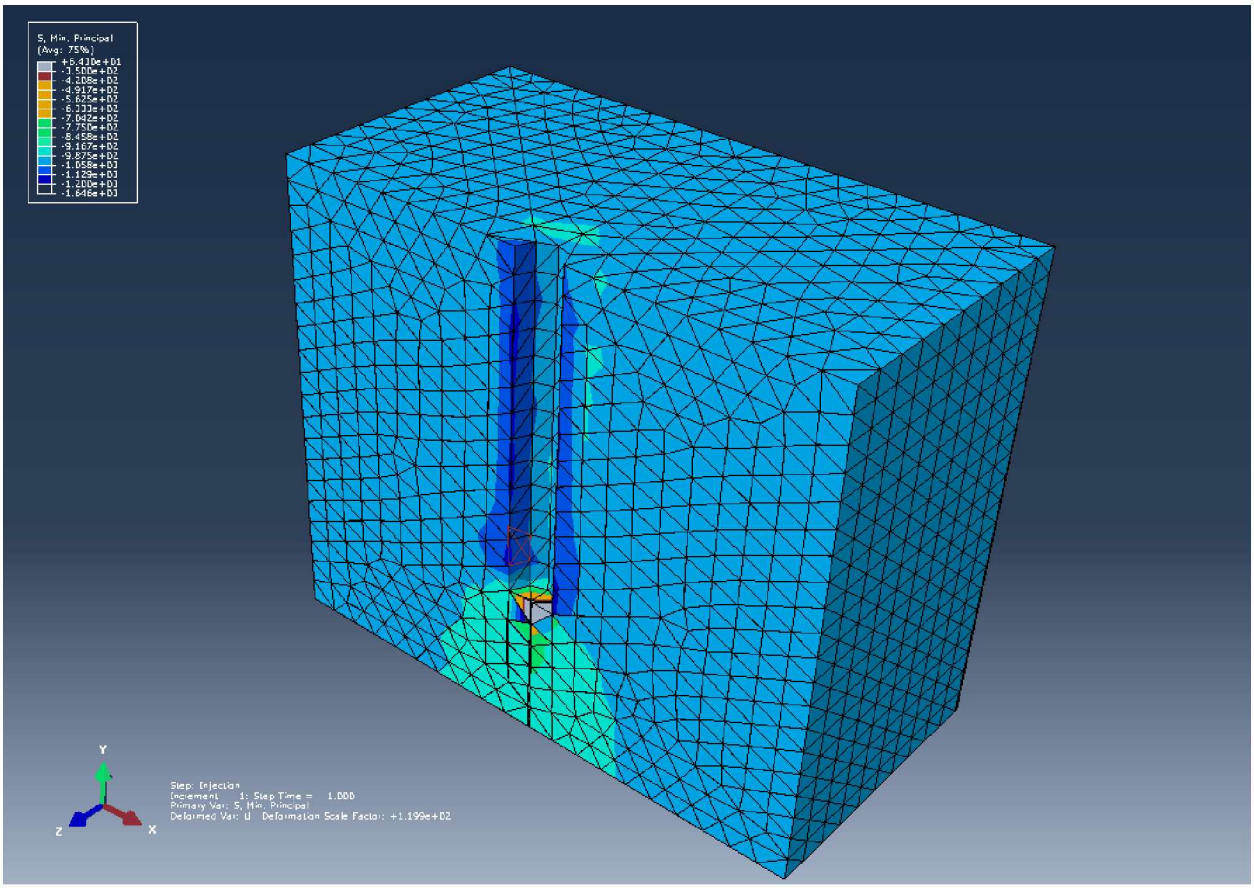

Figure 5-8 Principal stress plot along YX plane (test No. 2).

The stress conditions in all five performed experiments were applied to the built computer model. Through trial and error, the minimum pressure required to meet Equation 5-3 was determined for each case (5 psi interval was used in each attempt). All results are summarized in Table 5-1

Table 5-1 Minimum P_{HF} in each test determined using computer simulation.

Test #	$\sigma_v\ (psi)$	$\sigma_h\ (psi)$	$\sigma_H\ (psi)$	$\sigma_H - \sigma_h\ (psi)$	$P_{HF}(psi)$
1	1000	100	200	100	415
2	1000	100	300	200	310
3	1000	100	400	300	205
4	1000	100	500	400	115
5	1000	100	600	500	15

As shown in Figure 5-9, results from the experimental and numerical simulations match each other well, giving confidence that the numerical model can be used for further simulations.

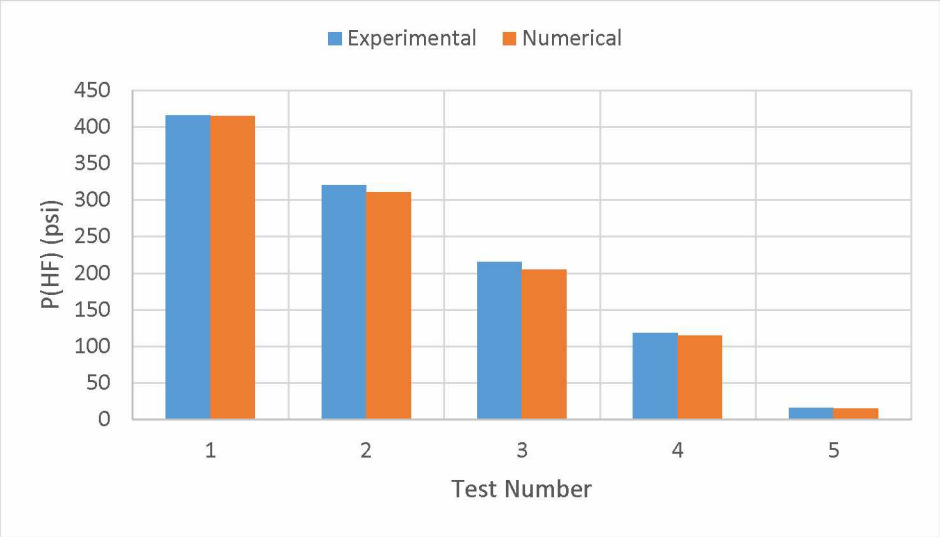

Figure 5-9 Comparison of experimental simulation versus numerical simulation.

Several models were run with different vertical stress and different levels of horizontal stress. Since the compressive strength of material was 1600 psi, applied vertical stress in each simulation was less than this value. In each simulation, through trial and error, the minimum pressure required to initiate HF was obtained. The stress conditions and results of all tests are listed in Table 5-2. From the simulations results, it can be stated that by increasing vertical stress at the same horizontal stress conditions, the minimum pressure required to initiate HF, slightly increases.

Table 5-2 Finding minimum P_{HF} at different vertical stress and levels of horizontal stress.

Test #	$\sigma_v\ (psi)$	$\sigma_h\ (psi)$	$\sigma_H\ (psi)$	$\sigma_H - \sigma_h\ (psi)$	$P_{HF}(psi)$
1	800	100	200	100	400
2	800	100	300	200	295
3	800	100	400	300	200
4	800	100	500	400	95
5	800	100	600	500	10
6	1000	100	200	100	415

Table 5-3 Finding minimum P_{HF} at different vertical stress and levels of horizontal stress (continued).

Test #	$\sigma_v\ (psi)$	$\sigma_h\ (psi)$	$\sigma_H\ (psi)$	$\sigma_H - \sigma_h\ (psi)$	$P_{HF}(psi)$
7	1000	100	300	200	310
8	1000	100	400	300	205
9	1000	100	500	400	115
10	1000	100	600	500	15
11	1200	100	200	100	435
12	1200	100	300	200	330
13	1200	100	400	300	215
14	1200	100	500	400	120
15	1200	100	600	500	30
16	800	200	300	100	605
17	800	200	400	200	500
18	800	200	500	300	395
19	800	200	600	400	300
20	800	200	700	500	195
21	1000	200	300	100	615
22	1000	200	400	200	510
23	1000	200	500	300	420
24	1000	200	600	400	305
25	1000	200	700	500	220
26	1200	200	300	100	630
27	1200	200	400	200	525
28	1200	200	500	300	430
29	1200	200	600	400	320
30	1200	200	700	500	235

Based on the results, R software was used to develop a 3D HF criterion for the used material. A multiple linear regression model was generated with four predictors or regressors (x1 = vertical stress, x2 = minimum horizontal stress, x3 = maximum horizontal stress, x4 = tensile strength). Y is the response or dependent variable, which in this case is the minimum required pressure to initiate HF. Figure 5-10 shows a screenshot of the generated results from the R software. The first column is the coefficient of each predictor that was estimated by R.

```
Coefficients:
    Estimate Std. Error t value Pr(>|t|)
x1  0.068750   0.006523   10.54 7.02e-11 ***
x2  3.010833   0.022596  133.25  < 2e-16 ***
x3 -1.000833   0.007532 -132.88  < 2e-16 ***
x4  0.784409   0.024778   31.66  < 2e-16 ***
---
Signif. codes:  0 '***' 0.001 '**' 0.01 '*' 0.05 '.' 0.1 ' ' 1

Residual standard error: 5.834 on 26 degrees of freedom
Multiple R-squared:  0.9998, Adjusted R-squared:  0.9997
F-statistic: 2.828e+04 on 4 and 26 DF,  p-value: < 2.2e-16
```

Figure 5-10 A screenshot of the generated results using the R software.

Equation 5-5 is the developed 3D HF criterion for the used material:

$$P_{HF} = 0.07(\sigma_v) + 3.01(\sigma_h) - (\sigma_H) + 0.79(T) \quad (5\text{-}5)$$

From the developed equation it can be stated that for a vertical well in a shallow formation, vertical stress has the least effect among all stress components on the minimum pressure required to initiate HF. Pore pressure in this simulation was assumed to be zero.

CHAPTER 6 CONCLUDING REMARKS AND RECOMMENDATIONS

In this study, a laboratory apparatus for simulating the HF process at a small scale was built. Hydraulic fractures were initiated in vertical holes drilled in cubic specimens made of plaster under various stress conditions. The hydraulic pressures applied at fracturing were observed and recorded. Furthermore, based on the specimen dimensions in the laboratory experiments, finite element models were developed to simulate the HF numerically under various stress fields; the results were compared with the laboratory experimental results.

The laboratory experiments of HF at a small scale were highly successful. In all cases, vertical hydraulic fractures formed since the applied vertical stress was the highest. It was observed that the vertical hydraulic fracture propagated along the maximum horizontal stress direction and perpendicular to the minimum horizontal stress direction. This is in agreement with the theory of HF propagation. It was observed that when vertical stress was kept constant, and the differential horizontal stress was increased by 100 psi, the minimum pressure required to initiate HF decreased almost 100 psi. These results were in agreement with 2D failure criterion of HF.

A numerical model was developed based on the conditions applied in the laboratory experiments. The results obtained from computer simulations were close to those obtained from experiments, verifying the applicability of the computer model. Therefore, additional scenarios with different stress conditions were run using the numerical model. The results indicated that the hydraulic pressure needed to initiate fracture was influenced by the maximum horizontal stress, the minimum horizontal stress, the vertical stress, and the tensile strength of the used material, with the vertical stress having the most effect; however, the vertical stress appeared to have minimal impact on HF. Based on the numerical simulations, a 3D failure criterion for HF was developed using a statistical software package, R.

The statistical analysis results suggested that the HF pressure required to initiate hydraulic fractures (P_{HF}) is a function of the vertical stress (σ_v), the maximum horizontal stress (σ_H), the minimum horizontal stress (σ_h) and the tensile strength of the material (T) in the following relationship:

$$P_{HF} = 0.07(\sigma_v) + 3.01(\sigma_h) - (\sigma_H) + 0.79(T) \quad (6\text{-}1)$$

It can be stated that in shallow formations as simulated, vertical stress has the least effect among stress components on the minimum pressure required to initiate HF.

There were some challenges with the experiment that can be improved in the future:

- The rock box was heavy (almost 40 kg). It is recommended to build a lighter box by using less steel, which would be easier to handle.
- The size of the box can be enlarged to have bigger specimens.
- For preparing the specimen, instead of the wood mold that was constructed in this research, it is recommended to make a mold from other material like Lexan to have a permanent mold.
- The strength properties of plaster are low, which does not allow the application of high stress. It is recommended to use other materials like cement or real shale samples to simulate high in situ stress conditions that are closer to what is happening in the real environment.

With the current experimental apparatus, it is possible to perform some other tests to investigate the effects of different parameters on HF propagation. One of the hot topics in petroleum industry is the effect of natural fractures in a shale formation while HF is being performed in that formation. The interaction of natural fracture and hydraulic fracture can be studied and simulated by using the built setup. The effects of drilling fluid on the HF also can be studied using this setup. For a real time picture of fracture propagation, one can use ultrasonic sensors attached to the specimen. It is recommended to drill inclined boreholes in the cubic specimens at different angles and test them with the experimental apparatus under different stress conditions. It is also recommended to generate computer models of an inclined borehole and develop a failure criterion for this case.

REFERENCES

1. EEC Environmental - A Brief History of Hydraulic Fracturing. [Online] November 19, 2011. http://eecenvironmental.com/services/258-a-brief-history-of-hydraulic-fracturing.

2. Morton, Michael Quentin. GEOEXPRO - Unlocking the Earth - A Short History of Hydraulic Fracturing. [Online] 2013. http://www.geoexpro.com/articles/2014/02/unlocking-the-earth-a-short-history-of-hydraulic-fracturing.

3. Shooters – A "Fracking" History. *American Oil and Gas Historical Society.* [Online].

4. *Differentiating Applications of Hydraulic Fracturing.* Joel, Adams. and Rowe, Clem. Brisbane, Australia : s.n., 2013. ISRM International Conference for Effective and Sustainable Hydraulic Fracturing.

5. Troy Cook, Jack Perrin. U.S. Energy Information Administration. [Online] March 15, 2016. https://www.eia.gov/todayinenergy/detail.php?id=25372.

6. United States Department of Energy. Modern Shale Gas Development in the United States: An Update. *National Energy Technology Laboratory (NETL).* [Online] September 2013. https://www.netl.doe.gov/File%20Library/Research/Oil-Gas/shale-gas-primer-update-2013.pdf.

7. Hydraulic Fracturing - Unlocking America's Natural Gas Resources. [Online] February 2017. http://www.api.org/oil-and-natural-gas/energy-primers/hydraulic-fracturing.

8. Hydraulic Fracturing - Graph of Oil and Shale Formations. [Online] 2016. http://www.api.org/~/media/APIWebsite/oil-and-natural-gas/primers/hf-oil-gas-production.png?la=en.

9. Ground Truth Trekking - Unconventional Oil and Gas in Alaska. [Online] April 13, 2015. http://www.groundtruthtrekking.org/Issues/AlaskaOilandGas/unconventional-petroleum-shale-oil-gas-alaska-great-bear-north-slope-hydraulic-fracturing.html.

10. Alaska Oil and Gas Competitiveness Review Board. Alaska Oil and Gas Competitiveness Report 2015. [Online] February 27, 2015.

11. Houseknecht, David, USGS. Assessment of Potential Oil adn Gas Resources in Source Rocks (Shale) of the Alaska North Slope. [Online] 2012.

12. Panel, National Science Foundation (NSF) Blue Ribbon. Simulation-Based Engineering Science. [Online] May 1, 2006. https://www.nsf.gov/pubs/reports/sbes_final_report.pdf.

13. *Analysis of stresses and strains near the end of cracking traversing a plate.* Irwin, G.R. 24, 1957, Journal of Applied Mechanics, pp. 361-364.

14. *Off-Balance Growth: A New Concept in Hydraulic Fracturing.* Daneshy, A. 04, April 2003, Journal of Petroleum Technology, Vol. 55, pp. 78 - 85.

15. *The distribution of stress in the neighbourhood of a crack in an elastic solid.* Sneddon, L.N. 1009, 1946, Proc. Royal Soc. London, Vol. 187, pp. 229-260.

16. *Extension of Griffith's theory of rupture to three dimensions.* Sack, R.A. 1946, Proc. Phys. Soc. London, Vol. 58, pp. 729-736.

17. *The Effects of Existing Fractures in Rocks on the Extension of Hydraulic Fractures.* Lamount, N. and Jessen, F.W. 02, February 1963, Journal of Petroleum Technology, Vol. 15, pp. 203-209.

18. *Hydraulic Fracture Propagation in the Presence of Planes of Weakness.* Daneshy, Ali. Amsterdam, Netherlands : s.n., 1974. SPE European Spring Meeting.

19. *Hydraulic Fracture Propagation in Layered Formations.* Daneshy, Ali. 01, s.l. : Society of Petroleum Engineers, February 1978, Society of Petroleum Engineers Journal, Vol. 18, pp. 33-41.

20. *Effects of Friction on Hydraulic Fracture Growth near Unbonded Interfaces in Rocks.* Anderson, Gordon. 01, s.l. : Society of Petroleum Engineers, February 1981, Society of Petroleum Engineers Journal, Vol. 21, pp. 21-29.

21. *An Experimental Study of Interaction between Hydraulically Induced and Pre-Existing Fractures.* Blanton, Thomas. Pittsburgh : Society of Petroleum Engineers, 1982. SPE Unconventional Gas Recovery Symposium.

22. *Effect of Stress Distribution on Hydraulic Fracture Geometry: A Laboratory Simulation Study in One Meter Cubic Blocks.* Ahmed, Usman, et al. Denver : Society of Petroleum Engineers, 1983. SPE/DOE Low Permeability Gas Reservoirs Symposium.

23. *Hydraulic Fracture Propagation in Layered Rock: Experimental Studies of Fracture Containment.* Teufel, Lawrence and Clark, James. 01, s.l. : Society of Petroleum Engineers, February 1984, Society of Petroleum Engineers Journal, Vol. 24, pp. 19-32.

24. *Numerical and Physical Studies of Fluid-Driven Fracture Propagation in Jointed Rock.* Shaffer, R.J., et al. Pittsburgh, Pennsylvania : Society of Petroleum Engineers, 1984. SPE Unconventional Gas Recovery Symposium.

25. *Propagation of Hydraulically and Dynamically Induced Fractures in Naturally Fractured Reservoirs.* Blanton, Thomas. Louisville, Kentucky : Society of Petroleum Engineers, 1986. SPE Unconventional Gas Technology Symposium.

26. *Influence of Geologic Discontinuities on Hydraulic Fracture Propagation.* Warpinski, N.R. and Teufel, L.W. 02, s.l. : Society of Petroleum Engineers, 1987, Journal of Petroleum Technology, Vol. 39, pp. 209-220.

27. *Laboratory Observations of the Effect of Geological Discontinuities on Hydrofracture Propagation.* Blair, Stephan, et al. Morgantown, West Virginia : American Rock Mechanics Association, 1989. The 30th U.S. Symposium on Rock Mechanics (USRMS).

28. *Experimental Hydraulic Fracture Propagation in a Multi-Fractured Medium.* Beugelsdijk, L.J., De Pater, C.J. and Sato, K. Yokohama, Japan : Society of Petroleum Engineers, 2000. SPE Asia Pacific Conference on Integrated Modelling for Asset Management.

29. *Experiments and numerical simulation of hydraulic fracturing in naturally fractured rock.* De Pater, C.J. and Beugelsdijk, L.J. Anchorage, Alaska : American Rock Mechanics Association, 2005. Alaska Rocks 2005, The 40th U.S. Symposium on Rock Mechanics (USRMS).

30. *Laboratory Hydraulic Fracturing Test on a Rock with Artificial Discontinuities.* Casas, L., et al. San Antonio, Texas, USA : Society of Petroleum Engineers, 2006. SPE Annual Technical Conference and Exhibition.

31. *Experimental Investigation of Fracture Interaction between Natural Fractures and Hydraulic Fracture in Naturally Fractured Reservoirs.* Zhou, Jian and Xue, Chengjin. Vienna, Austria : Society of Petroleum Engineers, 2011. SPE EUROPEC/EAGE Annual Conference and Exhibition.

32. *Laboratory Hydraulic Fracturing Tests on Small Homogeneous and Laminated Blocks.* Athavale, A.S. and Miskimins, J.L. San Francisco, California : American Rock Mechanics Association, 2008. The 42nd U.S. Rock Mechanics Symposium (USRMS).

33. *Laboratory scale model testing of well stimulation by use of mechanical impulse hadraulic fracturing.* Frash, L.P., Gutierrez, Marte and Hampton, Jesse. 03, s.l. : Society of Petroleum Engineers, June 2014, SPE Journal, Vol. 20, pp. 536-549.

34. Bing, Hou, et al. *Experimental investigation on the non-planar propagation of hydraulic fracture in Fractured Shale Reservoir.* Beijing, China : School of Engineering Bulletin, China University of Petroleum,, 2014.

35. *The opening of a Griffith cracks under internal pressure.* Sneddon, I and Elliot, H. 1946, Q. Appl. Math, Vol. 4, pp. 262-267.

36. *Widths of hydraulic fractures.* Perkins, T and Kern, L. 9, 1961, PE J. Pet. Tech., Vol. 13, pp. 937-949.

37. *Propagation of a vertical hydraulic fracture.* Nordgren, R P. 8, 1972, SPE, Vol. 12, pp. 306-314.

38. *Formation of vertical fractures by means of highly viscous liquid.* Khristianovic, S and Zheltov, Y. 1955. Proceedings of the 4th World Petroleum Congress.

39. *A rapid method of predicting width and extent of hydraulically induced fractures.* Geertsma, J and de Klerk, F. 12, 1969, Petroleum Technology, Vol. 21, pp. 1571-1581.

40. *Computer simulation of hydraulic fractures.* Adachi, J, et al. 5, 2007, International Journal of Rock Mechanics and Mineral Science, Vol. 44, pp. 739-757.

41. *A review of hydraulic fracture models and development of an improved Pseudo-3D model for stimulating tight oil/gas sand.* Rahman, M. 15, 2010, Energy Sources, Vol. 32, pp. 1416-1436.

42. *A finite element method for crack growth without remeshing.* Moes, N, Dolbow, J and Belytschko, T. 1, 1999, International journal of numerical analysis methods in geomechanics, Vol. 46, pp. 131-150.

43. *Discrete Fracture Network Modeling of Hydraulic Stimulation, Coupling Flow and Geomechanics.* McClure, M. and Horne, R. 2013, Springer International Publishing.

44. *A discrete numerical model for granular assemblies.* Cundall, P. and Strack, O. 1, 1979, Geotechnique, Vol. 29, pp. 47-65.

45. *3-D numerical simulation of hydraulic fracturing in a CBM reservoir.* Zou, Junpeng, et al. 2017, Natural Gas Science and Engineering, Vol. 37, pp. 386-396.

46. *A unified finite element method for the simulation of hydraulic fracturing with and without fluid lag.* Bao, J.Q., Fathi, E. and Ameri, S. 2016, Engineering Fracture Mechanics, Vol. 162, pp. 164-178.

47. *Numerical study on hydraulic fracturing in tight gas formation in consideration of thermal effects and THM coupled processes.* Feng, Wentao, et al. 2016, Petroleum Science and Engineering, Vol. 146, pp. 241-254.

48. *The effect of natural fractures on hydraulic fracturing propagation in coal seams.* Wang, Tao, et al. 2017, Petroleum Science and Engineering, Vol. 150.

49. ASTM. *Standard test method for unconfined compressive strength of intact rock core specimens.* s.l. : American Society for Testing and Materials, 1986.

50. *Standard method of test for elastic moduli of rock core specimens in uniaxial compression.* s.l. : American Society for Testing and Materials. D 3148-72.

51. Brady, B.H.G. and Brown, E.T. *Rock Mechanics for Underground Mining.* New York : Kluwer Academic , 2005.

52. *Measurement of tensile strength by diametral compression of discs and annuli.* Mellor, M. and Hawkes, I. 1971, Engineering Geology, Vol. 5, pp. 173-225.

53. ASTM. *Standard method of test for triaxial compressive strength of undrained rock core specimens without pore pressure measurements.* s.l. : American Society for Testing and Materials D 2624-67.

54. *Mechanics of Hydraulic Fracturing.* Hubbert, M. King and Willis, David G. s.l. : Society of Petroleum Engineers, 1957, Vol. 210.

55. Zobac, Mark. *Reservoir Geomechanics.* s.l. : Cambridge University, 2007.

56. Fjaer, E, et al. *Petroleum realted rock mechanics.* Amsterdam : Elsevier, 2008.